STUDIES ON PREPARATION AND CHARACTERISTICS OF $Ga_{1-x}Al_xAs$ LIQUID PHASE EPITAXIAL FILMS

SHOJI ISOZUMI

1979

STUDIES ON
PREPARATION AND CHARACTERISTICS OF $Ga_{1-x}Al_xAs$ LIQUID PHASE EPITAXIAL FILMS

by

SHOJI ISOZUMI

A Thesis Submitted to
Kyoto University
for The Partial Requirements of
The Degree of Doctor of Engineering

1979

CONTENTS

I. INTRODUCTION

I.1. General Introduction

Applications of a liquid phase epitaxial (LPE) growth method to III-V compounds were originated by Nelson[1] in 1963. He demonstrated this method was very useful for the fabrication of GaAs p-n junction of tunnel and laser diodes. In the same year, Hall[2] determined the solubility of III-V compounds in Ga and In liquid. However, it was in 1965 that the phase diagrams of binary III-V systems was precisely determined by Thurmond[3]. At that time, LPE growth method took an important position as one of the crystal growth techniques because the knowldges about the phase diagram is essential for it. On the other hand, the phase diagrams of ternary III-V systems were obtained later on. In the case of Ga-Al-As system, it was determined by Ilegems and Pearson in 1968[4].

In various mixed crystal systems of III-V compounds, $Ga_{1-x}Al_xAs$ system is most widely used. This is mainly due to the unique property that the lattice constant is well matched with that of GaAs for the entire composition range at the growth temperature. As a result, both the epitaxial layer and the GaAs-$Ga_{1-x}Al_xAs$ heterojunction interface are free from dislocations except for the threading ones from the substrate. Another reason why this mixed crystal is widely used is that the energy gap corresponds to a useful

wavelength region from near infrared to red. Then, applications to photo-lamps emitting the light in this region have been investigated by many workers. Whereas, in the recent years, more attentions have been paid to the near infrared region because it was found advantageous to utilize the light of about 0.8 μm for fiber-optical communication systems. Double heterostructure lasers[5),6)] and high radiance light emitting diodes[7),8)] using this material have been playing important roles as light sources for the communication systems.

It is well known that the continuous operation of GaAs-$Ga_{1-x}Al_xAs$ double heterostructure laser diodes was first demonstrated by Hayashi et al.[5),6)] in 1970. Their success is attributed to the excellent property of this heterojunction and the development of a new LPE technique[9)]. This heterojunction does not result in the interface recombination centers usually exsisting at such boundaries, and is extremely useful for providing carrier and optical confinement in semiconductor lasers. The LPE method developed by them was named "Sliding Method" later. It permitted a successive growth of multiple layers with the control of both the thickness and the characteristics of each layer.

It can be said that the LPE growth technology of $Ga_{1-x}Al_xAs$ which had been developed before 1970 was intensively demonstrated by their success in the double heterostructure lasers. Since their work was almost perfect, up to present, there have been few landmarks in this field. It is neccessary, however,

to improve their techniques for the applications to other devices.

The epitaxial wafer for the double heterostructure lasers is composed of GaAs and/or $Ga_{1-x}Al_xAs$ layers successively grown on the GaAs substrate. The thickness of each layer is within the range of 0.1 - 3 μm. In the case of such a thin layer growth, the phase diagram gives almost complete data for the control of the composition of each layer. The phase diagram predicts both a saturated liquidus composition at a given temperature by the liquidus line and the composition of the solid equilibrated with the liquid by the solidus line. On the other hand, other devices such as light emitting diodes sometimes requires thicker epitaxial $Ga_{1-x}Al_xAs$ films for high device performances. The solidus composition changes as the growth proceeds because the consumption of the solute atoms into the solid substantially causes a change of the liquidus composition. Besides, a temperature drop during the growth cycle changes the distribution coefficient of each constitutive element. Consequently, not only the phase diagram but knowldges about the solidus composition change during the growth cycle are essential for the control of the thick $Ga_{1-x}Al_xAs$ films which is required for the light emitting diodes.

The growth of thick $Ga_{1-x}Al_xAs$ films presents some other accompaning difficulties. The LPE wafer for high radiance light emitting diodes are required to have multiple layers

structures to achieve high device performances by utilizing heterojunctions, and the thicknesses of both the thick layer and the successive thin layers should be precisely controlled. Whereas, during the growth of the thick layer, the liquidus compositions are continuously changing. Then, the growth rate of each layer is also continuously changing because the growth rate is strongly dependent on the liquidus composition in Ga-Al-As system.[10] This problem leads to the difficulty in the prediction of the each layer thickness. For the analyses on such a complicated case, detailed knowldges about the growth mechanisms of $Ga_{1-x}Al_xAs$ and the solute diffusivity in Ga-Al-As liquid. However, there have been few reports in this field.

Another difficulty is more practical one which we experience when the thick and multi-structured LPE wafers are prepared by the conventional "Sliding Method" developed by Hayashi et al.[9] In order to obtain a thick (for example, 50 μm) LPE layer, the cooling interval of a few ten's is required. During the growth of this layer, the liquids for the successive thin layers are also cooled. Then, if the conventional method is used for the growth, the successive liquids would be covered with precipitated solids because the magnitude of the supercooling is a few °C at most. A large improvement in the growth system is neccessary to prevent this phenomenon.

In this thesis, the theoretical and experimental studies on these basic problems are described. On the bases of these

analyses, the LPE growth technology of $Ga_{1-x}Al_xAs$ wafers for light emitting diodes used in fiber-optical communication systems, and the characteristics of the LPE films are also described.

In section I.2, the progress in LPE growth of III-V compounds are reviewed. This section is especially prepared for better understanding of the historical backgrounds in this field.

In chapter II, the studies on the preparation of $Ga_{1-x}Al_xAs$ LPE wafers are described. In section II.2, Ga-Al-As ternary phase diagram is discussed. It is shown that the precise choice of the thermodynamic data is neccessary for the analyses described in the following chapters. In section II.3, tne basic problems in LPE growth of $Ga_{1-x}Al_xAs$ are discussed using the experimental results in the early stage of the studies.

In chapter III, the solidus composition change of ternary compounds during the growth cycle is analyzed. The results in this chapter is effectively applied to the design of thick $Ga_{1-x}Al_xAs$ LPE films as is shown in chapter V.

In chapter IV, the analyses on the growth rate of $Ga_{1-x}Al_xAs$ are described. In section IV.2, the theoretical backgrownds are reviewed. In sections IV.3 and IV.4, the strong dependence of the growth rate on the liquidus composition in Ga-Al-As system is analyzed from both the theory and the experiments. The growth of $Ga_{1-x}Al_xAs$ is shown to be an arsenic diffusion controlled process in the main. Arsenic

diffusivity in the Ga-Al-As liquid and its temperature dependence are discussed.

On the bases of the results in the preceding chapters, the growth conditions to obtain a 50 μm thick $Ga_{1-x}Al_xAs$ LPE films are analyzed in chapter V. It is shown that the very low cooling rate and the thin liquid are essential for the surface flatness and the thickness control.

In chapter VI, an unique LPE growth system, which enables to prepare a thick and multiple-layer structured $Ga_{1-x}Al_xAs$ wafer, is presented. The LPE wafer grown in this system consists of a 50 μm thick layer and a subsequent thin layer, and is suitable for the effective extraction of the emitted light from the crystal.

In chapter VII, $Ga_{1-x}Al_xAs$ LPE films are characterized from the points of the contained defects and the degradation phenomena of the light emitting diodes prepared from them. In section VII.2, the structure and the properties of the high radiance light emitting diodes are described. In section VII.3, it is shown that the degradation phenomena of $Ga_{1-x}Al_xAs$ light emitting diodes can be classified into two modes. In section VII.4, the dark line defects in the rapidly degraded light emitting diodes are analyzed by TEM observations. The structures and the growth mechanisms of the dark line defects are described.

In chapter VIII, these studies are summarized.

I.2. Progress in Liquid Phase Epitaxial Growth of III-V Compounds

In semiconductor materials for optoelectronic devices, the binary compounds formed from the elements of groups III and V are particularly important for their fundamental properties. Since their existence was first reported by Welker et al.[11] in 1952, they have been studied extensively, and are now widely used technologically. In the semiconductor industry at present, GaAs, GaP, AlAs and their mixed crystals are used for optoelectronic devices and microwave devices.

Since the efficiency of these electroluminescent devices depends on the competition between the desired radiative process and undesired non-radiative processes, which is favoured by impurities or crystal defects, it is clearly necessary to prepare the material to a high degree of purity and crystalline perfection. All of the III-V compounds have high melting points and appreciable vapour pressures at their melting points. These factors lead to several problems in the growth of pure single crystal. At the high temperature the molten semiconductors tend to be contaminated by crucible materials. Furthermore, high pressures under which some preparations must be carried out lead to severe problems in the design of the growth apparatus.

GaAs has a melting point of 1240°C and exerts an arsenic pressure of 0.9 atmospheres at the melting point. The vapour pressure of elemental arsenic reaches the same value at 610°C

and increases rapidly with temperature. Then, if one attempts to combine the elements gallium and arsenic by heating together the appropriate quantities to the melting point of the compound, the arsenic pressure in the system may rise to a very high value and an explosion is almost inevitable. This problem can be overcome if the elements are heated in a system containing two temperature zones, the arsenic being held at 610°C and the gallium being held at 1240°C. In this way, the arsenic vapour pressure will be held at 0.9 atmospheres and the reaction with gallium will proceed to give molten gallium arsenide.

However, this method has limitation in the purity and the crystal perfection. For example, the limitation of the purity of GaAs by this method is believed to be 10^{16} cm^{-3} for electron concentration. That is due to the contamination of sillicon from silica crucible and complex defects peculiar to such a high energy gap semiconductor as GaAs. The crystal by this method essentially contains vacancies of the elemental atoms, which form complex defects with the residual impurities. They lead to the undesired non-radiative recombination centers in electroluminescent devices. These problems are inevitable when the crystal is grown from the melting point.

The epitaxial growth techniques have overcome these problems. The basic concept of an epitaxial growth is that one commences with an orientated single-crystal slice, or substrate, of the material grown by the method described above, and grows

the further layer of the material with higher purity and higher perfection on the substrate. In epitaxial techniques, the material is grown either from the liquid phase or from the vapor phase at a temperature which is considerably below its melting pont. This can reduce the contamination of the material caused by any interaction with a hot crucible and thus enables very pure material to be produced. Alternatively, intentional dopant elements can be introduced into the growth system so that doped semiconductor layers with desired carrier concentration can be grown.

In the case of GaAs, both the vapor phase epitaxy (VPE) and the liquid phase epitaxy (LPE) provided the most purified crystals. Dilorenzo[12] obtained residual electron concentration $n = 1.4 \times 10^{12}$ cm^{-3} and electron mobility $\mu(77°K) = 2.2 \times 10^{5}$ $cm^2/V \cdot sec$ by VPE using H_2-Ga-$AsCl_3$ system. Whereas, Miki et al.[13] obtained $n = 2.5 \times 10^{13}$ cm^{-3} and $\mu(77°K) = 2.2 \times 10^{5}$ cm^2/V sec by LPE from Ga solution. In their data, the residual electron concentration by VPE is lower than that by the LPE. However, electron mobilities obtained by both method are nearly the same values each other. This means crystals by VPE contain more deep impurities or crystal defects responsible for scattering processes of electrons.

The natures of these crystal defects are closely related to the deviation of the compounds from its stoichiometry. The vacancies of the elemental atoms caused by the non-stoichiometry act as deep trapping centers by interacting with impurity

atoms or interstitial atoms. In Figs.1 and 2, electron traps and hole traps measured by several kinds of methods are respectively shown for GaAs crystals obtained by the melt growth, VPE and LPE. It should be noticed that crystals obtained by the melt growth and VPE contains both many electron and hole traps, whereas LPE crystals contain only two native hole traps (indicated as LA and LB in Fig.2.). Consequently, LPE is superior to the other methods for obtaining perfect crystals, and has been widely used in the production of electroluminescent devices.

Most LPE growth systems fall into one of two classifications: (a) transient systems, involving the controlled cooling of a solution in which the desired constituents have been dissolved; or (b) steady-state systems, in which the system temperature is essentially constant and material is transported by the use of thermal gradient. In the explanation of these systems, it is convenient to choose a particular example. The growth of GaAs from Ga solution is chosen due to the extensive work which has been done on this system. The Ga-As phase diagram obtained by Hansen[14] is shown in Fig.3 for the illustration.

If a solution of composition X_A and temperature T_A (point A in Fig.3) is brought into contact with a GaAs substrate also at temperature T_A, the system equilibrium is unchanged. This is so since the point A lies on the liquidus line of the phase diagram and the solution is already saturated with arsenic.

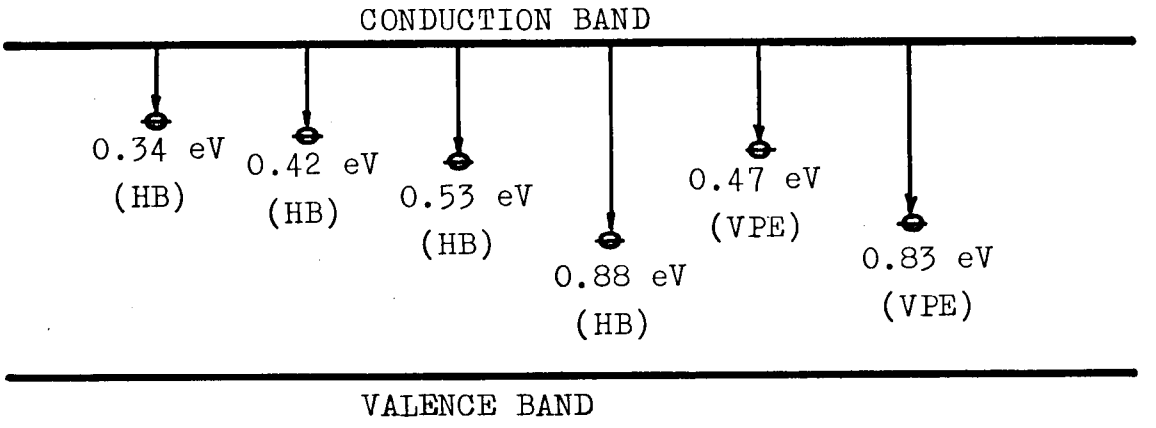

Fig.I-1. Electron traps in GaAs[51]. No electron trap has been observed in LPE GaAs.

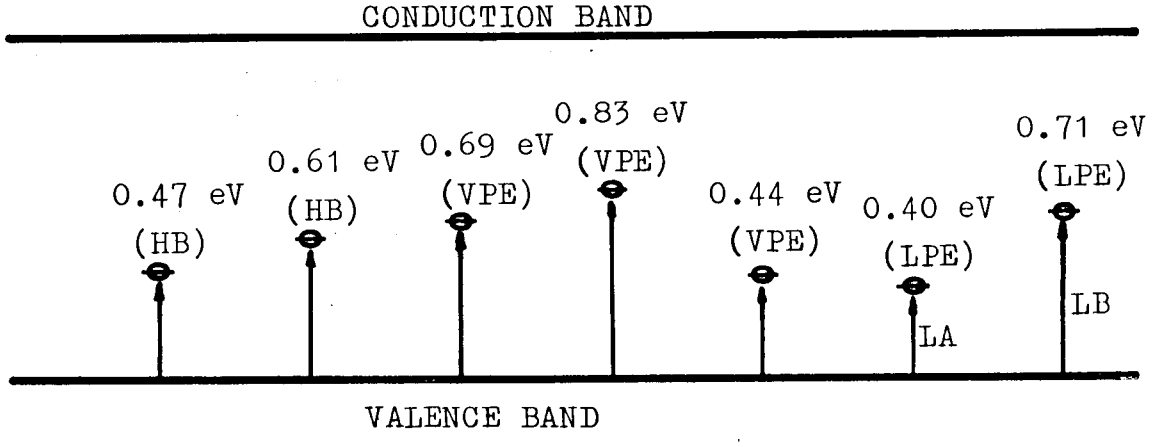

Fig.I-2. Hole traps in GaAs[51].

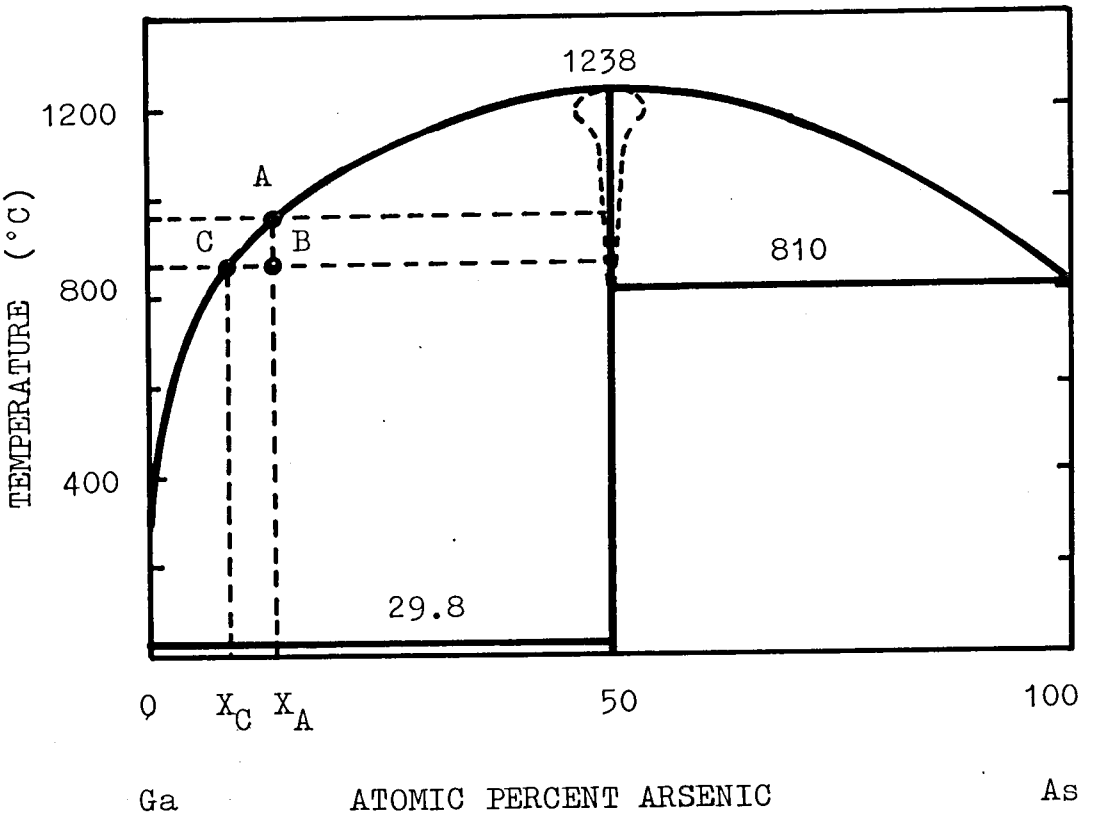

Fig. I-3. Ga-As binary phase diagram[14].

If the system is then cooled to point B, the solution becomes supersaturated, and GaAs precipitates from the melt. When an As-saturated Ga solution is cooled, the decreasing solubility of arsenic with decreasing temperature causes arsenic to precipitate in the form of GaAs, bringing the liquid to composition X_c. The growth occurs more readily on the GaAs substrate than in the bulk of the melt and an epitaxial film is grown. This is a principal idea of the transient system. This growth method was first applied to the fabrication of tunnel and laser diodes by Nelson [1]. His growth system is shown in Fig.4. A graphite boat contains a GaAs substrate wafer clamped in one end and a Ga-GaAs mixture in the other. The boat is inserted into a furnace in a tilted position, as shown Fig.4, to maintain isolation of the substrate and the melt. As the system is heated to a temperature of 800-900°C, GaAs dissolves to saturate the melt with arsenic. The furnace is then tipped to allow the melt to flow over the substrate, after which the system is cooled to produce the epitaxial deposition. After cooling by several hundred degrees, the furnace is tipped to decant the melt, with drainage usually being incomplete. Subsequent cooling to room temperature produces some additional growth.

The second major classification of LPE growth systems is the steady-state method. Consider a system in which a GaAs substrate is held at temperature T_B and a GaAs source crystal is held at a higher temperature T_A, with the space

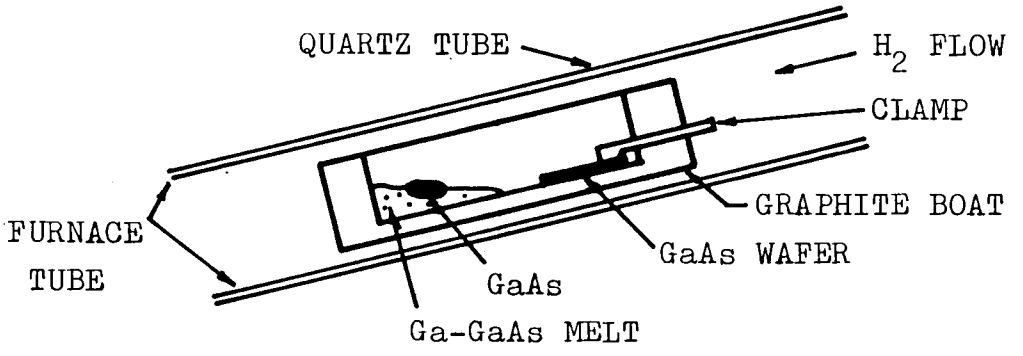

Fig. I-4. Tipping growth system for LPE growth of GaAs[1].

filled with gallium. As the system approaches equilibrium, more GaAs will be dissolved at the hotter source than at the cooler substrate. Then arsenic atoms diffuse from the vicinity of the source to the vicinity of the substrate. A condition of supersaturation is thus created at the substrate and the growth will occur. Although this idea is well known as the temperature gradient method and was successfully applied to the growth of silicon from aluminum solution by Pfann[15),16)], the application of it to the growth of III-V compounds is, in practice, difficult because of the very low growth rate and the poor reproducibility.

Consequently the LPE growth of III-V compounds advanced using the transient systems. It has been used more widely for the growth of GaAs than for any other materials, largely due to a greater number and variety of device structures to which GaAs lends itself. The process was first applied to the growth of heavily doped p or n layer on inversed type substrate to form p-n junctions. With Gunn's[17)] discovery of microwave oscillations in n-type GaAs, the emphasis shifted away from the p-n junction and toward the bulk properties of the material. It soon became evident that a new breed of electronic devices had been conceived and with it a new and more demanding set of materials had been required. Gunn diodes require very homogeneous free electron concentrations[18)] in the 10^{15} cm^{-3} range or lower[19)-21)], usually with an active layer thickness less than 10 μm. In this stage of the

progresses, the demand for LPE growth techniques was restricted in a single and relatively thick layer. Whereas, the method originated by Nelson had not been able to satisfy the increasing demands for the control of layer thickness or surface flatness, mainly due to the poor removal of the solution after the growth. In this method, the system is cooled several hundred degrees with the melt and the substrate remaining in contact. Reproducibility of layer thickness then depends on the fraction of the crystallizing solute which is deposited on the substrate. Often this fraction is small and not reproducible owing to the formation of crystallites within the melt, and serving to make dimensional control of the layer difficult. If the growth is terminated by tipping back to decant the melt at some elevated temperature, droplets often adhere to the surface, causing additional sporadic growth on subsequent cooling to room temperature.

One approach to better dimensional control is the use of vertical dipping systems[22)-29)]. If the melt and substrate are separated after the growth by withdrawing the substrate through the top surface of the melts, the greatest use is made of gravity and surface tension for complete drainage. Dawson[22)] reported the use of such a system for the growth of epitaxial GaAs layers from gallium solutions. Their system, shown in Fig.5, provides separate holders for the source and substrate wafers. The melt is saturated with arsenic

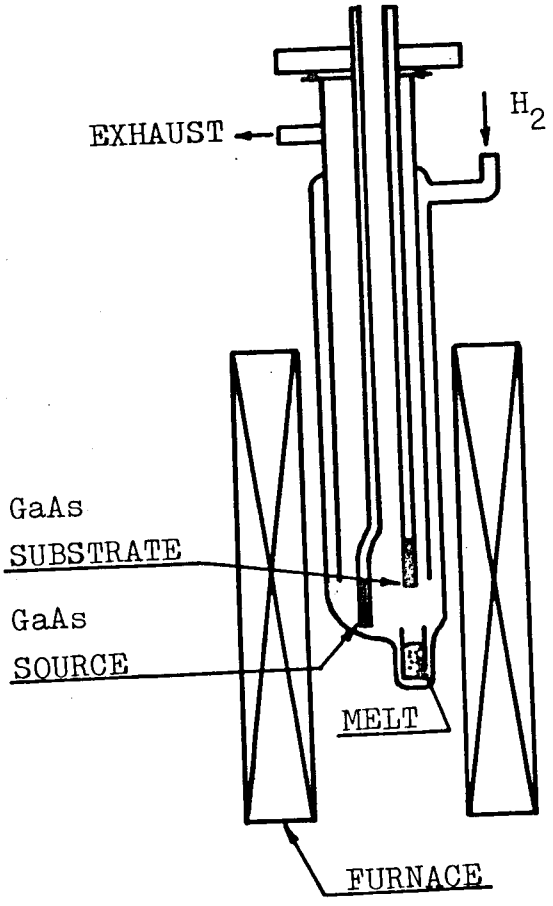

Fig. I-5. Vertical dipping system for LPE growth of GaAs[22].

by dipping the source piece into the melt. After withdrawal of the source, the substrate is inserted into the melt and the furnace is cooled to produce growth. Using low cooling rates to prevent excessive supersaturation, smooth films were grown from which the melt drained completely as the substrate was withdrawn. By establishing the temperature control of $\pm$ 0.01°C, very small total cooling ranges could be used, producing films ranging in thickness of 1 - 20 μm. However, this method was revealed to have limitations in the uniformity of the layers and still in the complete drain of the melt. The former is mainly due to the essential difficulty of establishing the constant temperature zone in vertical furnaces, on the other hand, the latter is often caused by the appearance of crystallines at the surface of the melt especially in a case of a large cooling interval.

Panish et al.[30),31)] first designed a sliding system with a wiping mechanism in a horizontal furnace, which was more suitable for establishing longer constant temperature zone than vertical ones. Their system is schematically shown in Fig.6. The melt is contained in a well and the substrate is delivered to a clean melt surface by a slider whcih first wipes the melt surface free of any solid material. After the growth, the substrate is slid off from the melt, and simultaneously, complete wiping of the melt by the surface tension and the scraping action of the wall

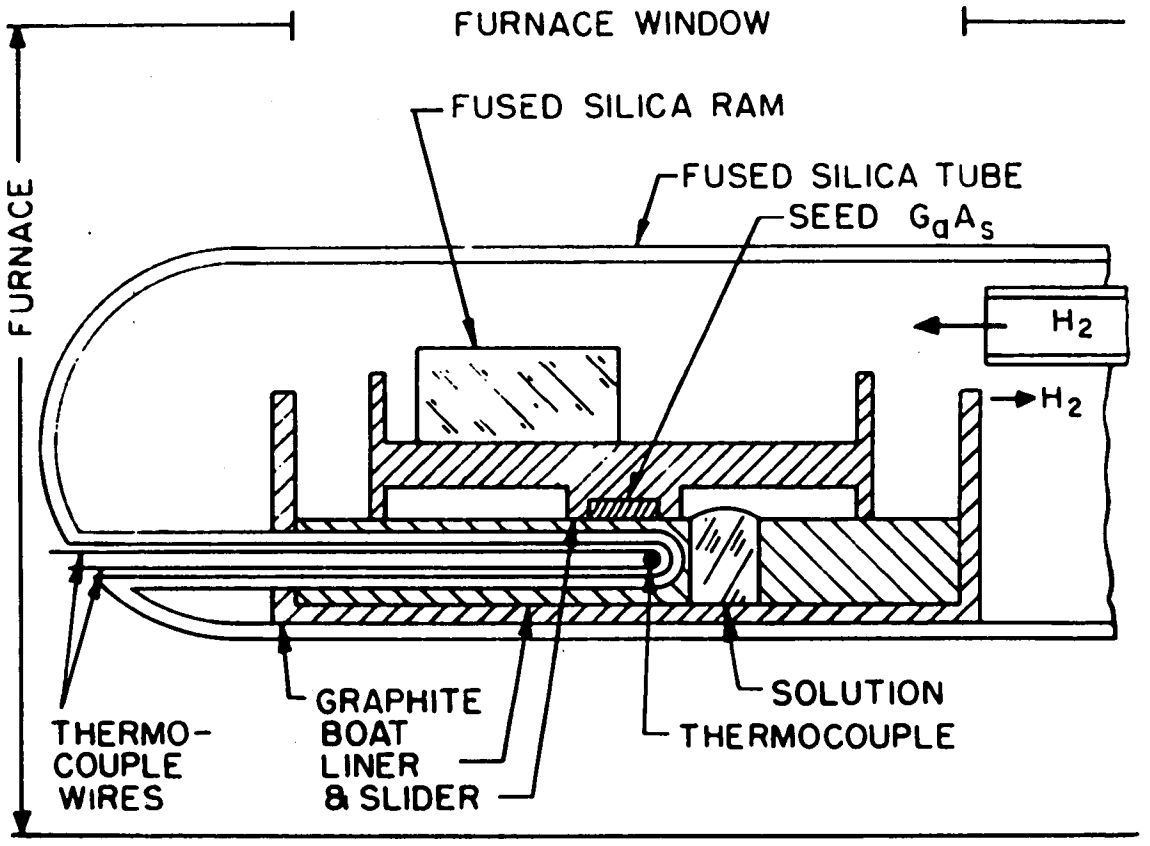

Fig. I-6. Holizontal sliding system for LPE growth of $Ga_{1-x}Al_xAs$[30].

edge. They successfully applied this method to the growth of $Ga_{1-x}Al_xAs$ layers from the solution containing aluminum.

This design was later modified as shown in Fig.7 for the growth of the multilyer structures required for heterostructure lasers[9]. As is shown in this figure, a slider system contains four solutions. The premeasured solutions are chosen to be nearly saturated with arsenic at the temperature at which the growth is initiated. After a time for thermal equilibration, the system is cooled at a constant rate and the solution holder is positioned to bring each melt successively into contact with the substrate. In this manner, four LPE layers with a complicated structure for double heterostructure lasers were grown with an extreme planarity of each layer. From such a LPE wafer, Hayashi et al.[5),6)] were able to fabricate lasers operating continuously at room temperature and above. Their success made this system very famous as "Sliding Method". This method and the modified ones[42),43),34)] have successfully provided multilayers LPE wafers for opto-electronic devices, Gunn diodes[32)-34)], IMPATT diodes[34)-39)] and FETs[40),41)]. All the results of them proved that this method was powerful in the preparation of thin and complicated multilayer structures, and was more advantageous even than any vapour phase epitaxial growth methods.

Another aspect of progresses in the LPE growth is the advances of multi-wafers growth techniques developed for

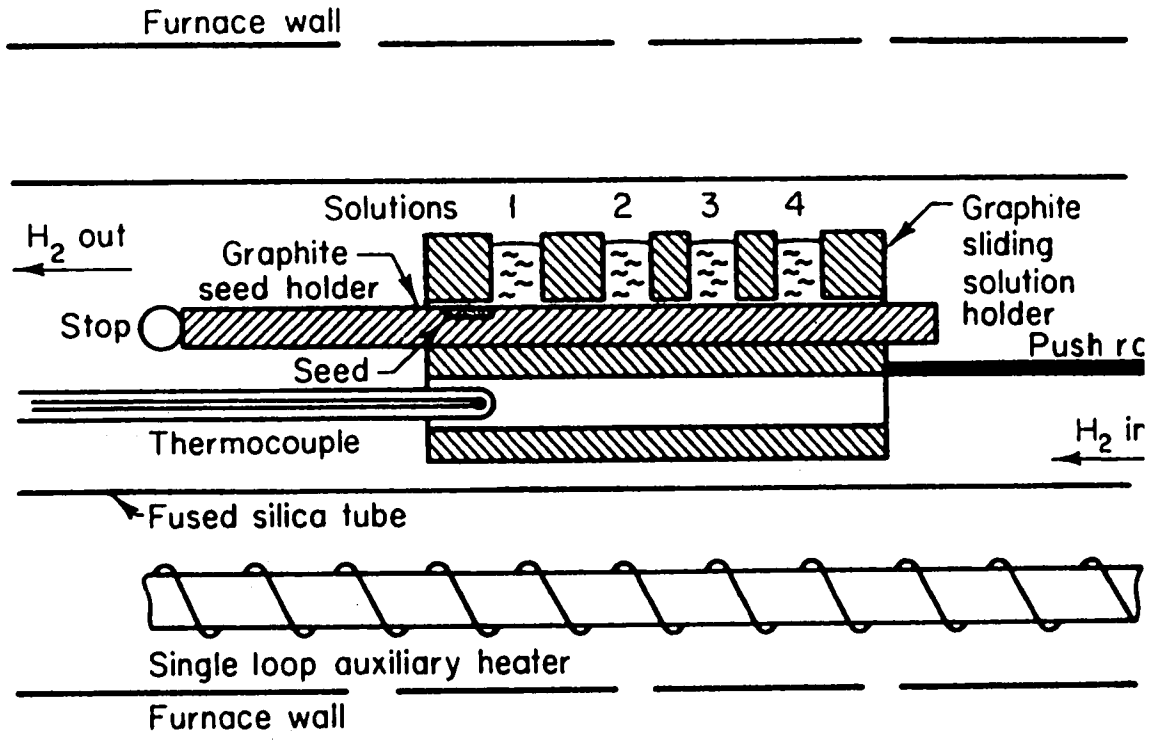

Fig. I-7. LPE growth system for double heterostructure lasers using a sliding solution holder[9].

the large scale productions of GaP displays and GaAs:Si infrared lamps. In these cases, the cost required to produce a LPE wafer is the most important factor in designing growth systems. This requirement has been satisfied by decreasing the volume of gallium solutions used for one LPE wafer and by the development of multi-wafer processing systems. Takahama et al.[44] developed a multi-wafers dipping system as shown in Fig.8. In this system, 10-12 GaP substrates spaced each other with 1-3 mm distance were fixed at a substrate holder. By dipping the substrates into the solution (GaP + Ga + dopants), gallium melt uniformly spreaded into these thin spaces between each substrate, and the growth was initiated. The growth was terminated by withdrawing the substrates from the solution. Similiar systems have been developed by many workers[45)-47)]. Whereas, in these systems, there is a disadvantage that the adhesion of the thin melts with the substrates sometimes interrupts a smooth drain of the melts after the growth.

Bergh et al.[48] introduced the sliding technique into multi-wafers processing system. Their system was designed in which a large volume of a saturated melt was sectioned into many small but equal thin melts (aliquot) for each substrate. The key to forming aliquots was wetting the substrate by a large volume of the melt in an apparatus constructed of nonwetted materials. The part of the apparatus are shown in Fig.9. A melt reservoir was held in the frame with cover

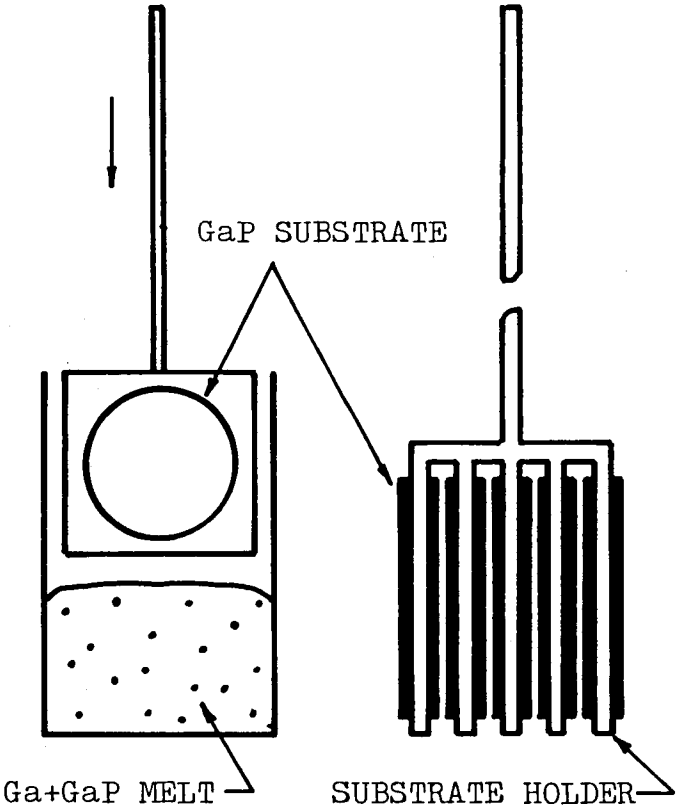

Fig. I-8. Multi-wafers dipping system for LPE growth of GaP[44].

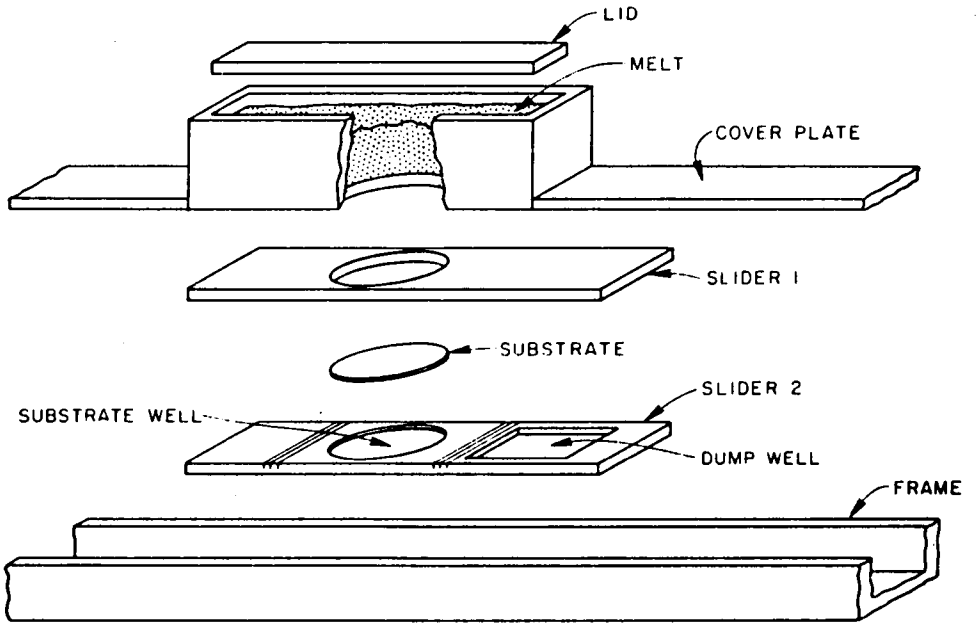

Fig. I-9. Parts of the double slider LPE apparatus[48].

plates to seal the top of the frame. Two sliders are positioned into the frame, moving underneath the reservoir and cover plates from left to right. Slider 2 contains the substrates and the dump well used in the removal of the aliquots from the substrates when the growth was terminated. Slider 1 had an opening slightly larger than the substrate and was used to form the aliquots. Both sliders were aligned under the reservoir and simultaneously translated from left to right to form the aliquots. Fig.10 demonstrates the operational steps for a multislices LPE deposition. Each slider pair contained one substrate and one dump well. After the saturated melt was formed ;(a), the slider pairs were moved along sequentially to form the desired number of aliquots ;(b) and (c). After the LPE deposition was accomplished, the sliders on the top were moved to wipe off the aliquots, thereby terminating the growth ;(d). This system was characterized by a high deposition efficiency and smooth surface morphologies. The authors reported that close to 100 % deposition efficiency and hence excellent control over layer thickness and uniformity was obtained with aliquot melts of less than 1 mm.

Saul et al[49),50)] proposed another sliding system for a mass production of Si-doped $Ga_{1-x}Al_xAs$ LPE wafers. Schematic illustrations of their system are shown in Fig.11. The system was designed for simultaneous epitaxial growth on 12 substrates. Functionally, it consisted of alternating movable and sta-

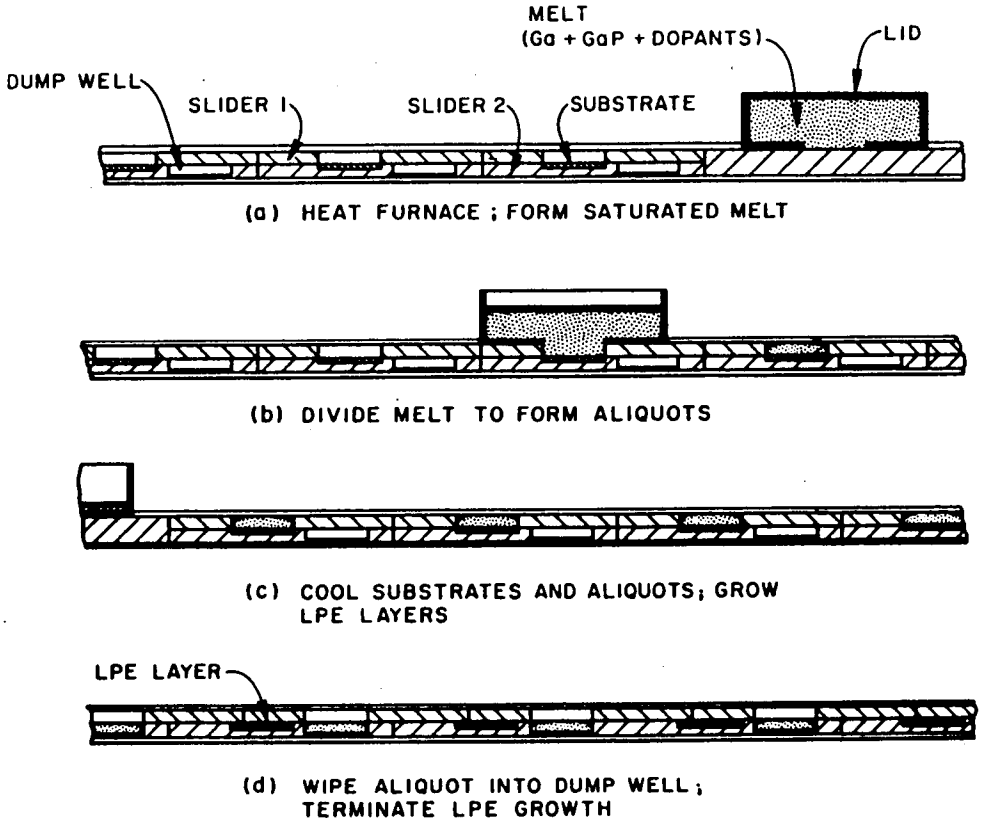

Fig. I-10. Multislices LPE deposition in a double slider aliquot LPE apparatus[48].

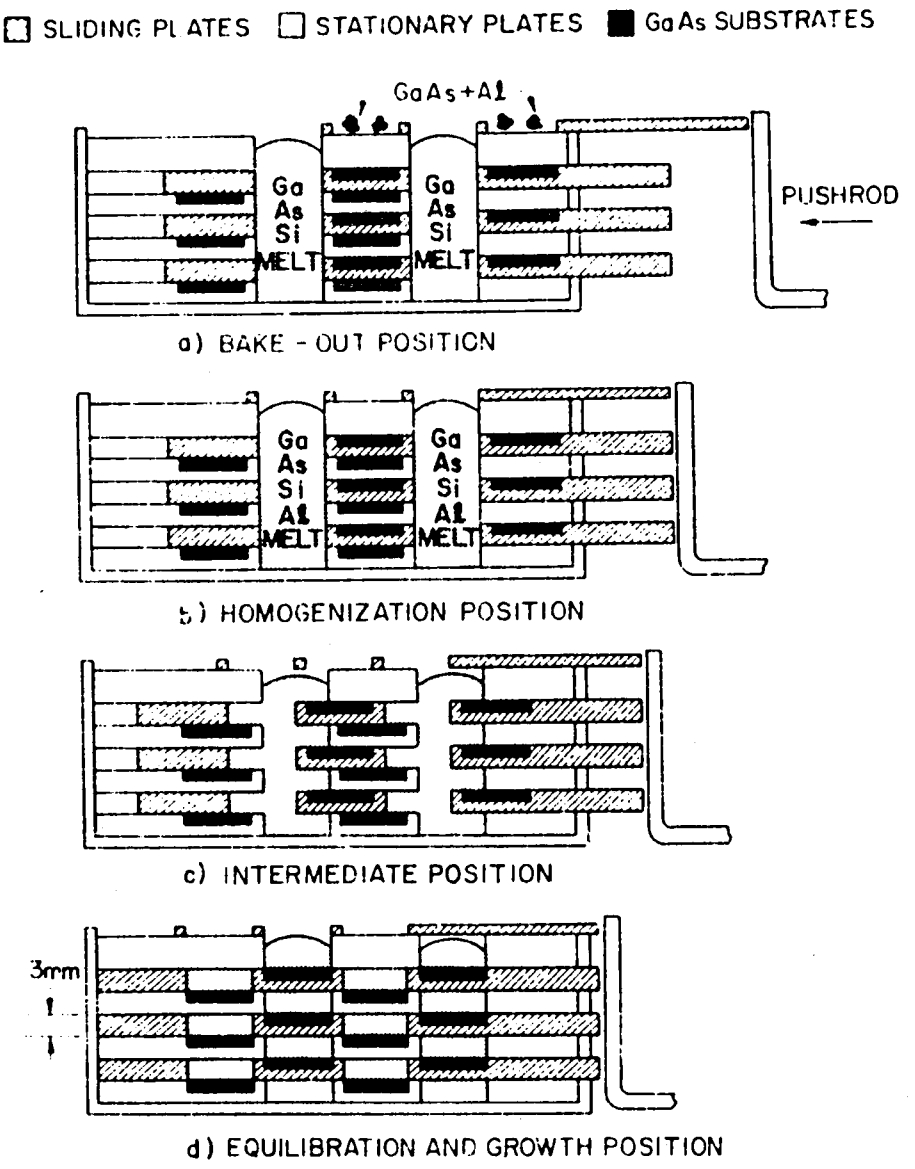

Fig. I-11. Stacked-slider-type fixture for the growth of Si-doped $Ga_{1-x}Al_xAs$ LPE layers[49),50)].

tionary graphite plates, each having machined depressions to accomodate substrates and the holes to form the cavities for the growth solutions. The spacing of depressions and holes permitted the arrangement shown in Fig.11, in which two large cavities exist for the preparation of homogeneous liquid solutions. Each of the substrate wafers was isolated from the melt. In addition, the top plate contained holes for the temporaty storage of both aluminum and the GaAs source material used to bring the melt to a condition of near saturation with arsenic. This plate was subsequently moved to drop these materials into their respective solutions during the growth cycle. From the wafers obtained by this system, they fabricated graded band-gap $Ga_{1-x}Al_xAs$ LEDs having external quantum efficiency as high as 27 %.

The present aspects of LPE growth techniques can be represented by the various kinds of sliding systems and the multiwafers processing systems. The workers in this field take interests in the enlargement of the growth area.. Their intensive efforts will establish a new technology to grow LPE wafers as large as Si wafers in the future.

REFERENCES OF CHAPTER I.

(1) H. Nelson, RCA Rev. 24 (1963).

(2) R. N. Hall, J. Electrochem. Soc. 110 (1963) 385.

(3) C. D. Thurmond, J. Phys. Chem. Solids 26 (1965) 785.

(4) M. Ilegems and G. L. Pearson, Proc. 1968 Symp. on GaAs, Dallas (Inst. Phys. and Phys. Soc. London 1969) 3.

(5) I. Hayashi, M. B. Panish, P. W. Foy and S. Sumski, Appl. Phys. Lett. 17 (1970) 109.

(6) I. Hayashi, M. B. Panish and F. K. Reinhart, J. Appl. Phys. 42 (1971) 1929.

(7) C. A. Burrus and B. I. Miller, Opt. Commun. 4 (1971) 307.

(8) M. Abe, I. Umebu, O. Hasegawa, S. Yamakoshi, T. Yamaoka, T. Kotani, H. Okada and H. Takanashi, IEEE Trans. on Electron Device ED-24 (1977) 990.

(9) M. B. Panish, S. Sumski and I. Hayashi, Met. Trans. 2 (1971) 795.

(10) S. Isozumi, Y. Komatsu, N. Okazaki, S. Koyama and T. Kotani, J. Crystal Growth 41 (1977) 166.

(11) H. Welker, Uber neue Halbleitende Verbindungen, Z. Naturforschg. 7a (1952) 744.

(12) J. V. Dilorenzo, J. Crystal Growth 17 (1972) 189.

(13) H. Miki, Japan J. Appl. Phys. 10 (1971) 509.

(14) M. Hansen, Constitution of Binary Alloys (McGraw-Hill N. Y. 1958) 165.

15) W. G. Pfann, Zone Melting, 2nd Ed. (John Wiley and Sons, N. Y. 1966) 259.

16) W. G. Pfann, J. Metals 203 (1955) 961.

17) J. B. Gunn, Solid State Commun. 1 (1963) 88.

18) J. A. Copeland, IEEE Trans. on Electron Devices ED-14 (1967) 497.

19) S. Christensson, D. W. Woodard and L. F. Eastman, IEEE Trans. on Electron Devices ED-17 (1970) 732.

20) D. P. Brady, S. Knight, K. L. Lawley and M. Uenohara, Proc. 1st Symp. on GaAs (Inst. Phys. Phys. Soc., London 1967) 162.

21) A. G. Foyt and C. M. Wolfe, Proc. 1st Symp. on GaAs (Inst. Phys. Phys. Soc., London 1967) 181.

22) L. R. Dowson and J. M. Whelan, Bull. Am. Phys. Soc. Series 2 13 (1968) 375.

23) R. Solomon, Proc. 2nd Symp. on GaAs (Inst. Phys. Phys. Soc., London 1969) 11.

24) E. W. Williams and D. M. Blacknall, Trans. Met. Soc. AIME 239 (1967) 387.

25) H. Rupprecht, Proc. 1st Symp. on GaAs (Inst. Phys. Phys. Soc., London 1967) 57.

26) K. K. Shih, J. M. Woodall, S. E. Blum and L. M. Foster, J. Appl. Phys. 39 (1968) 2962.

27) S. Mnight, L. R. Dawson, J. V. DoLorenzo and W. A. Johnson, Proc. 3rd Symp. on GaAs (Inst. Phys. Phys. Soc., London 1971) 108.

28) J. M. Woodall, H. Rupprecht and W. Reuter, J. Electrocem. Soc. 116 (1969) 899.

29) R. H. Deitch, J. Crystal Growth 7 (1970) 69.

30) M. B. Panish and S. Sumski, J. Phys. Chem. Solids 30 (1969) 129.

31) M. B. Panish, I. Hayashi and S. Sumski, IEEE J. Quantum. Electronics 5 (1969) 210.

32) J. F. Caldwell and F. E. Rosztoczy, Proc. 4th Int. Symp. on GaAs and Related Compounds, (Inst. of Phys., London 1973) 240.

33) F. E. Rosztoczy, R. E. Goldwasser and T. G. Ruttan, Microwave J. 16 (1973) 51.

34) F. E. Rosztoczy and J. Kinoshita, J. Electrochem. Soc. 121 (1974) 439.

35) F. E. Rosztoczy, J. F. Caldwell, J. Kinoshita and M. Omori, Appl. Phys. Lett. 19 (1973) 525.

36) M. Omori, F. E. Rosztoczy and R. Hayashi, Proc. IEEE 61 (1973) 255.

37) M. Migitaka, Proc. 1971 European Microwave Conf. 1 (1971) 1.

38) H. C. Huang, IEEE Trans, ED-20 (1973) 482.

39) A. Doi, T. Toyabe and M. Migitaka, Proc. 5th Conf. on Solid State Devices, Tokyo in 1973.

40) C. A. Liechti, E. Gowen and J. Cohen, 1972 IEEE Int. Solid State Circuit Conf. THPM 14.2.

41) A. Doi, T. Asano and M. Migitaka, J. Crystal Growth

39 (1977) 353.

(42) H. F. Lockwood and M. Ettemberg., J. Crystal Growth 15 (1972) 81.

(43) R. M. Totemski, J. Electrochem. Soc. 119 (1972) 277.

(44) T. Yamaguchi and T. Niina, Japan J. Appl. Phys. 15 (1975) 1219.

(45) M. Ohshima and Y. Sedine, National Tech. Rep. 22 (1976) 631.

(46) O. G. Lorimor, W. H. Hackett and R. Z. Bachrach, J. Electrochem. Soc. 120 (1973) 1424.

(47) O. G. Lorimor, R. H. Saul, L. R. Dawson and C. R. Paola, Solid State Electronics. 16 (1973) 1289.

(48) A. A. Bergh, R. H. Saul and C. R. Paola, J. Electrochem. Soc. 120 (1973) 1558.

(49) R. H. Saul and O. G. Lorimor, J. Crystal Growth 27 (1974) 183.

(50) L. R. Dawson, J. Appl. Phys., 48 (1977) 2485.

(51) T. Ikoma, OYOBYTSURI 46 (1977) 519.

II. PREPARATION OF $Ga_{1-x}Al_xAs$ LIQUID PHASE EPITAXIAL FILMS

II.1. Introduction

$Ga_{1-x}Al_xAs$ is the most remarkable system in ternary III-V compounds owing to the unique property that both the band-gap and the refractive index continuously change corresponding to the composition with little change of the lattice constant. The lattice constant is well matched with that of GaAs for the entire composition range. In Fig. II-1, the lattice constants of GaAs and AlAs are shown vs. temperature[1]. This figure shows that the lattice constant of AlAs is completely matched with that of GaAs at 900°C and the mismatching ratio is less than 10^{-3} even at room temperature. Owing to such a small lattice mismatching with GaAs, $Ga_{1-x}Al_xAs$ epitaxial layers grown on GaAs substrate do not contain any misfit dislocation usually introduced in other III-V ternary compounds. This leads to the high perfection of the crystal and the facility of growing the epitaxial layers.

In Fig.II.2, the bandgap of this crystal is shown as a function of the composition[2]. The direct gap increases from 1.47 eV of GaAs up to 1.86 eV of $Ga_{0.62}Al_{0.38}As$. This range corresponds to the wavelength region from near infrared to red. Then, applications to photo-lamps emitting the light in this region have been investigated by many workers. Whereas, in the recent years, more attentions have been paid to the near infrared region because it was found advantageous

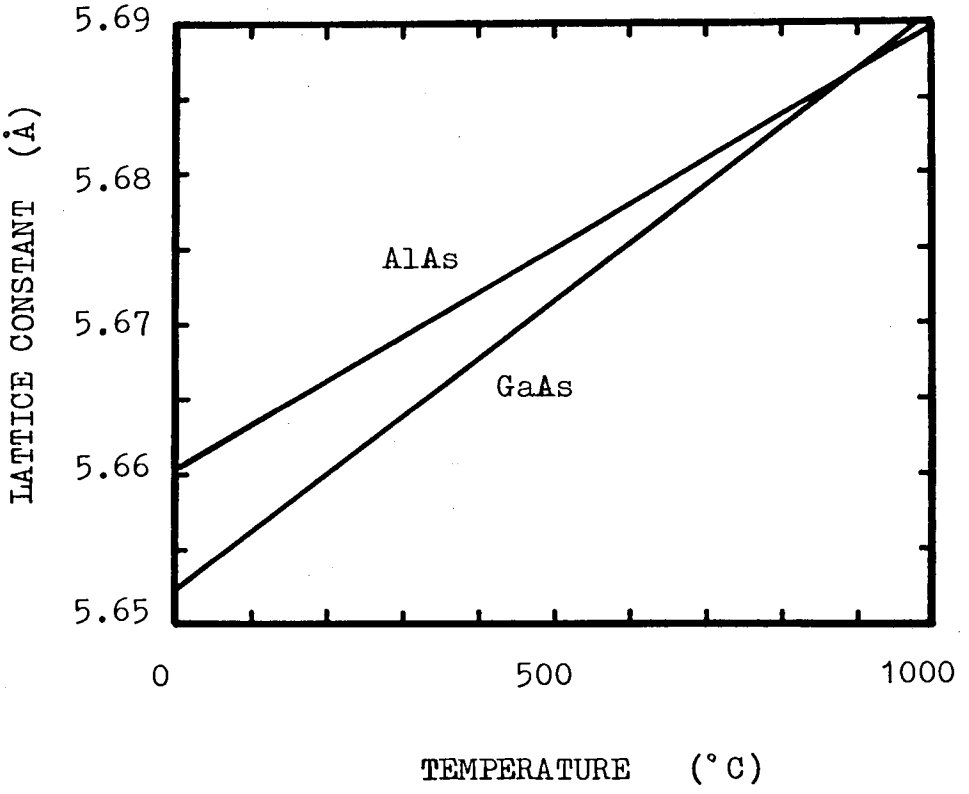

Fig. II-1. Lattice parameters of AlAs and GaAs versus temperature[1].

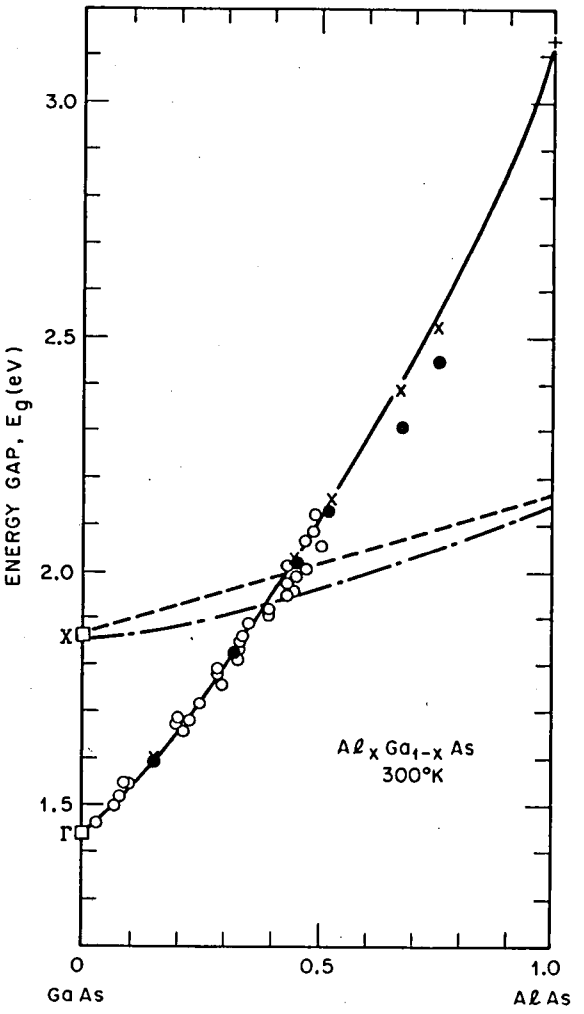

Fig. II-2. Bandgap of $Ga_{1-x}Al_xAs$ against composition[2].

to utilize the light of about 0.8 μm for fiber-optical communication systems. Double heterostructure lasers[3),4)] and high radiance light emitting diodes[5),6)] fabricated from this material have been successfully used as light sources in these systems. These devices effectively utilize the remarkable properties of GaAs-$Ga_{1-x}Al_xAs$ heterojunction for confining the injected carriers or the emitted photons in the active regions.

On the other hand, these devices require the epitaxial layers that their compositions and thicknesses are precisely controlled for high device performances. The epitaxial wafers are also required to contain smooth surfaces for photoprocessings usually adopted for device fabrications. To satisfy these requirements for epitaxial wafers, knowledges about the phase diagram and the LPE growth thechnique of "Sliding Method"[7)] are essential.

In this chapter, the theory of Ga-Al-As ternary phase diagram and the growth experiments of $Ga_{1-x}Al_xAs$ in the early stage of the studies are described. The experimetal results will contribute to both the selection of the thermodynamic data and the extraction of the problems in the growth technique.

II.2. Ga-Al-As Ternary Phase Diagram

A very useful calculational technique for the phase diagrams of III-V systems is one which Vieland[8], following a more general treatment due to Wagner[9], applied to binary compounds. Ilegems[10] and Ilegems and Pearson[11] first extended it to several ternary III-V systems.

In this treatment, the solid solution of a composition $A_{1-x}B_xC$ is treated as a mixture of AC and BC, and each of them are equilibriumed with the corresponding elements in the liquid. That means the chemical potentials (μ) of AC and BC in the solid are equal respectively to the sum of the chemical potemtials of A and C, and B and C in the liquid:

$$\mu_{AC}^{S}(\theta) = \mu_{A}^{L}(\theta) + \mu_{C}^{L}(\theta), \qquad \ldots (II.1)$$

$$\mu_{BC}^{S}(\theta) = \mu_{B}^{L}(\theta) + \mu_{C}^{L}(\theta), \qquad \ldots (II.2)$$

where θ is temperature. The chemical potentials in the liquid are given by the equations of the form:

$$\mu_{A}^{L}(\theta) = \mu_{A}^{OL}(\theta) + R\theta \ln \gamma_A X_A^L , \qquad \ldots (II.3)$$

and in the solid by

$$\mu_{AC}^{S}(\theta) = \mu_{AC}^{OS}(\theta) + R\theta \ln \gamma_{AC}(1-X) . \qquad \ldots (II.4)$$

Here, the superscripts OL and OS represent the pure state of the liquid phase and the solid phase, γ the activity coefficient , R the gas constant, respectively. X_i designates the atomic

fraction of element i in the liquid. X is the mole fraction of BC in the solid. The chemical potential of the pure compound which appears in eq.(II.4) can be related to the chemical potentials of its constituents in the liquid by the following equation given by Vieland[8]:

$$\mu_{AC}^{OS}(\theta) = \mu_A^{sl}(\theta) + \mu_C^{sl}(\theta) - \Delta S_{AC}^F(\theta_{AC}^F - \theta) - \Delta C_p(\theta_{AC}^F - \theta - \theta \ln(\theta_{AC}^F/\theta)) \quad \ldots \text{(II.5)}$$

where ΔS^F is the entropy of fusion of the compound, ΔC_p the difference in specific heat between the compound and its supercooled liquid, θ_{AC}^F the temperature of fusion of the compound, and where the superscript sl refers to the stochiometric liquid.

The activity coefficients of the constituents in the liquid are given by the following equations[11]:

$$R\theta \ln \gamma_A = \Omega_{AC}^L (X_C^L)^2 + \Omega_{AB}^L (X_B^L)^2 + (\Omega_{AC}^L + \Omega_{AB}^L - \Omega_{BC}^L) X_B^L X_C^L \quad \text{(II.6)}$$

$$R\theta \ln \gamma_B = \Omega_{BC}^L (X_C^L)^2 + \Omega_{AB}^L (X_A^L)^2 + (\Omega_{BC}^L + \Omega_{AB}^L - \Omega_{AC}^L) X_A^L X_C^L \quad \text{(II.7)}$$

$$R\theta \ln \gamma_C = \Omega_{AC}^L (X_A^L)^2 + \Omega_{BC}^L (X_B^L)^2 + (\Omega_{AC}^L + \Omega_{BC}^L + \Omega_{AB}^L) X_A^L X_B^L \quad \text{(II.8)}$$

where Ω_{ij}^L is the interaction parameter between the two liquid constituents i and j. For the solid phase,

$$R\theta \ln \gamma_{AC} = \Omega^{S}(1-X)^{2}, \qquad \ldots \text{(II.9)}$$

$$R\theta \ln \gamma_{BC} = \Omega^{S}X^{2}, \qquad \ldots \text{(II.10)}$$

where Ω^{S} is the interaction parameter between AC and BC in the solid.

Substituting eqs.(II.3), (II.4) and (II.5), and the same equations obtained by cyclic permutation of the indices into eqs.(II.1) and (II.2), neglecting the specific heat terms, that:

$$\ln \gamma_{AC}(1-X) = \ln 4X_A^{L}X_C^{L} + \ln(\gamma_A\gamma_C/\gamma_A^{sl}\gamma_C^{sl}) + \Delta S_{AC}^{F}(\theta_{AC}^{F} - \theta)/R\theta, \qquad \ldots \text{(II.11)}$$

$$\ln \gamma_{BC}X = \ln 4X_B^{L}X_C^{L} + \ln(\gamma_B\gamma_C/\gamma_B^{sl}\gamma_C^{sl}) + \Delta S_{BC}^{F}(\theta_{BC}^{F} - \theta)/R\theta, \qquad \ldots \text{(II.12)}$$

The set of eqs.(II.6)-(II.12) gives complete expressions for the phase diagram. In these equations ΔS_{ij}^{F} and θ_{ij}^{F} are constants and Ω's are approximated by constants or simple linear functions of temperature[12),13)]. Since they have no analytical expression, a computer solution must be used for the calculation.

For the calculation of Ga-Al-As phase diagram, there are two sets of the thermodynamic data by Ilegems and Pearson[11)], and Panish and Ilegems[13)] as shown in Table.II-1. In both data, the interaction parameter of the solid is taken equal to zero on the basis of the fact that the lattice mismatch between

		Data-1[11]	Data-2[13]
ΔS^F (cal·mol^{-1}·K^{-1})	GaAs	16.64	16.64
	AlAs	22.8	15.6
θ^F (°C)	GaAs	1238	1238
	AlAs	1740	1770
Ω^L_{i-j} (cal·mol^{-1})	Ga-As	-9.16θ + 5160	-9.16θ + 5160
	Al-As	-9.16θ + 9040	-12θ + 600
	Ga-Al	104	104
Ω^S (cal·mol^{-1})		0	0

Table.II-1. Thermodynamic data of Ga-Al-As system.

GaAs and AlAs is negligibly small. Since the activity coefficient of the solid is equal to 1 when Ω^S is equal to zero, eqs.(II.11) and (II.12) are simplified as follows:

$$1-X = 4X_{Ga}{}^{L}X_{As}{}^{L} \frac{\gamma_{Ga}\gamma_{As}}{\gamma_{Ga}^{sl}\gamma_{As}^{sl}} \exp(\Delta S_{GaAs}{}^{F}(\theta_{GaAs}{}^{F} - \theta)/R\theta), \quad \text{.. (II.13)}$$

$$X = 4X_{Al}{}^{L}X_{As}{}^{L} \frac{\gamma_{Al}\gamma_{As}}{\gamma_{Al}^{sl}\gamma_{As}^{sl}} \exp(\Delta S_{AlAs}{}^{F}(\theta_{AlAs}{}^{F} - \theta)/R\theta), \quad \text{(II.14)}$$

where

$$X_{Ga}{}^{L} + X_{Al}{}^{L} + X_{As}{}^{L} = 1 . \quad \text{.. (II.15)}$$

Using eqs.(II.13) and (II.14), X is easily eliminated and the resultant equation gives the liquidus surface. The solidus line is obtained by substituting the calculated liquidus data into eq.(II.13) or eq.(II.14).

The results of the calculations using the thermodynamic data listed in Table II-1 are shown in Figs.II-3 and II-4. There is little difference between the liquidus isotherm calculated by data-1 and the one calculated by data-2, whereas the solidus isotherms are slightly different one another. It is obvious that data-1 gives a higher X than data-2.

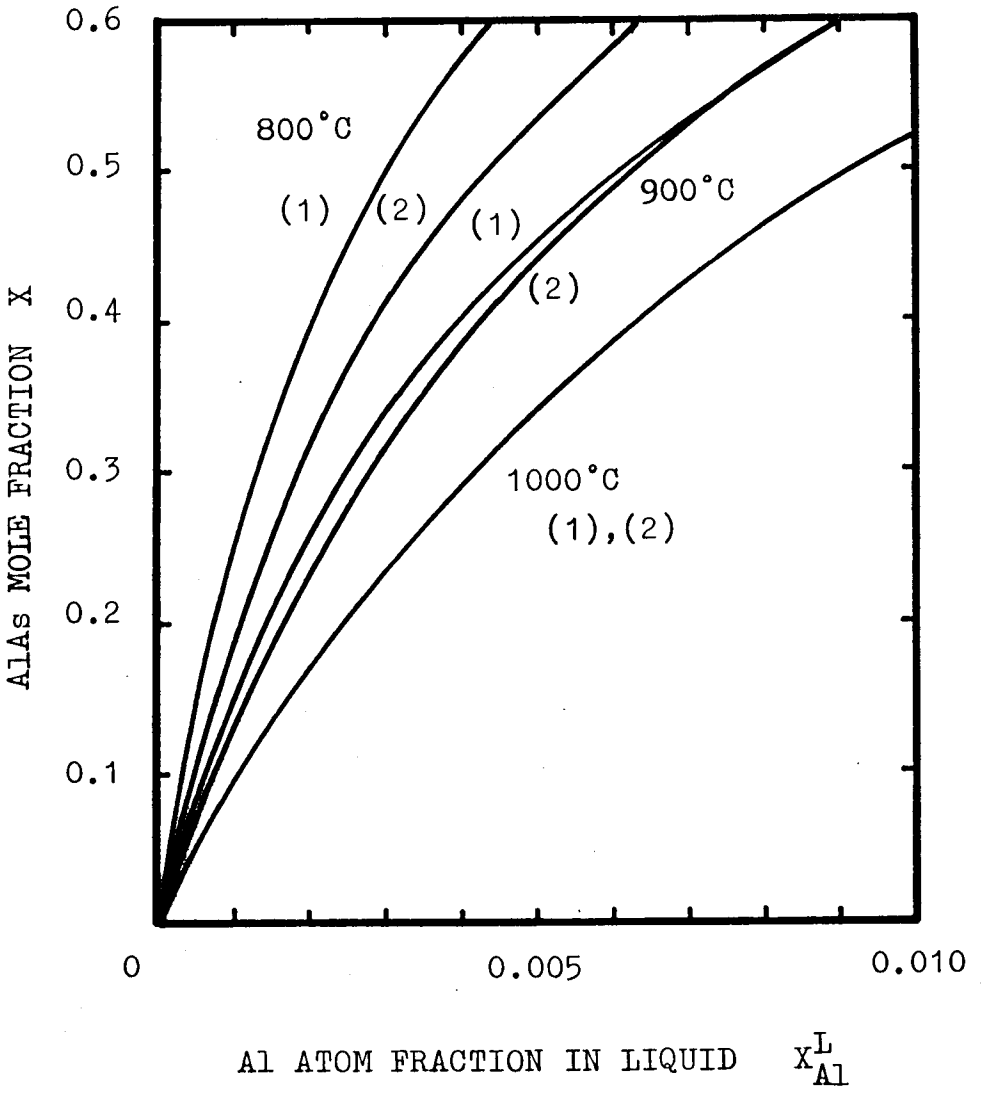

Fig. II-3. Solidus isotherms versus aluminum atomic fraction in liquid. (1): data-1[11], (2): data-2[13].

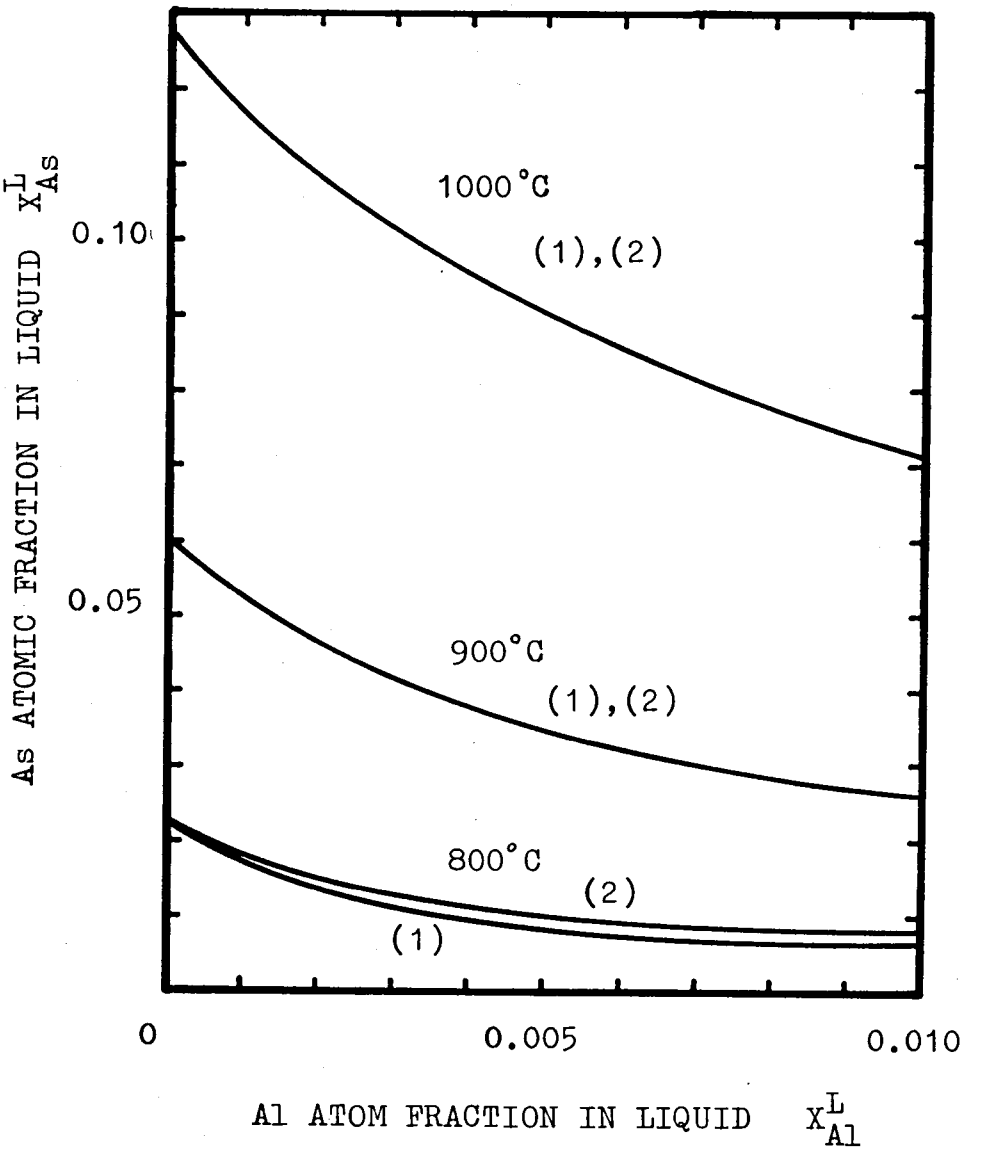

Fig. II-4. Liquidus isotherms versus aluminum atomic fraction in liquid. (1): data-1[11], (2): data-2[13].

II.3. Liquid Phase Epitaxial Growth of $Ga_{1-x}Al_xAs$

The phase diagram described in the previous section is the basis of the studies on $Ga_{1-x}Al_xAs$. It predicts both a saturation condition in the liquid and the composition of the solid deposited from the liquid. Moreover, the analyses described in the following chapters are always based on the the phase diagram. Although the difference between the solidus isotherms calculated by data-1 and data-2, it may become a large difference in the more detailed analyses. Consequently, LPE growth experiments were carried out to examine which set of thermodynamic data gives the accurate results.

The LPE growth apparatus used for the experiments is shown in Fig.II-5. It consisted of a furnace, a silica tube through which a purified H_2 flow was maintained, and a graphite boat. The graphite boat consists of a slider with a container for the solution, and a holder with a set of slots to contain the source and growth seeds. A (100) oriented GaAs doped with tellurium and a slice of undoped poli-GaAs were used for the substrate and the source seed, respectively. At the start of a run, the required components for the solution and a insufficient amount of GaAs for the saturation were placed in the solution container, and the seeds were placed into the slots as illustrated. The apparatus was brought to the starting temperature and maintained there for an hour. Temperature control was to about $\pm$ 0.1°C. Prior to the growth onto the substrate, the melt was placed onto the source seed for 40

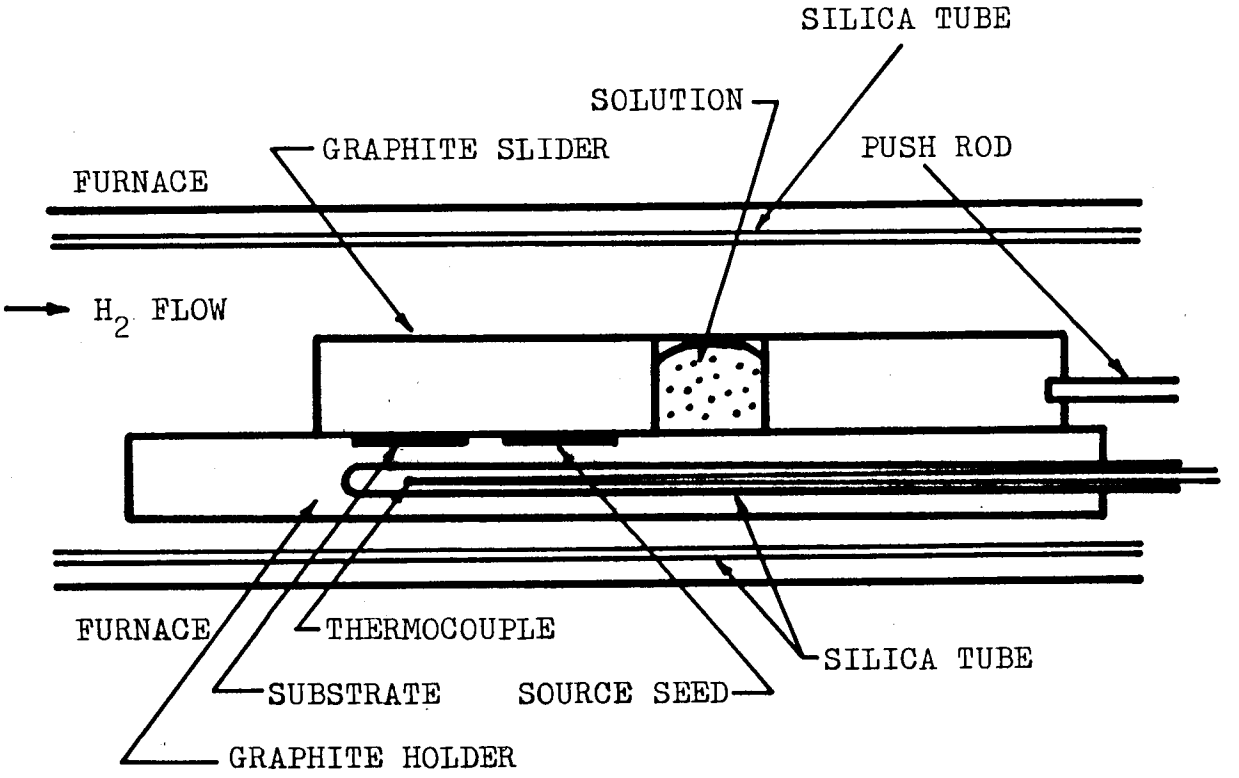

Fig. II-5. Apparatus for growth of LPE layers.

minutes to achieve saturation in the solution. Then, the growth was initiated just at saturation at a cooling rate of 0.2°C/min by sliding the solution from the source seed onto the substrate. The cooling intervals (Δ) were 5°C for thin LPE layers, and 50 - 150°C for thick layers.

The weight loss of the source seed, which was partially dissolved for saturating the solution, was measured after the growth. From the sum of the weight loss and the amount of GaAs initially dissolved in the solution, the liquidus data were obtained. Using the LPE wafers, the solidus data were obtained by two methods. At the surface of the thin LPE layers, photoluminescence spectrums were measured at room temperature by exciting the crystal using a argon ion laser. Then, the photon energy of the edge emission was converted to the solidus composition using the data shown in Fig.II-2. The thick LPE layers were cleaved along the (110) plane, and the quantitative analyses of gallium by electron probe micro analyses (EPMA) were carried out on the cleaved face. The energy of electron beam and the detecting angle of X-ray were respectively 25 KeV and 45°. The intensity ratio of Ga-Kα X-ray at the LPE layer, and at the GaAs substrate was converted to the solidus composition with correcting the effects of the atomic number, the absorption and the fluorerescence[14]. The data for the conversion is shown in Fig.II-6. Finally, the solidus data were obtained from the value of the LPE layer nearest to the substrate.

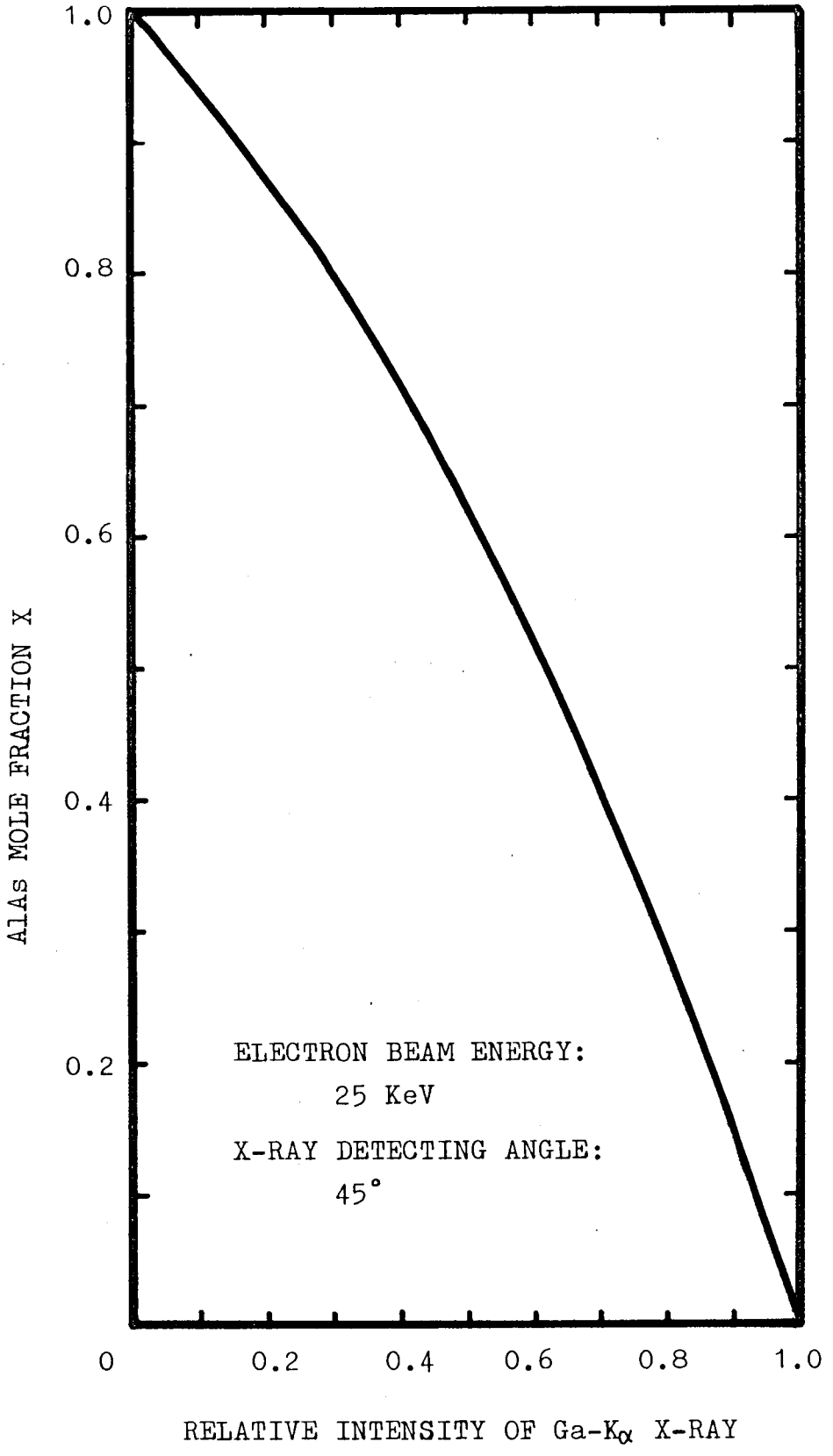

Fig. II-6. Conversion data for quantitative EPMA analyses of $Ga_{1-x}Al_xAs$.

The results of the experimentally obtained solidus data are shown in Fig.II-7 with the calculated lines. In this figure, all the solidus data are plotted without distinguishing each method of the measurements because the difference of the measured values by two methods was proved within $\pm$ 2 %. It is obvious from this figure that the experimental values agree with the theoretical curves calculated from data-2. The data-1 gives much higher values of the solidus composition than the experimental ones.

The liquidus data are shown in Fig.II-8 with the data in the literature[13]. The solid lines show the theoretical values calculated from data-2. The experimental data and the other obviously agree with the theoretical curves.

This series of LPE growth experiments revealed the facts that the LPE layers obtained by this growth apparatus were generally poor, and that the solidus composition considerably distributed in the thick LPE layers. In Fig.II-9, a photograph of a typical surface of as-grown wafer is shown. The surface is seen to be irregular by the dispersed white spots or the projections like hillocks. Besides, in the growth of thick LPE layers, the solution removal after the growth could not be sometimes accomplished. In such a case, the melt had been in contact with the substrate for the whole cooling cycle down to room temperature, and the irregularity of the resultant LPE layer was more emphasized. In Fig.II-10, one of the reuslts of EPMA measurements for the thick LPE layers is shown.

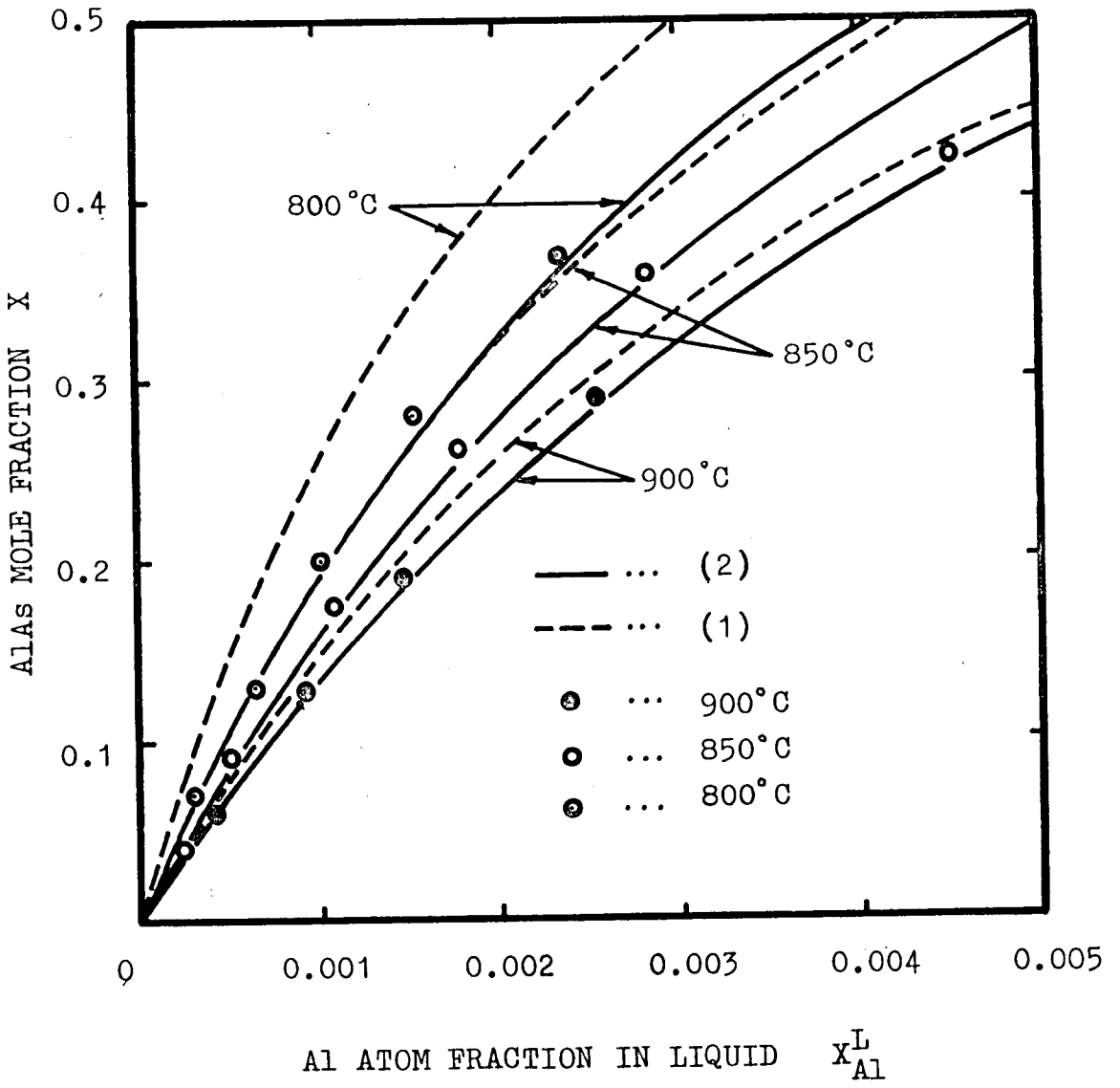

Fig. II-7. Solidus isotherms versus aluminum atomic fraction in liquid. (1): data-1[11], (2): data-2[13].

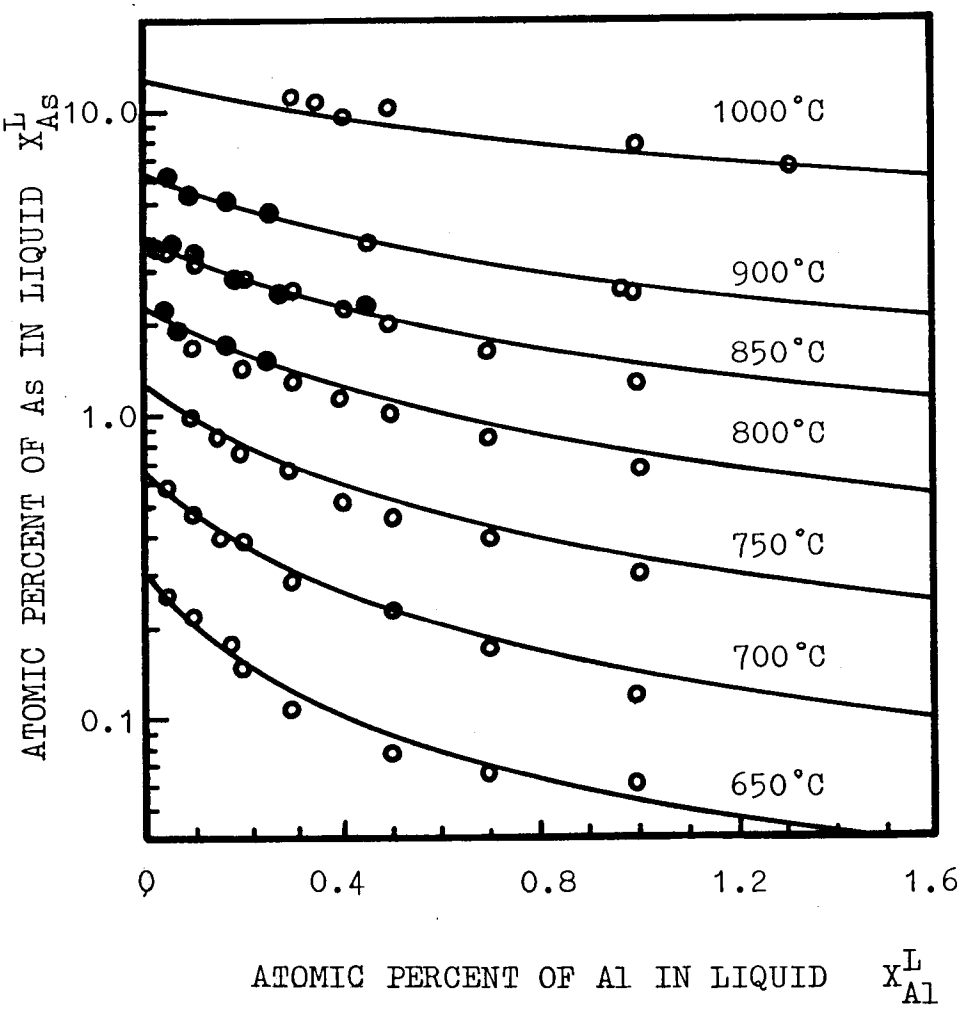

Fig. II-8. Liquidus isotherms versus aluminum atomic percent in liquid. O: Panish and Ilegems[13], ● : This work.

Fig. II-9. A photograph of the typical surface of $Ga_{1-x}Al_xAs$ LPE wafer grown by the apparatus shown in Fig.II-5.

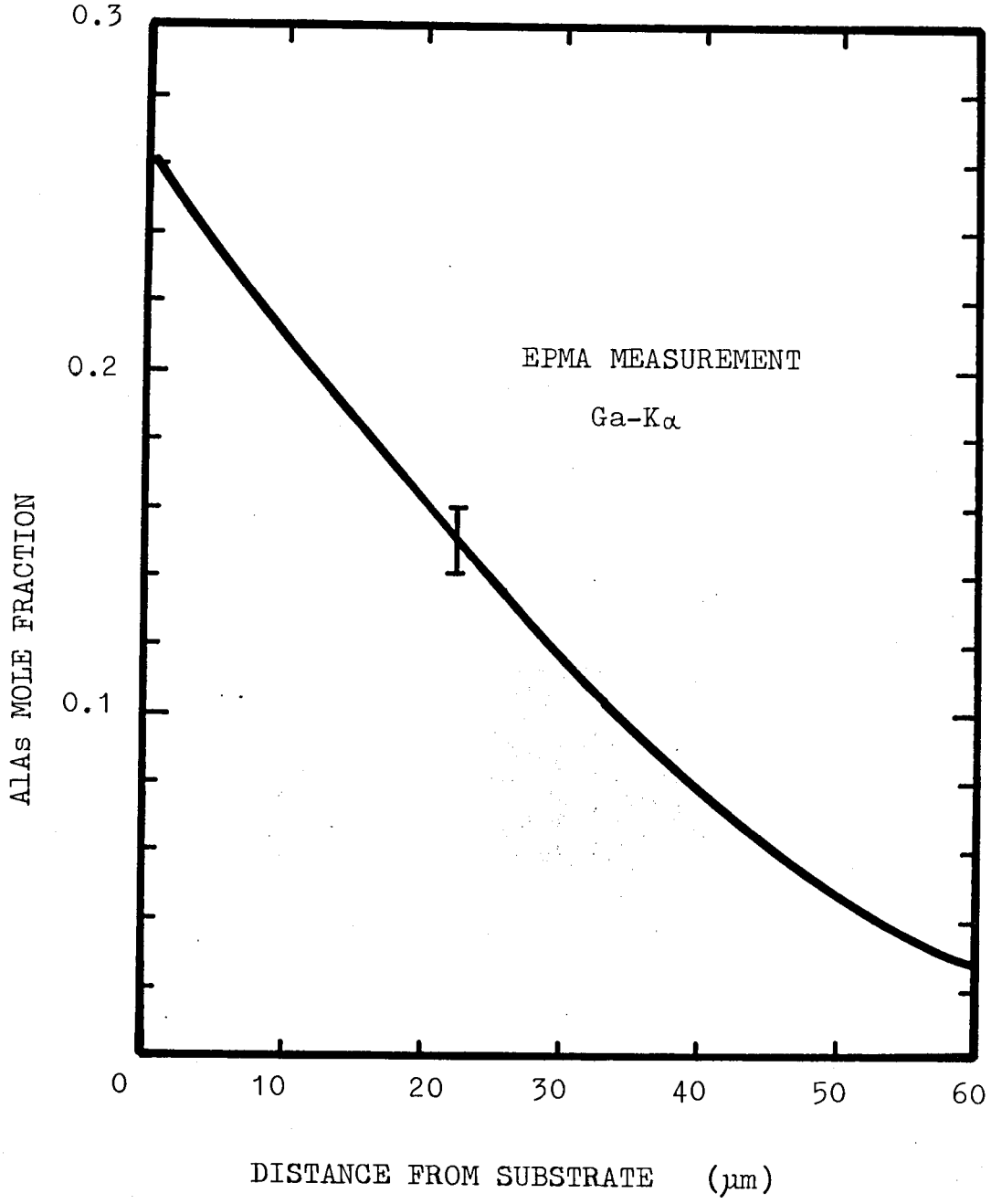

Fig. II-10. Composition distribution in $Ga_{1-x}Al_xAs$ LPE layer.

The LPE layer in this figure was grown from 900°C to 800°C. During this growth cycle, X decreased from 0.26 to 0.03. The soldus line in the phase diagram only predicts the solidus composition at the start of the growth (i.e. X = 0.26 at 900 °C). This problem leads to the difficulty of predicting the actual composition in the LPE layers.

II.4. Discussion.

In section II.2, the theory of the phase diagram of ternary III-V systems has been described. The theory is based on the quasi-regular solution model providing that the interaction parameters are linear functions of temperature. Although a more detailed model has been proposed, it has been proved that there is no difference in the accuracy of the calculated results[15].

From the comparison between the calculated values and the experimental ones, the thermodynamic data by Panish and Ilegems [13] have been found to give the more accurate phase diagram of Ga-Al-As system than the data by Ilegems and Pearson[11]. In the latter data, the interaction parameter between aluminum and arsenic is thought to be overestimated. The accuracy of the phase diagram by Panish and Ilegems is remarkable over a wide temperature range, whereas it should be noticed that such a remarkable accuracy cannot be expected in the calculated phase diagrams of other III-V ternary systems except for Ga-Al-P system.[16] The accuracy in Ga-Al-As system is maily attributed to the facts that the solid in this system can be treated as an ideal solid solution, and that the interaction parameters in the liquid are well approximated by simple linear functions of temperature over a wide temperature range.

In this series of the growth experiments, the obtained LPE layers were found to be very poor. This problem was caused mainly by high activity of aluminum in the liquid.

In the early papers reported on the preparation of $Ga_{1-x}Al_xAs$ by LPE growth method, such difficulties were always emphasized. Panish et al.[17] reported that the tipping technique developed by Nelson[18] for GaAs could not be used, particularly for solutions containing appreciable amounts of aluminum, because of the formation of an Al_2O_3 scum on the liquid surface. Rupprecht et al.[19] also reported that, even in an ultrapure hydrogen ambient, a stable oxide scum was formed on the solution surface. They thought the scum was formed by the reaction of aluminum in the liquid with the gas released from the graphite cell during the heating cycle, and the presence of such a stable oxide scum on the solution surface resulted in the deterioration of the wetting between the substrate and the solution. The white spots seen in Fig.II-9 also corresponds with such scums adhering to the surface of the substrate at the start of the growth.

Since the LPE wafers for opto-electronic devices are required to contain smooth surfaces, the ploblems caused by scums must be overcomed. Woodall et al[20] developed a dipping system as shown in Fig.II-11 for this purpose. In their system, the wetting between the substrate and the liquid was greatly improved because the substrate was inserted through the oxide scum at the surface of the solution into the liquid. Panish et al.[17] developed a modified tipping system shown in Fig.I-6. In this system, the solution was held stationary in a recess in the bottom of a graphite boat. The substrate

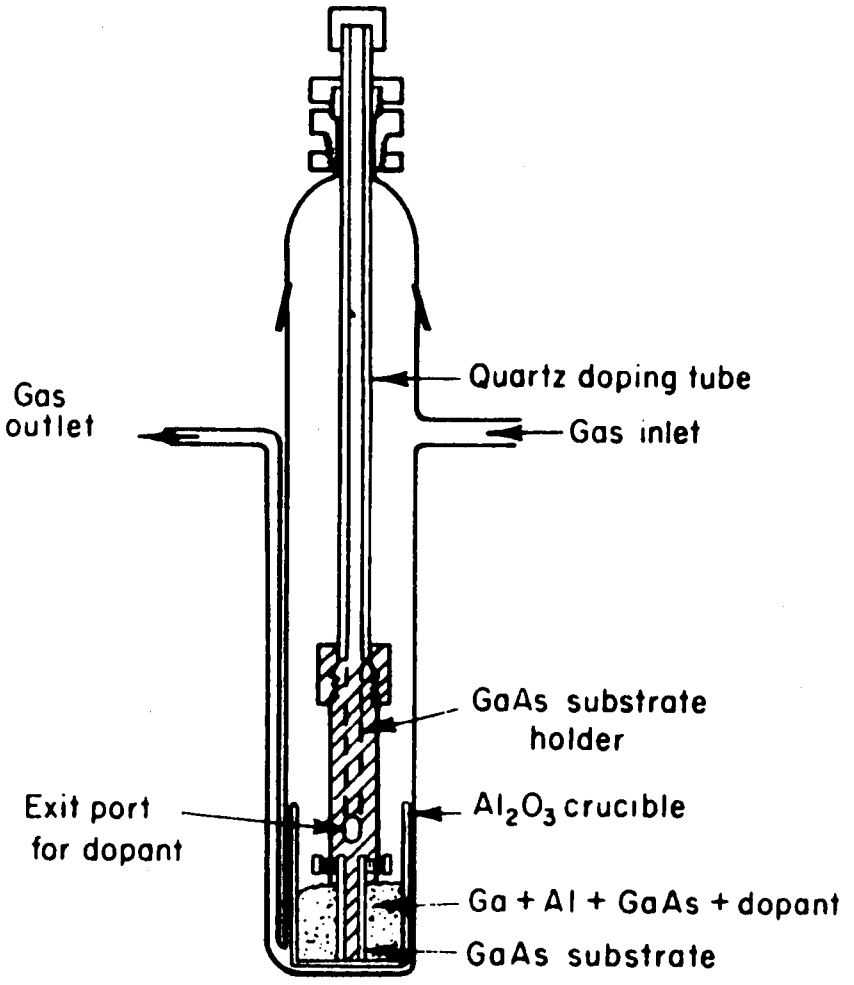

Fig. II-11. LPE growth apparatus for $Ga_{1-x}Al_xAs$ by Woodall et al.[20)]

was carried by moving the slider which simultaneously wiped away the oxide scum from the surface of the solution and deposits the substrate on a clean solution. Blum et al.[21] developed a modified sliding system shown in Fig.II-12. In this figure, it can be seen that the GaAs substrate is held within the graphite holder. A piece of polycrystalline GaAs is held stationary at the other end of the holder. The melt which contains gallium, aluminum, and the neccessary dopant is laid above the source material inside the sliding graphite top plate 2 and held flat under pressure due to the graphite top plate 1. The upper top plate 1 has covered compartments in it so that specific additions of dopants such as tellurium or zinc can be made, or the addition of aluminum-gallium alloy to the melt during growth and adjustment of the bandgap can be made. The most important advantage is that the solution is always in contact with the source material. This contact prevents the bottom surface of the solution from oxidation. Then, the resultant LPE layer, they reported, was enough smooth and any effect of the oxidation of the solution was not observed.

In these methods described above, the key to the overall improvement of the growth apparatus will exist. However, it should be noticed that these methods cannot be directly applied to the multi-layers growth. For the growth of multilayers, a sliding system as shown in Fig.I-7 is essential. Whereas, in this system, bottom surfaces of the solutions are in

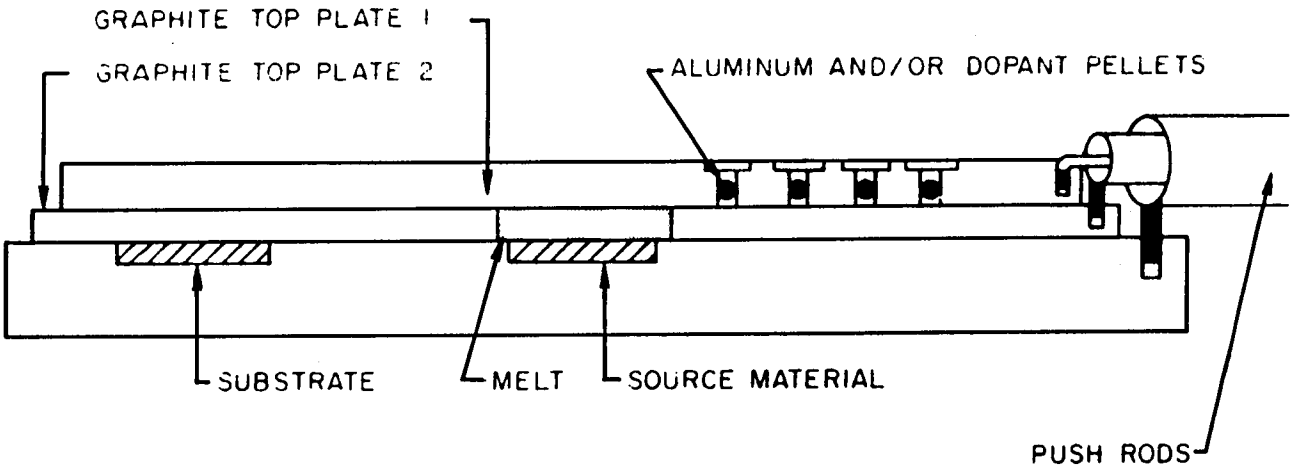

Fig. II-12. LPE growth apparatus for $Ga_{1-x}Al_xAs$ by Blum and Shih[21].

contact with the graphite before the growth. Then, the reaction of aluminum in the liquid with the gas released from the graphite will occur. This situation has been already verified by the experiments using a similar boat shown in Fig.II-5.

The solidus composition in the thick LPE layer has been found to distribute as shown in Fig.II-10. The AlAs mole fraction X decreases far from the initial composition predicted by the phase diagram as the growth proceeds. Whereas, the active layer of the devices is usually formed near the surface of the epitaxial layer. Consequently, not only the phase diagram but an analytical technique for the prediction of the solidus composition change are essential for the growth of thick LPE layers.

II.5. Conclusions.

The theory of the phase diagram of ternary III-V systems was described. The theory is based on the quasi-regular solution model providing that the interaction parameters are linear functions of temperature. Using the thermodynamic data in literatures[11),13)], Ga-Al-As ternary phase diagrams were calculated based on this model.

From the comparison between the calculated values and the experimental ones, the thermodynamic data by Panish and Ilegems [13)] was found to give the more accurate phase diagram of Ga-Al-As than the data by Ilegems and Pearson[11)].

A conventional sliding method used in the growth experiments was found disadvantageous for the growth of $Ga_{1-x}Al_xAs$. The irregularity of the obtained LPE layers was caused by the Al_2O_3 scum which was formed by the reaction of aluminum in the liquid with the gas released from the graphite cell during the heating cycle. Then, the key to to the averall improvement of the growth apparatus was discussed by reviewing the other methods in literatures.

It was found that the solidus composition considerably distributed in the thick LPE layer. The AlAs mole fraction decreased far from the initial composition predicted by the phase diagram as the growth proceeded. Then, an analytical technique for the prediction of the solidus composition change is essential for the growth of thick LPE layers.

REFERENCES OF CHAPTER II.

(1) M. Ettenberg and R. J. Paff, J. Appl. Phys. 41 (1970) 3926.

(2) M. B. Panish, J. Appl. Phys. 44 (1973) 2667.

(3) I. Hayashi, M. B. Panish, P. W. Foy and S. Sumski, Appl. Phys. Lett. 17 (1970) 109.

(4) I. Hayashi, M. B. Panish and F. K. Reinhart, J. Appl. Phys. 42 (1971) 1929.

(5) C. A. Burrus and B. I. Miller, Opt. Commun. 4 (1971) 307.

(6) M. Abe, I. Umebu, O. Hasegawa, S. Yamakoshi, T. Yamaoka, T. Kotani, H. Okada and H. Takanashi, IEEE Trans. on Electron Device ED-24 (1977) 990.

(7) M. B. Panish, S. Sumski and I. Hayashi, Met. Trans. 2 (1971) 795.

(8) L. J. Vieland, Acta Met. 11 (1963) 137.

(9) C. Wagner, Acta Met. 6 (1958) 309.

(10) M. Ilegems, Ph. D. Thesis, Stanford Univ., Calif. (1970).

(11) M. Ilegems and G. L. Pearson, Proc. 1968 Symp. on GaAs, Dallas (Inst. Phys. and Phys. Soc. London 1969) 3.

(12) M. B. Panish, J. Crystal Growth 27 (1974) 6.

(13) M. B. Panish and M. Ilegems, Progress in Solid State Physics Vol.7 (Pergamon, New York. 1972) pp.39-83.

(14) Toyota Central Res. and Dev. Labs., "Diagrams and Tables for Quantitative Electron Probe Microanalysis." (Tokyo, 1970).

(15) K. Osamura, J. Inoue and Y. Murakami, J. Electrochem. Soc. 119 (1972) 103.

(16) M. Ilegems and M. B. Panish, J. Crystal Growth 20 (1973) 77.

(17) M. B. Panish and S. Sumski, J. Phys. Chem. Solid 30 (1969) 129.

(18) H. Nelson, RCA Rev. 24 (1963) 603.

(19) H. Rupprecht, J. M. Woodall and G. D. Pettit, Appl. Phys. Lett. 11 (1967) 81.

(20) J. M. Woodall, H. Rupprecht and W. Reuter, J. Electrochem. Soc. 116 (1969) 899.

(21) J. M. Blum and K. K. Shih, Proc. IEEE 59 (1971) 1498.

III. COMPOSITION CHANGE DURING EPITAXIAL GROWTH OF TERNARY COMPOUNDS.

III.1. Introduction.

In the LPE growth of binary compounds, such as GaAs, there is no difficulty in the control of the composition because the deposited solid always maintains the stoichiometry. On the other hand, the composition of LPE $Ga_{1-x}Al_xAs$ is a function of both temperature and the liquidus composition. In a case of the LPE growth of a relatively thin layer, Ga-Al-As ternary phase diagram[1),2)] gives complete data for the composition control. However, the solidus composition changes during the growth cycle of thick layers as is described in the previous chapter. Woodall et al.[3)] pointed out that the aluminum concentration decreased with distance away from the substrate and that the composition gradient decreased with increasing aluminum concentration. They explained this behavior in terms of the behavior of the distribution coefficient of aluminum, k_{Al}. It was found that k_{Al} was always greater than one and it decreased with increasing aluminum concentration. When k_{Al} is greater than one, the consumption of aluminum atoms into the solid substantially causes a rapid decrease of aluminum concentration in the liquid. The higher k_{Al}, the more melt is depleted of aluminum for each incremental volume element frozen, and therefore the steeper the profile.

Ilegems[4] first carried out detailed analyses on this problem by numerical calculations. His calculation was based on a assumption that the solution was entirely equilibrated with the solid. In such a case, deposition onto a substrate results in the solution losing nutrients in correspondence with the composition of the ternary solid formed. After an incremental deposition, the solution is assumed uniform throughout with a new composition calculated by substracting the amount of each component deposited from the amount of each that was previously in the solution. He followed this procedure only by the numerical calculations.

In this chapter, the theory of the composition change[5),6)] is described. An theoretical expression about the decreasing rate of each nutrient is derived, and the calculated results using this expression are compared with the experimental ones.

III.2. Calculation of The Deposition Path over The Liquidus Surface in Ga-Al-As system.

In the growth of a ternary compound expressed as $A_{1-x}B_xC$, total numbers of C atoms and B atoms in the solution (m_C^L and m_B^L) are related to the total numbers of atoms in the solution (M^L) thus:

$$m_C^L = X_C^L M^L , \qquad \ldots (III.1)$$

$$m_B^L = X_B^L M^L , \qquad \ldots (III.2)$$

where X_C^L and X_B^L are the atomic fractions of C and B in the solution, respectively. The values of the changing rate of M^L multiplied by the solidus concentrations of C and B are equal to the changing rate of m_C^L and m_B^L, respectively:

$$dm_C^L/d\theta = X_C^S \, dM^L/d\theta , \qquad \ldots (III.3)$$

$$dm_B^L/d\theta = \frac{X}{2} \, dM^L/d\theta , \qquad \ldots (III.4)$$

where X_C^S is the atomic fraction of C in the solid. Differentiation of eqs.(III.1) and (III.2) with respect to temperature gives the following equations:

$$\frac{dm_C^L}{d\theta} = \frac{dX_C^L}{d\theta} M^L + X_C^L \frac{dM^L}{d\theta} , \qquad \ldots (III.5)$$

$$\frac{dm_B^L}{d\theta} = \frac{dX_B^L}{d\theta} M^L + X_B^L \frac{dM^L}{d\theta} . \qquad \ldots (III.6)$$

From eqs.(III.3) and (III.5),

$$(X_C^S - X_C^L)\frac{dM^L}{d\theta} = \frac{dX_C^L}{d\theta} M^L \ , \qquad \ldots \text{(III.7)}$$

and from eqs.(III.4) and (III.6),

$$(\frac{X}{2} - X_B^L)\frac{dM^L}{d\theta} = \frac{dX_B^L}{d\theta} M^L \ , \qquad \ldots \text{(III.8)}$$

are obtained. Using eqs. (III.7) and (III.8), $dM^L/d\theta$ and M^L are eliminated, and the following relation is obtained:

$$\frac{X_C^S - X_C^L}{dX_C^L/d\theta} = \frac{X/2 - X_B^L}{dX_B^L/d\theta} \ . \qquad \ldots \text{(III.9)}$$

This equation gives the relationship between the changing rate of the solutes (B and C) and the compositions of the solid and the liquid.

In Ga-Al-As system, A, B, and C correspond to Ga, Al, and As, respectively. A small drop of temperature ($\delta\theta$) results in the small decreases of arsenic and aluminum (δX_{As}^L and δX_{Al}^L) in the solution. This relation is expressed as follows from eq.(III.9):

$$\frac{X_{As}^S - X_{As}^L}{\delta X_{As}^L} = \frac{X/2 - X_{Al}^L}{\delta X_{Al}^L} \ . \qquad \ldots \text{(III.10)}$$

From eq.(III.10) and the phase diagram, δX_{Al}^L was calculated for a given δX_{As}^L at the temperature of θ_0. After the calculation of δX_{Al}^L, the new equilibrium temperature ($\theta - \delta\theta$) and the new solidus composition which corresponds to the new liquidus compositions of $X_{As}^L - \delta X_{As}^L$ and $X_{Al}^L - \delta X_{Al}^L$ were calculated from the phase diagram. In this procedure, the

value of $\delta X_{As}^{L}/X_{As}^{L}$ should be chosen as an enough small value for the accurate calculation. In this case, it was taken equal to 1×10^{-3} and the corresponding $\delta\theta$ was less than 0.5°C. It was also veryfied that a further reduction of $\delta X_{As}^{L}/X_{As}^{L}$ had no effect on the accuracy of the culculation. The procedure described above repeated until the entire cooling cycle was finished. The calculated results are shown in Figs.III-1 - III.3.

The LPE layer thickness (T) deposited during the cooling cycle was also calculated as follows. The amount of arsenic atoms in the solid deposited from the liquid corresponding to a temperature drop $\delta\theta$ is equal to the amount of losed arsenic atoms in the liquid. Then, the following equation is given:

$$\delta T \cdot S \cdot C_{As}^{S} = \delta X_{As}^{L} \cdot M \ , \qquad .. \ (III.11)$$

where δT, S, and C_{As}^{S} are respectively the LPE layer thickness deposited during a temperature drop of $\delta\theta$, the growth area, and the arsenic atom density in the solid. From eq.(III.11),

$$\delta T = (\delta X_{As}^{L} \ M)/(S \ C_{As}^{S}) \ , \qquad .. \ (III.12)$$

is obtained. The total LPE layer thickness deposited during the entire cooling cycle was obtained by summing up δT corresponding to the each calculation step of the deposition path. The calculated LPE layer thicknesses corresponding to Fig.III-1 - III-3 are shown in Fig.III-4 in a case that the amount of gallium for the solution is 1 gr/cm^2.

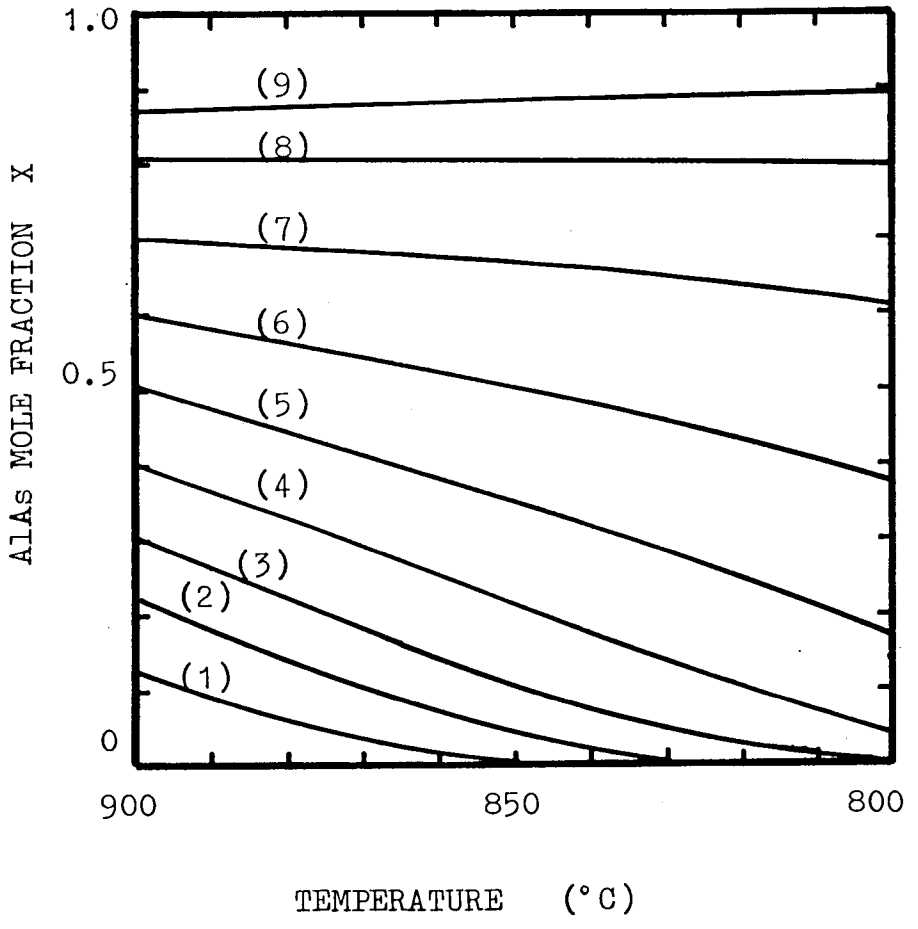

Fig. III-1. Changes of AlAs mole fraction in solids during the growth from 900°C to 800°C. Each curve in this figure corresponds to the curve denoted by the same number in Figs. III-2 - III-5.

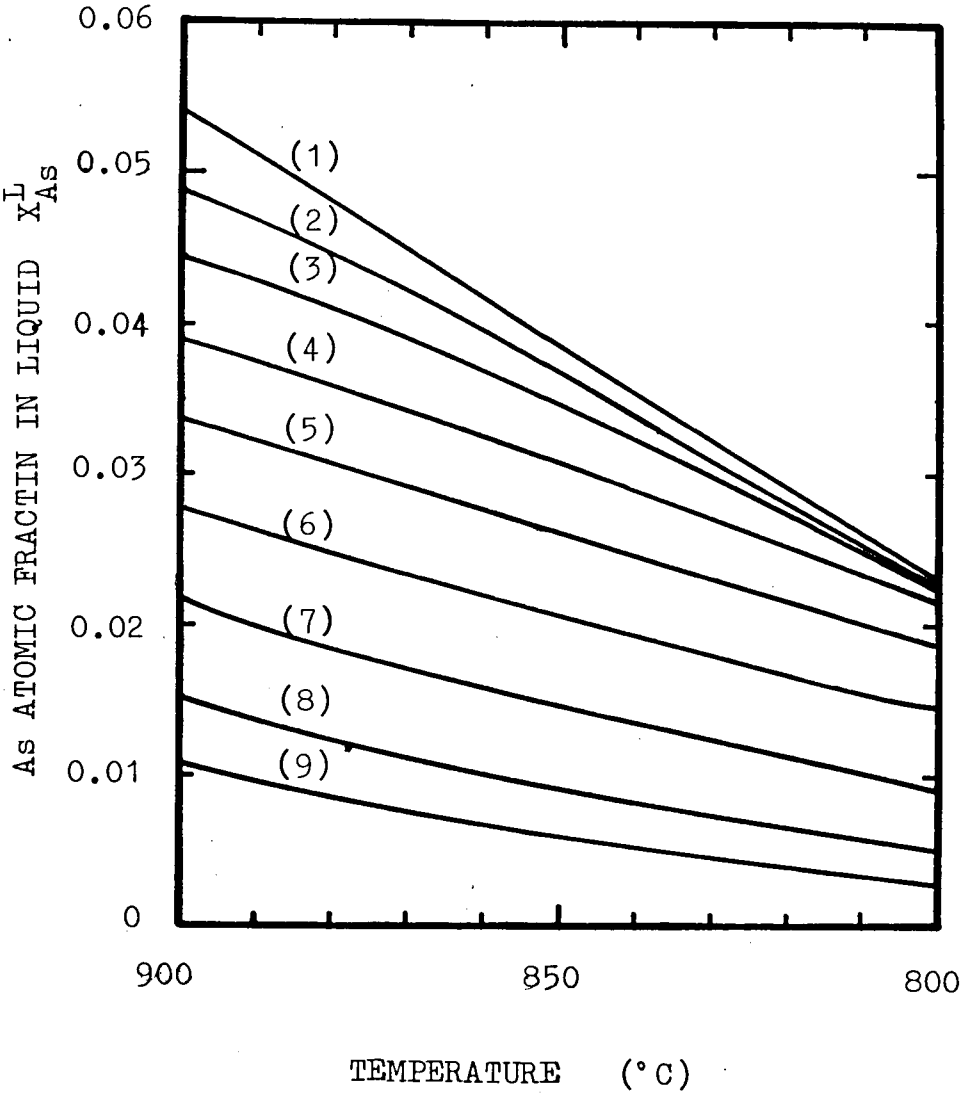

Fig. III-2. Changes of As atom fraction in liquids during the growth from 900°C to 800°C.

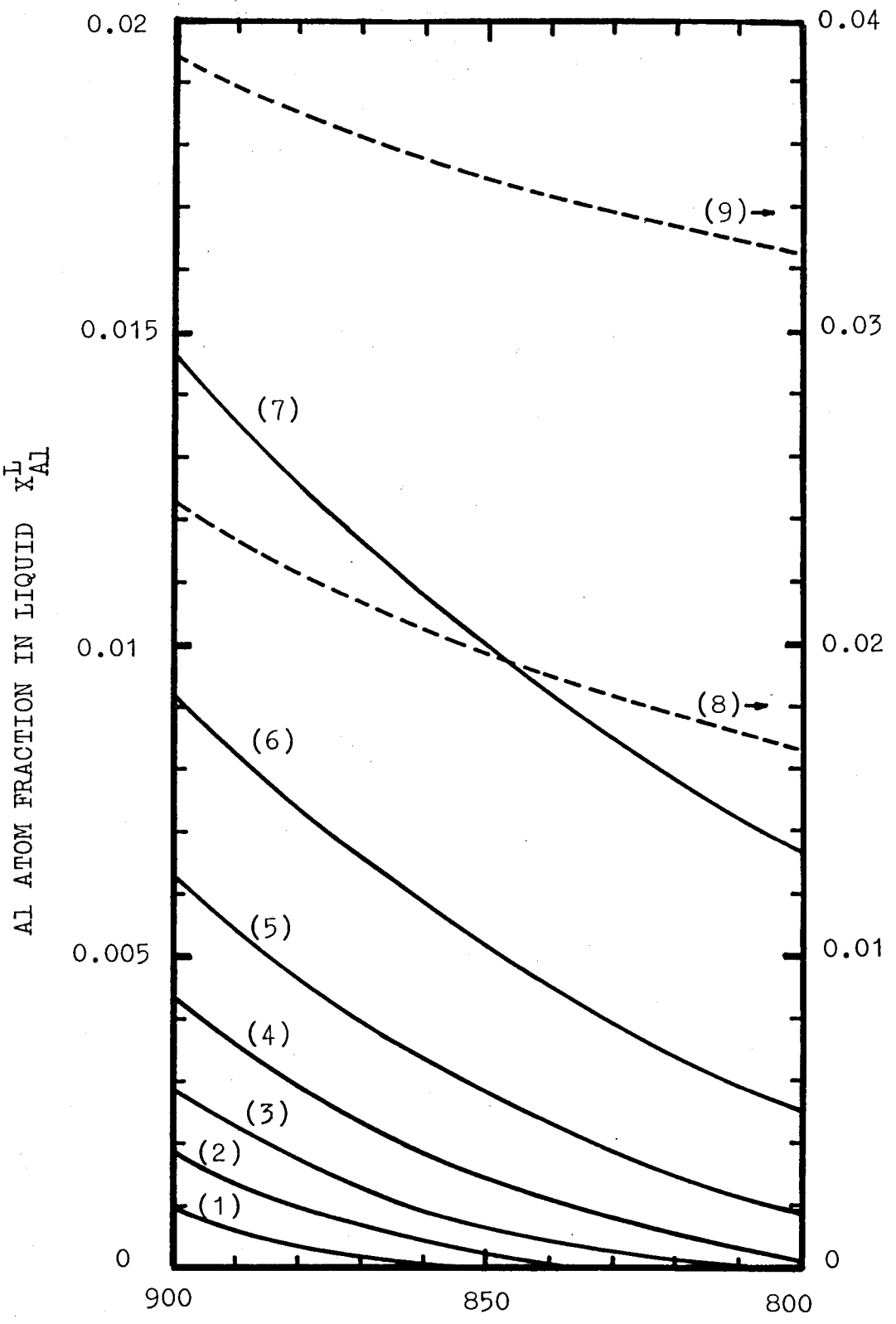

Fig. III-3. Changes of Al atom fraction in liquid during the growth from 900°C to 800°C.

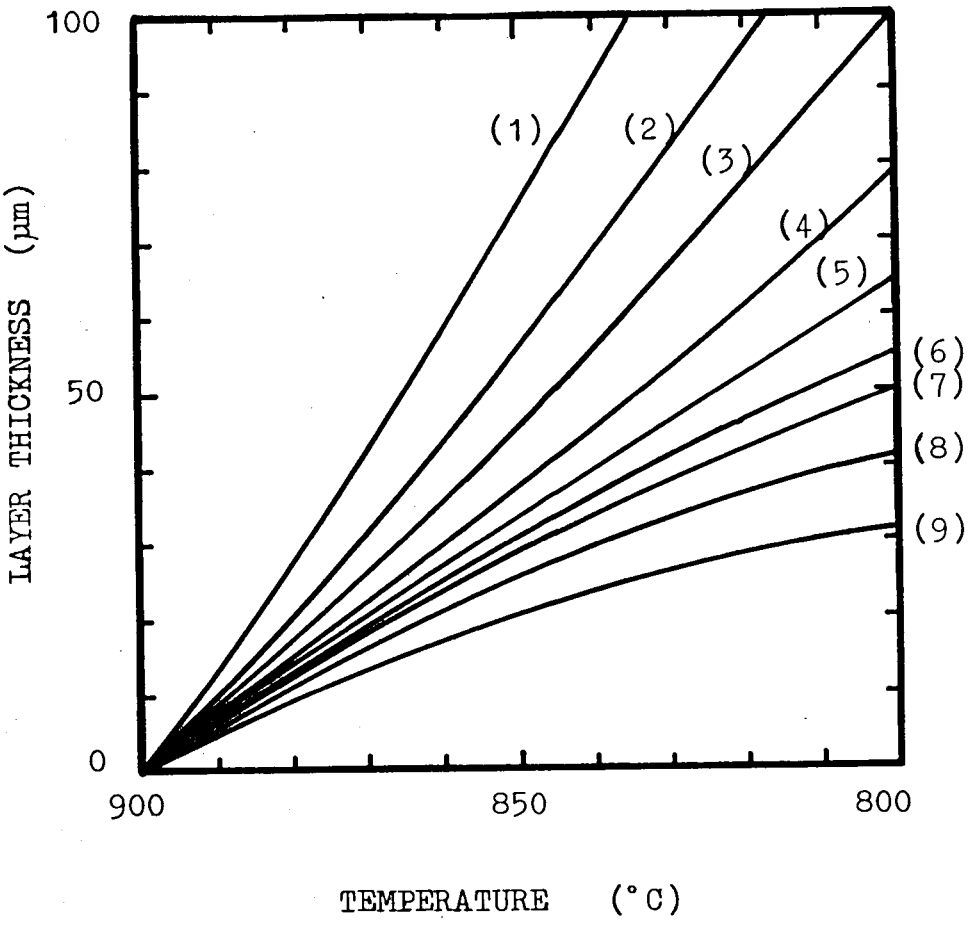

Fig. III-4. Thicknesses of the LPE layers during the growth from 900°C to 800°C.

III.3. Discussion.

The calculated solidus composition in Fig.III-1 shows decreasing tendency in the region $X < 0.8$. It is mainly caused by the high distribution coefficient of aluminum and the resultant depletion of aluminum in the solution. Whereas, X scarecely changes during the cooling cycle at $X \simeq 0.8$, and increases at $X > 0.8$. This complicated behavior of the soldification curve is explained as a result of the complex caused by aluminum depletion in the solution and the dependence of aluminum distribution coefficient on temperature. In Fig.III-5, the variation curves of aluminum distribution coefficients (k_{Al}) corresponding to Fig.III-1 -III-4 are shown. This figure shows the increasing tendency of k_{Al} with respect to θ. The increase of k_{Al} is balanced with the decrease of aluminum concentration in the solution at $X = 0.8$. This balance is broken in other regions, and that leads to the increasing solidification curves at $X > 0.8$, and the decreasing ones at $X < 0.8$.

In Fig.III-6, a calculated result is compared with experimental ones. The growth apparatus described in section II.3 was used for the experiments. The LPE layers were grown from 950°C ($X = 0.5$) to the temperatures plotted in this figure. The LPE layer thickness of each wafer was measured at the cleaved (110) face, and the composition at the surface was measured by EPMA or photoluminescence spectrums. The cooling rate and the amount of gallium for a solution were 0.1°C/min

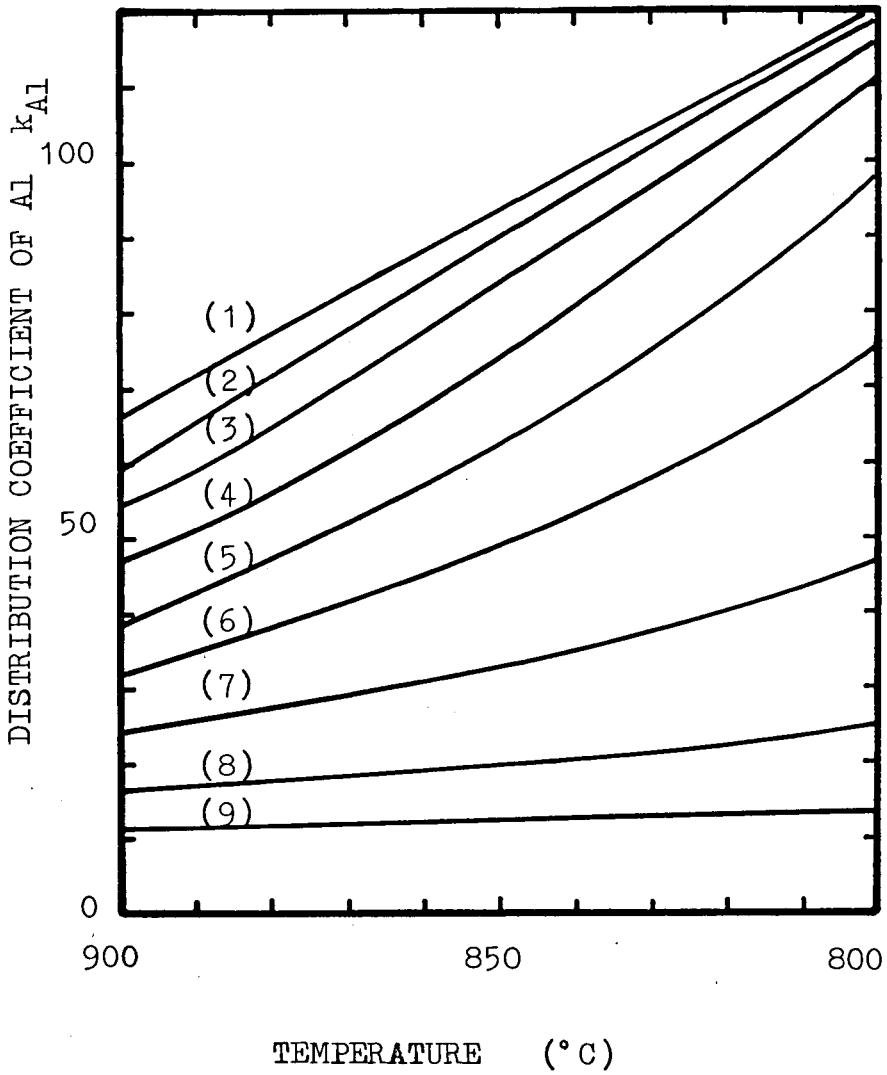

Fig. III-5. Changes of Al distribution coefficients during the growth from 900°C to 800°C.

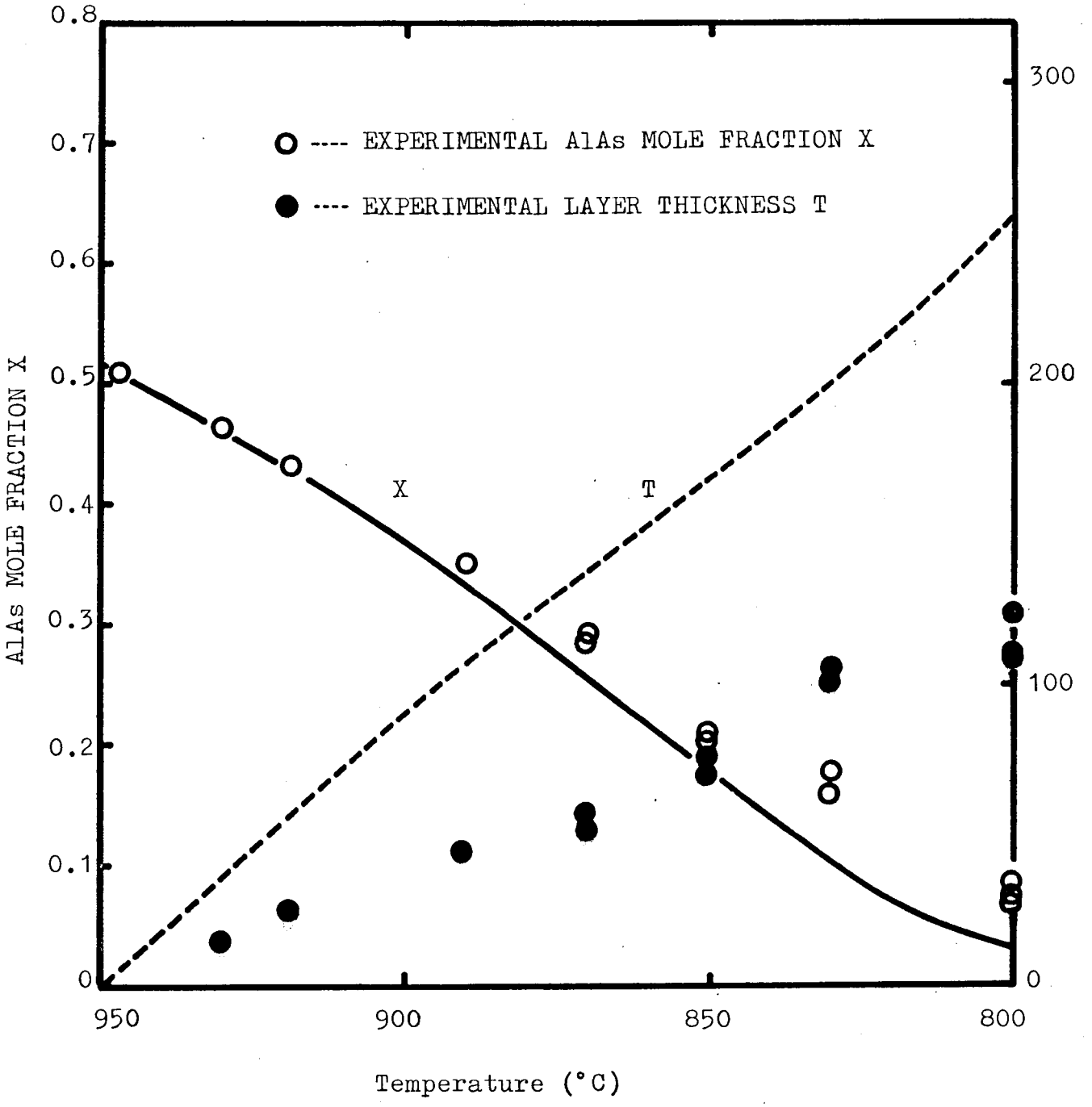

Fig.III-6. Variations of AlAs mole fraction in the solid, and the LPE layer thickness during the growth from 950 °C. Lines represent the theoretical values.

and 2 gr/cm^2, respectively. This figure shows that the actual profile of X deviates from the calculated one, and that the experimentally obtained growth rate is much lower than that predicted by the theory.

These deviations are caused mainly by the assumption on which the calculation was carried out. In this calculation, the solution was assumed uniform and in a equilibrium condition at any time of the growth. Whereas, in the process of an actual growth, the growth rate of the LPE layer is determined by the solute diffusion toward the solid-liquid interface from the solution. The consequence of the diffusion may cause a different deposition path or may give a smaller growth rate. Then, the deviation will become larger as the thicker solution is used for the growth. By the same reason, the faster cooling rate will give the larger deviation.

Another supposed reason for the deviation of the growth rate is that the appearance of spontaneous nucleations in the solution, and the resultant consumption of the solutes to them may decrease the LPE growth rate. The neighborhood of the surface of the solution far from the substrate is substantially supercooled as the growth proceeds. When the solution there is supercooled above the value of a critical supercooling temperature[7], spontaneous nucleations occur, and the solutes concentrations there are significantly reduced. This leads to a reduction of the LPE layer thickness.

For the quantitative analyses of these processes, a more

detailed theory based on the diffusion equations are essential. However, it should be noticed that the deviation of the composition profile is not so large in spite of the roughness of the theory. On the other hand, the deviation of the growth rate is very serious. More detailed analyses on this problem will given in chapter V.

III.4. Conclusions.

The theory of the composition change during the growth of ternary III-V compounds was described. A theoretical expression about the decreasing rate of each nutrient in the solution was derived, and the calculation of the deposition path in Ga-Al-As system was carried out based on it. The calculated results have shown that the solidus composition change during the growth cycle is determined by a competing process between the depletion of aluminum in the liquid, and the increase of the distribution coefficient of aluminum. In a case of the growth from 900 °C, the resultant solidification curve have shown increasing tendencies at $X > 0.8$, and decreasing ones at $X < 0.8$.

The calculated result was compared with the experiment of the growth from 950°C. It have been found, from this comparison, that the solidus compositions obtained by the experiments slightly deviate from the calculated values as the growth proceeds, and that the deviation between the actual layer thicknesses and the theoretical ones is very large.

REFERENCES OF CHAPTER III.

(1) M. Ilegems and G. L. Pearson, Proc. 1968 Sump. on GaAs, Dallas, (Inst. Phys. and Phys. Soc. London 1969).

(2) M. B. Panish and M. Ilegems, Progress in Solid State Physics Vol.7 (Pergamon, New York. 1972) pp.39-83.

(3) J. M. Woodall, H. Rupprecht and W. Reuter, J. Electrochem. Soc. 116 (1969) 899.

(4) M. Ilegems, Ph. D. Thesis, Stanford Univ., Calif. (1970).

(5) S. Isozumi, Y. Komatsu, N. Okazaki, S. Koyama and T. Kotani, J. Crystal Growth 41 (1977) 166.

(6) S. Isozumi, Y. Komatsu and T. Kotani, FUJITSU Scientific and Technical J. 6 (1979) to be published.

(7) A. Doi, T. Asano and M. Migitaka, J. Appl. Phys. 47 (1976) 1589.

IV. ANALYSIS ON THE GROWTH RATE OF $Ga_{1-x}Al_xAs$ EPITAXIAL FILMS.

IV.1. Introduction.

In general, actual LPE layer thicknesses are far different from the values predicted by calculating the excess amount of the solute corresponding to the temperature drop during the growth cycle. Tiller[1] first pointed out that solute transport by diffusion and convection, surface attachment kinetics and constitutional supercooling might be the causes of this difference. Later work by Tiller and Kang[2] developed this theme further in a theoretical vein. Ghez[3] calculated the growth rate from a semi-infinite melt when the growing interface, where interface kinetics were very fast, followed equilibrium condition. He showed that his theory yielded the same expression for the growth rate as those developed by Minden[4], and Small and Barnes[5]. Acçording to their theories, the layer thickness is proportional to the cooling rate (α), to the reciprocal of the slope of the liquidus curve (m), and to the growth time (t) taken to the 3/2 power. Moon and Kinoshita[6] have experimentally shown that this relation is valid in Ga-As system. Other mathematical solutions to the diffusion equation for situations encountered in LPE growth of binary compounds have been developed for finite melts by Rode[7] and Moon[8] under a linearized approximation for the liquidus concentration. Rode[9] and Hsieh[10] have verified their validity

experimentally.

Because of the simplicity of these expressions for the LPE layer thickness in binary systems, they are very effective for practical usages. Whereas, in ternary systems, it is impossible to obtain such a simple analytical expression for diffusion equations because the growth process is determined by diffusion of multicomponents in the liquid. Croossley and Small[11], and Ijuin and Gonda[12] extended a computer simulation technique[13] to the calculation of diffusion equation in Ga-Al-As system. By this technique, the result is obtained not in an analytical form, but in a numerical one. On the other hand, Moon and Kinoshita[6] have shown that the linear relationship between the layer thickness and the growth time to the 3/2 power, and the cooling rate, exsists in Ga-Al-As system and Ga-As-Sb system. This fact strongly indicates that the simple expression in binary systems still remains in ternary systems.

In this chapter, theories of the growth rate in binary system and ternary ones are described. The theory is compared with experimental results in Ga-Al-As system, and the growth process of $Ga_{1-x}Al_xAs$ and arsenic diffusivity in the Ga-Al-As liquid are discussed.

IV.2. LPE Growth Rate in Binary systems.

In the calculation of diffusion equations, the following assumptions are assumed in LPE growth. a) The rate-determining step in the growth is the diffusion in the growth solution. b) Convection is absence. c) The planarity of the solid-liquid interface is maintained. d) The solution is isothermal because the thermal diffusivity is roughly 10^4 greater in value than the mutual diffusivity of the liquid. e) The slope of the deposition path over the liquidus curve is approximated by a constant. f) The diffusivity of the solute in the liquid is constant. Under those conditions, the diffusion equation for the solute concentration (C) is expressed as follows:

$$D\,\partial^2 C/\partial x^2 = \partial C/\partial t \ , \qquad \ldots \text{(IV.1)}$$

where D, x and t are, respectively the diffusion coefficient, the distance normal to the solid-liquid interface, and the time. In the calculation of eq.(IV.1), the following boundary conditions are required:

$$C(x,\ 0) = C_0 \ , \qquad \ldots \text{(IV.2)}$$

$$C(\pm\, l,\ t) = C_0 - \alpha t/m \ , \qquad \ldots \text{(IV.3)}$$

where α = the cooling rate constatnt and m = the slope of the liquidus curve. C(x, t) is the solute concentration at x distant from the free surface of the growth solution. C_0 and l are the initial concentration at t = 0 and the solution thick-

ness, respectively. It should be noticed that the appropriate boundary conditions for the diffusion occurring between two plane sheets, $\pm$ l apart, are assumed in this approximation. This situation is schematically shown in Fig.IV-1. Under these boundary conditions, the gradient of the solute concentration $\partial C/\partial x$ is given as follows[8), 14)]:

$$\frac{\partial C}{\partial x} = \frac{\alpha l}{mD}\left(\frac{x}{l} - 2\sum_{n=0}^{\infty} \frac{(-1)^n}{\lambda_n} \left(- \frac{\lambda_n^2 Dt}{l^2} \right) \sin\left(\lambda_n \frac{x}{l}\right) \right) , \quad .. \text{(IV.4)}$$

where $\lambda_n = (n + \frac{1}{2})\pi$. By intengrating eq.(IV.4) with respect to t, the solute concentration is expressed as follows:

$$C(x, t) = C_0 + \frac{\alpha l}{mD} \left(- \frac{Dt}{l} - \frac{1}{2} + \frac{x^2}{2l} + 2 \sum_{n=0}^{\infty} \frac{(-1)^n}{\lambda_n^2} \exp\left(- \frac{\lambda_n^2 Dt}{l^2}\right) \right.$$
$$\left. x \frac{l}{\lambda_n} \cos\left(\lambda_n \frac{x}{l}\right) \right) \quad .. \text{(IV.5)}$$

The layer thickness (T) is obtained in a usual manner by integrating eq.(IV.4) with respect to t using mass conservation rule in the interface region. Provided $T \ll l$, then:

$$T = \int_0^t \frac{D}{C_s - C(l,t)} \left(-\left(\frac{\partial C}{\partial x}\right)_{x=l}\right) dt , \quad .. \text{(IV.6)}$$

where Cs is the solid concentration of the diffusing species. In an ususl LPE growth condition, C(l,t) is very small value comparing to Cs because of the use of a dilute solution for the growth. Consequently, eq.(IV.6) is approximated as follows:

$$T = -\int_0^t \frac{D}{C_s}\left(\frac{\partial C}{\partial x}\right)_{x=l} dt . \quad .. \text{(IV.7)}$$

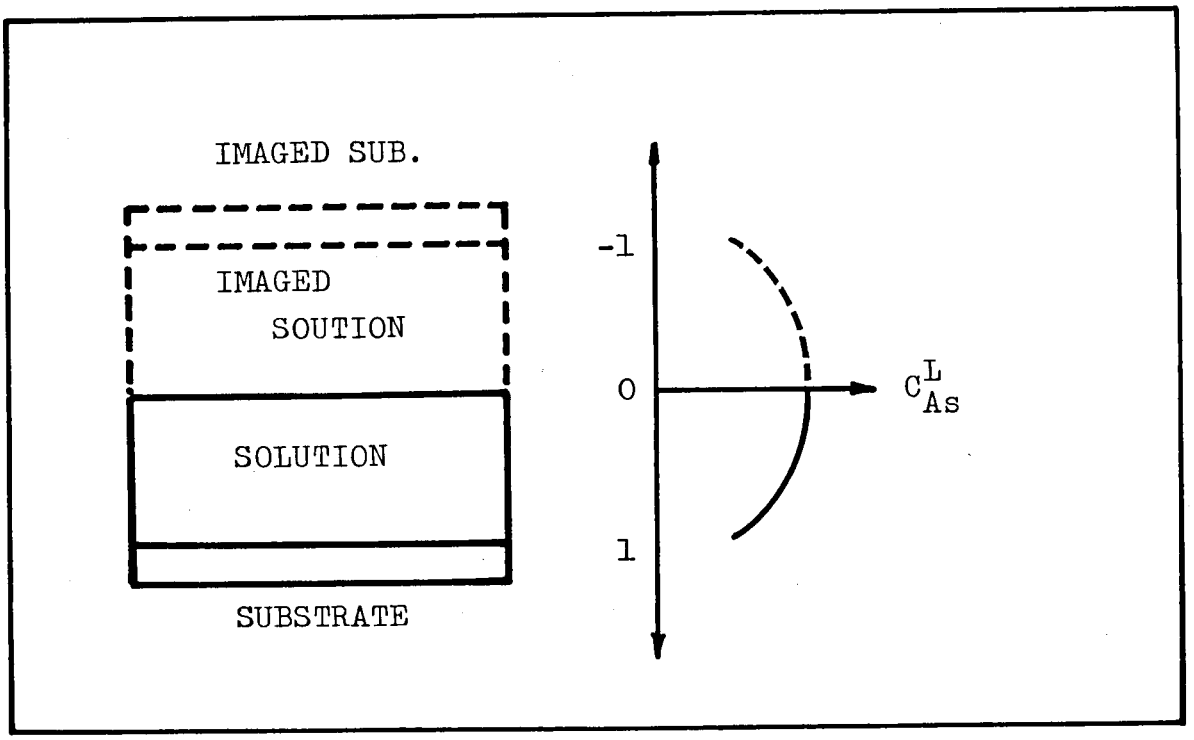

Fig.IV-1. Schematic illustration of the boundary condition in LPE growth. The diffusion of the solute is assumed to occur between two plane sheet, $\pm$ 1 apart.

From eqs.(IV.4) and (IV.7), the following equation is obtained:

$$T = \frac{\alpha}{C_s m}\left(1t + \frac{2l^3}{D}\left(\sum_{n=0}^{\infty} \frac{\exp(-\lambda_n^2\, Dt/l^2)}{\lambda_n^4} - \frac{1}{6} \right) \right). \quad \text{... (IV.8)}$$

When $Dt/l^2 < 1$, eq.(IV.8) comes close to:

$$T = \frac{4}{3}\frac{\alpha}{C_s m}\left(\frac{D}{\pi}\right)^{1/2} t^{3/2} . \quad \text{... (IV.9)}$$

And when $Dt/l^2 \gtrsim 1$,

$$T = \frac{\alpha l}{C_s m}\left(t - \frac{l^2}{3D} \right) . \quad \text{.. (IV.10)}$$

The comparison of the theory with the experiment was intensively carried out in Ga-As system by Rode[9] and Hsieh[10]. The results obtained by them are shown in Figs.IV-2 and IV-3. Those figures show the fairly good agreements of the experiments with the theory. Both experimental data show a clear proportional trend of the layer thickness to $t^{3/2}$ because their experimental condition belongs to the case of an infinite melt (eq.IV.9). In this condition, the growth rate increases in proportion to $t^{1/2}$. However, the increase is limited as Dt/l^2 comes close to 1. The solution in such a case is given by eq.(8) or eq.(10). During $Dt/l^2 < 1$, the solute concentration at the free surface of the solution ($C_{suf.}$) is maintained at its initial values of C_0. Whereas, when $Dt/l^2 \gtrsim 1$, the gradient of the solute concentration, and therefore, the flux of the solute atoms diffusing toward the growth interface are reduced owing to the decrease of $C_{surf.}$. This is one of possible reasons why the experimental points for larger t in Figs.IV-2

and IV-3 have a trend to fall a little below the extraporation of the line drawn through the points for small t. The second reason for expecting a decrease in T for longer t is precipitates of GaAs at the solution surface during the long growth run. Hsieh[10] reported that such precipitates were usually observed at 20-30 min after the solution were placed in contact with the substrate. By reducing the arsenic concentration in the solution, the formation of precipitates decreases T below the values predicted by the theory. The maximum amount of supercooling without spontaneous nucleations in the solution is called a critical supercooling temperature (Δ_c). The continuous reduction in temperature without a significant change in the solute concentration at the surface eventually causes supercooling there. When the amount of supercooling there exceeds the value of Δ_c, GaAs precipitates appear. These precipitates not only reduce the growth rate but deteriorate the planrity of the LPE layer. More detailed discussions about this problem will be given in chapter V.

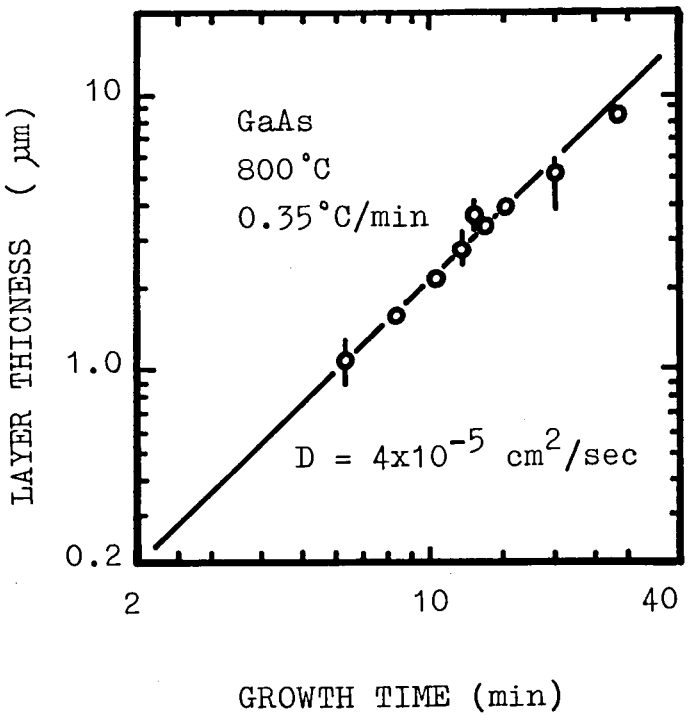

Fig.IV-2. LPE layer thickness as a function of growth time[9].

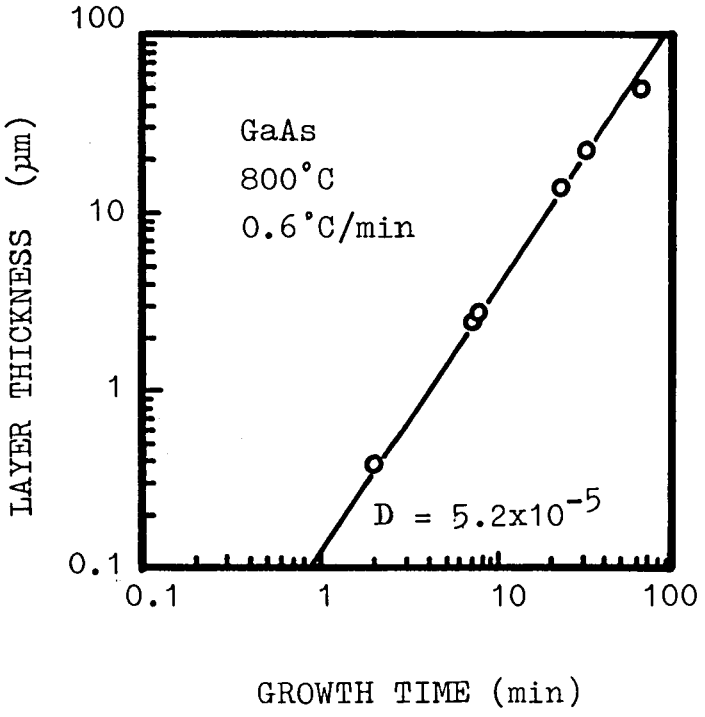

Fig.IV-3. LPE layer thickness as a function of growth time[10].

IV.3. Calculation of The Slope of The Deposition Path over The Liquidus Surface in Ga-Al-As System.

As is described in the previous section, LPE growth rate in binary systems is determined by the solute diffusion toward solid-liquid interface. The layer thickness is expressed by a simple solution of the one dimensional diffusion equation. The simplicity of the form of the solution is mainly due to the linear approximation of the deposition path.

Since the linear relationship between the layer thickness and the growth time to the 3/2 power, and the cooling rate, exists in Ga-Al-As system[6], the most important point for the application of eq.IV.9 to this system is to show the validity of the similar linear approximation of the deposition path.

In chapter III, the deposition path over the liquidus surface during the cooling cycle was analyzed in the case of $(A_{1-x},B_x)C$ type ternary compounds using the pseudoequilibrium model. In eq.(III.9), $dX_C^L/d\theta$ and $dX_B^L/d\theta$ represent the slopes of the components of C and B on the deposition path over the liquidus surface, respectively. Although this relation and the phase diagram give the deposition path as is described in chapter III, another relationship between $dX_C^L/d\theta$ and $dX_B^L/d\theta$ is neccessary for the calculation of the slopes.

Another relationship is derived from the differentiation of X_C^L assuming that θ and X_B^L are independent variables:

$$\frac{dX_C^L}{d\theta} = \left(\frac{\partial X_C^L}{\partial X_B^L}\right)_\theta \frac{dX_B^L}{d\theta} + \left(\frac{\partial X_C^L}{\partial \theta}\right)_{X_B^L} . \qquad .. \text{(IV.11)}$$

From eqs.(IV.11) and (III.9) , the following expressions are obtained:

$$\frac{dX_C^L}{d\theta} = \left(\frac{\partial X_C^L}{\partial \theta}\right)_{X_B^L} \Bigg/ \left\{1 - \left(\frac{\partial X_C^L}{\partial X_B^L}\right)_\theta \frac{X/2 - X_B^L}{X_C^S - X_C^L}\right\} , \qquad .. (IV.12)$$

$$\frac{dX_B^L}{d\theta} = \left(\frac{\partial X_C^L}{\partial \theta}\right)_{X_B^L} \Bigg/ \left\{\frac{X_C^S - X_C^L}{X/2 - X_B^L} - \left(\frac{\partial X_C^L}{\partial X_B^L}\right)_\theta\right\} , \qquad .. (IV.13)$$

In A_{III}-B_{III}-C_V systems, the C_V atom fraction in the liquid $B_{III}C_V$ mole fraction in the solid can be regarded as functions of temperature and the B_{III} atom fraction in the liquid. They are defined by the phase diagram. Therefore, we can obtain $\partial X_C^L/\partial\theta$ and $\partial X_C^L/\partial\theta$ directly from the phase diagram by numerical calculations. This means, since the other terms are in the phase diagram, $dX_C^L/d\theta$ and $dX_B^L/d\theta$ can be calculated from eqs. (IV.12) and (IV.13) based on the phase diagram.

In Ga-Al-As system, A, B, and C correspond to Ga, Al, and As, respectively. In eqs.(IV.12) and (IV.13), X corresponds to AlAs mole fraction in the solid and X_C^S is equal to 0.5. At a given X_{Al}^L, the arsenic atom fraction in the liquid corresponding to the temperatures of θ, $\theta+\delta\theta$, and $\theta-\delta\theta$ were calculated from the phase diagram. Then, they were approximated by a quadratic function, which was directly differentiated to obtain $(\partial X_{As}^L/\partial\theta)_{X_{Al}^L}$. In the same way as the calculation of $(\partial X_{As}^L/\partial\theta)_{X_{Al}^L}$, $(\partial X_{As}^L/\partial X_{Al}^L)_\theta$ was obtained by varing X_{Al}^L to $X_{Al}^L + \delta X_{Al}^L$ and $X_{Al}^L - \delta X_{Al}^L$ keeping θ constant. In this case, 5°C and $X_{Al}^L/100$ were chosen for $\delta\theta$ and δX_{Al}^L, respectively. The

results of the calculation of $dX_{As}^{L}/d\theta$ and $dX_{Al}^{L}/d\theta$ are shown Figs.IV-4 and IV-5 over the temperature range of 700-1000°C.

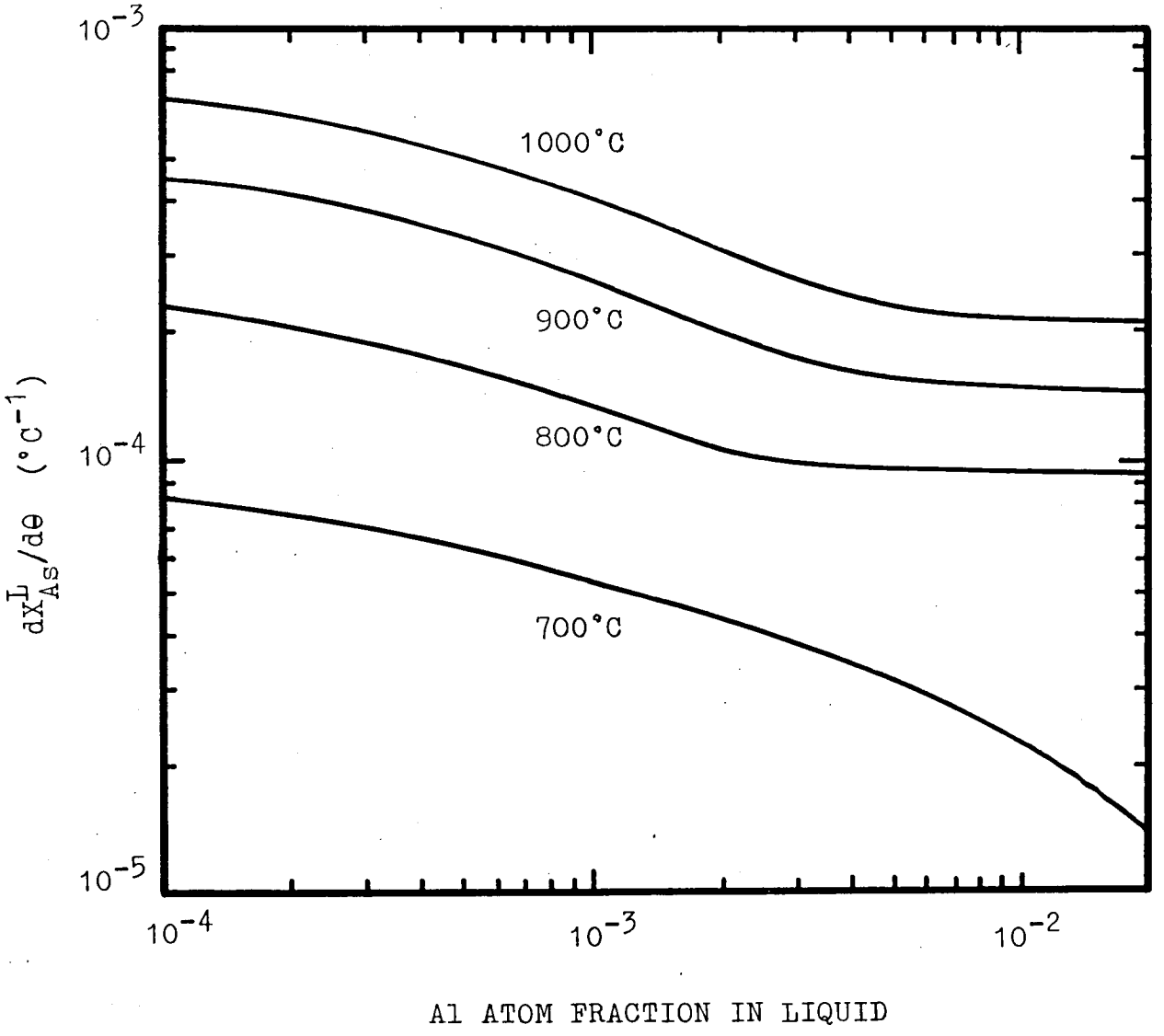

Fig.IV-4. Changing rate of As atom fraction during the cooling cycle as a function of the liquidus composition.

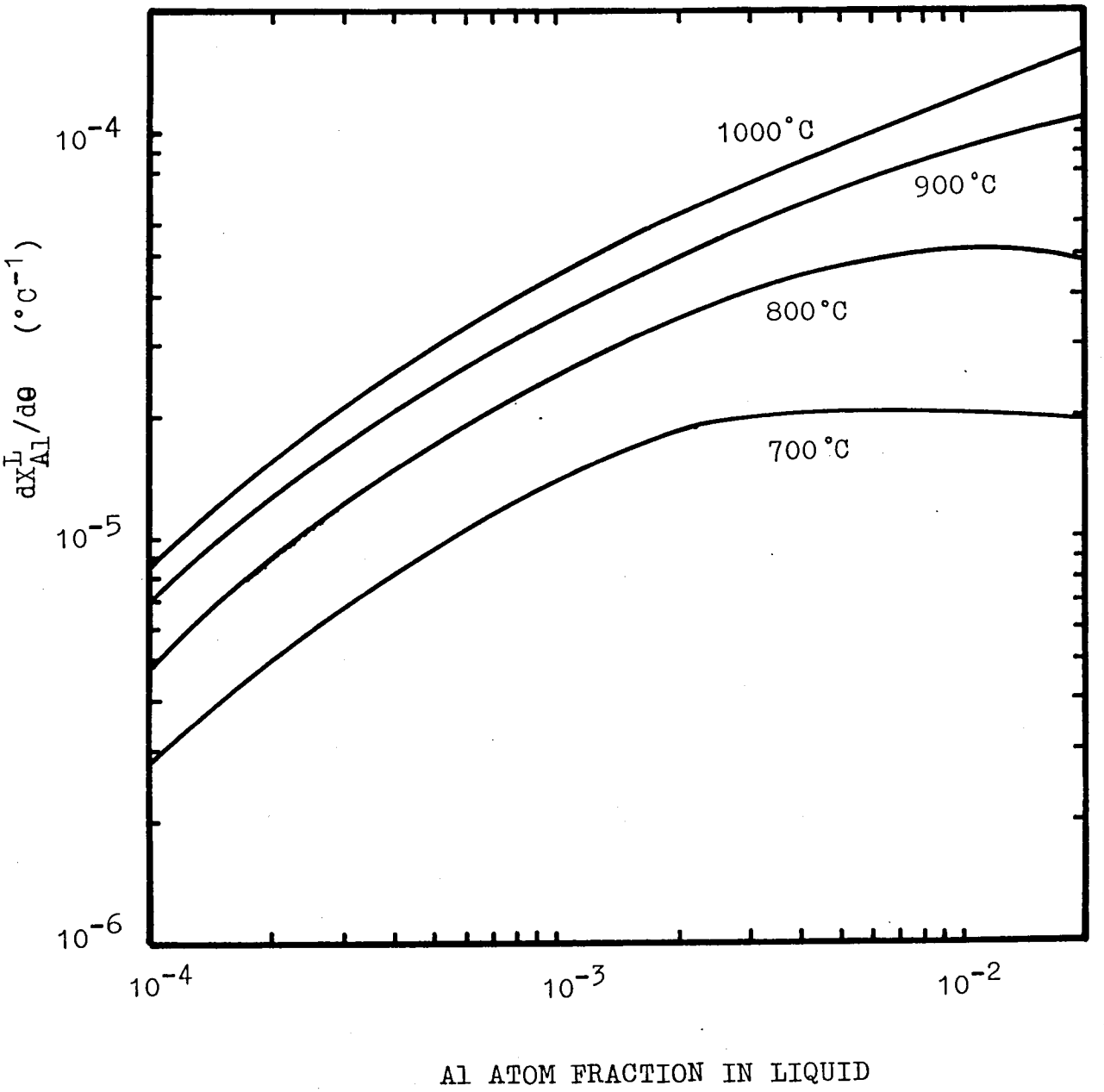

Fig.IV-5. Changing rate of Al atom fraction during the cooling cycle as a function of the liquidus composition.

IV.4 LPE Growth Rate in Ga-Al-As System.

The changing rate of arsenic concentration with respect to temperature ($dX_{As}^{L}/d\theta$) in Ga-Al-As system corresponds to 1/m in Ga-As system. Then, assuming that arsenic concentration at the solid-liquid interface decreases at this changing rate during the cooling cycle of $Ga_{1-x}Al_xAs$ LPE growth, eq.(IV.9) would be applicable to this ternary system. For examining this assumption, $Ga_{1-x}Al_xAs$ LPE growth on a GaAs (100) substrate was carried out using a sliding boat shown in Fig.IV-6. In this figure, a GaAs source wafer was kept in contact with the bottom of the melt in order to achieve equilibration. After keeping this situation at a certain temperature (θ_0) for 40 min, the growth was initiated just at saturation at a cooling rate of 1.0°C/min by sliding the melt from the source wafer onto the substrate. The LPE growth area and the weight of gallium for the melt were 3.5 cm^2 and 8 g, respectively.

The result of the first series of the growth experiments is shown in Fig.IV-7. In this experiment, the growth starting temperature (θ_0) was 900°C and the cooling interval (Δ) was varied at each growth run. Aluminum atom fraction in the liquid X_{Al}^{L} was 6.9×10^{-4} which corresponded to X=0.09. Fig.IV-7 shows a clear increasing tendency of T in proportion to $\Delta^{3/2}$. In a case of an infinite binary melt, T increases in proportion to $t^{3/2}$. Using the relation $\Delta = \alpha t$, eq.(IV.9) is expressed as follows:

$$T = \frac{4}{3} \frac{\alpha^{-1/2}}{C_s\, m} \left(\frac{D}{\pi}\right)^{1/2} \Delta^{3/2} \quad . \qquad .. \text{(IV.14)}$$

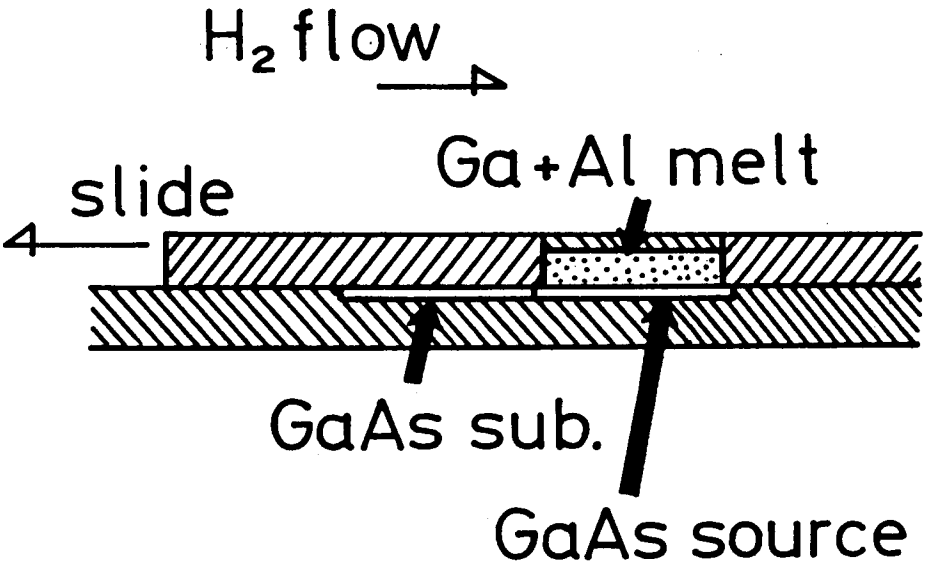

Fig.IV-6. LPE growth apparatus for the experiment of the growth rate in Ga-Al-As system.

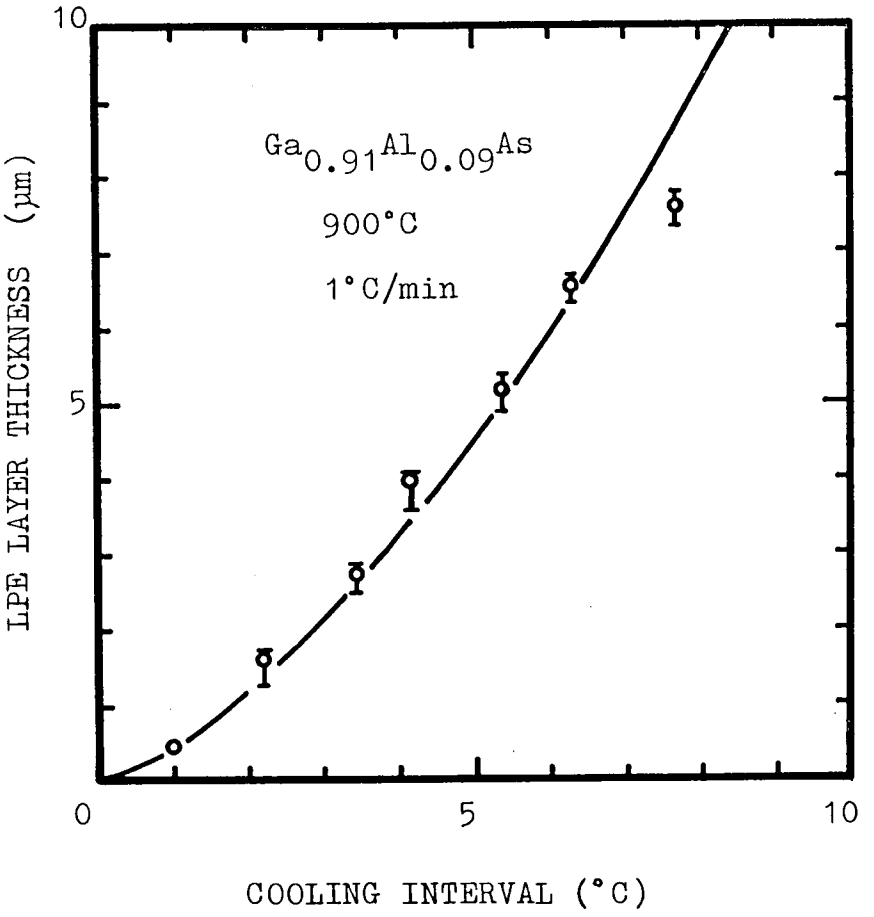

Fig.IV-7. LPE layer thickness as a function of the cooling rate.

Assuming the decreasing rate of arsenic atom fraction at the solid-liquid interface is equal to $dX_{As}^{L}/d\theta$ in eq.(IV.12), the following equation is derived:

$$T = \frac{4}{3}\frac{C_l}{C_s}\left(\frac{dX_{As}^{L}}{d\theta}\right)\alpha^{-1/2}\left(\frac{D}{\pi}\right)^{1/2}\Delta^{3/2}, \qquad \text{.. (IV.15)}$$

where C_l is the numbers of atoms per unit volume in the liquid. This value can be calculated directly from the liquid Ga density because the melt is dilute in this case. Taking the thermal expansion into account, ρ_l = 5.56 g/cm^3 and C_l = 4.80x10^{22}/cm^3 [15] were adopted. The experimentally set values of X_{Al}^{L} = 6.9 x10^{-4} and θ_0 = 900°C give $dX_{As}^{L}/d\theta$ = 2.9x10^{-4}°C^{-1}. Using these values and C_s = 2.22x10^{22}/cm^3, arsenic diffusion coefficient of D = 1x10^{-4} was calculated from eq.(IV.15). The LPE growth area S = 3.5 cm^2 and the weight of gallium for the melt w = 8 g give a thickness of the melt l = 0.41 cm. Then, the value of Dt/l^2 for a maximum Δ is 0.27. This means the growth condition in this experiment belongs to a case of the growth from infinite melt.

The second series of the growth experiments were carried out with Δ = 5°C. The growth was started from 850°C, 900°C, or 950°C. The liquidus composition range examined is from X_{Al}^{L} = 1.7x10^{-4} to 4.7x10^{-3}. In Fig.IV-8, the layer thickness are plotted versus $(dX_{As}^{L}/d\theta)/X_{As}^{S}$ to show the relationship between these two quantities. As is obvious from this figure, T increases in proportion to $(dX_{As}^{L}/d\theta)/X_{As}^{S}$ for each temperature. The straight lines in this figure represent the calculated values

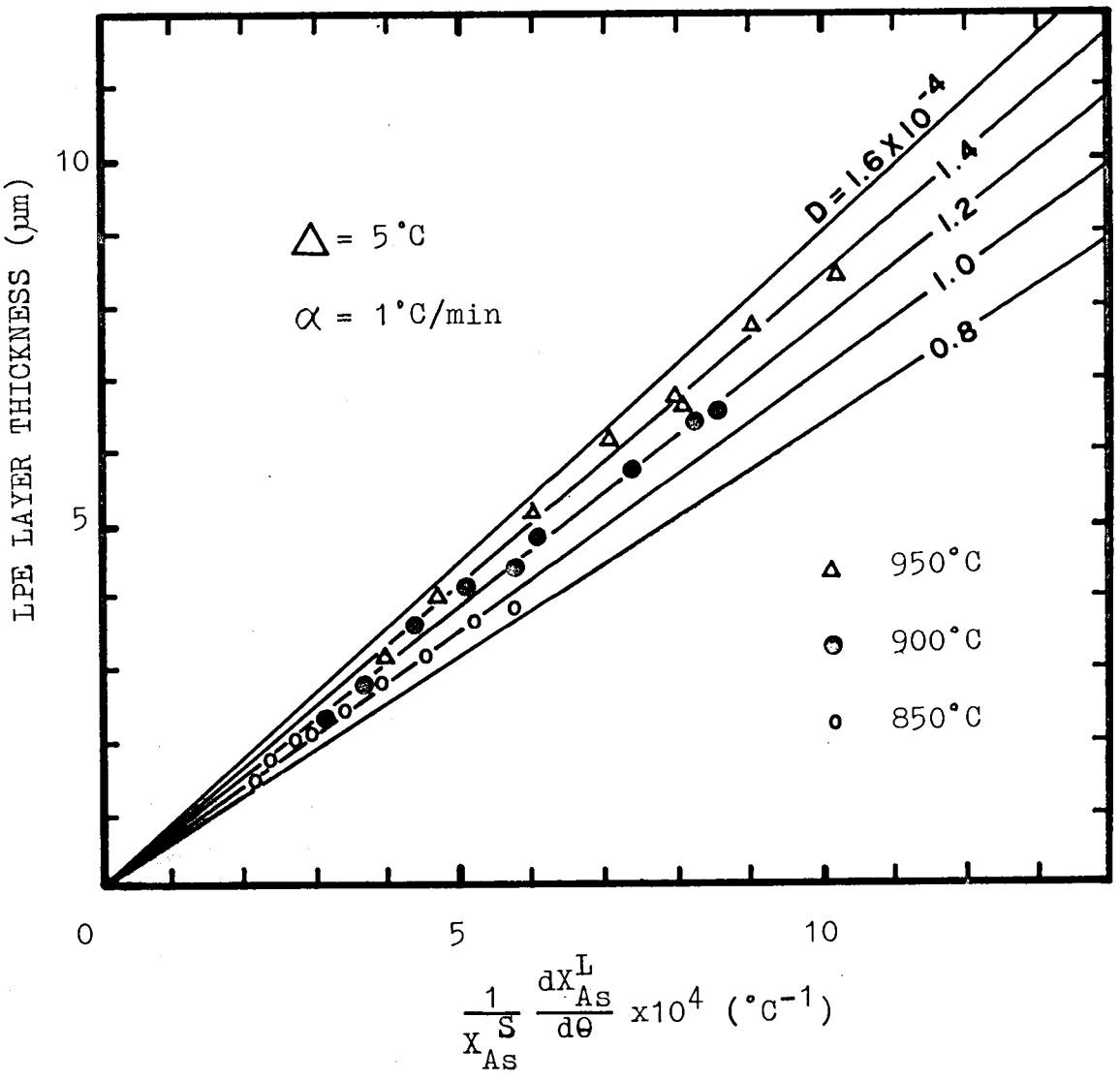

Fig.IV-8. LPE layer thickness versus the changing rate of As atom fraction in the liquid per As atom fraction in the solid. Lines for each As diffusivity were calculated from eq,(IV.15).

for various arsenic diffusivities in the liquid. The experimental data for 850°C, 900°C and 950°C are well approximated by the lines for $D = (1.0 \pm 0.2)\times10^{-4}$ cm^2/sec, $D = (1.2 \pm 0.2)\times10^{-4}$ cm^2/sec, and $D = (1.4 \pm 0.2)\times10^{-4}$ cm^2/sec, respectively. This result shows that the arsenic diffusivity in Ga-Al-As liquid has little dependence on the solution composition, but has a weak dependence on temperature.

From the results shown in Figs.IV-7 and IV-8, it has been established that the equation for LPE layer thickness in binary systems remains valid in Ga-Al-As system. This means the growth process of $Ga_{1-x}Al_xAs$ is mainly arsenic diffusion controlled, and that arsenic concentration at the solid-liquid interface decreases at the rate of $dX_{As}^{L}/d\theta$ given by eq.(IV.12) in the adopted growth condition.

IV.5. Discussion.

The driving force of LPE growth is the decrease of the solute concentration at the solid-liquid interface. The theory in binary systems described in section IV.2 is based on a assumption that the equilibrium is always maintained at the solid-liquid interface. The simplicity of the form of the solutions for the diffusion equation is attributed to the boundary condition in which the equilibrium condition at the solid-liquid interface is approximated by a linear function shown in eq.(IV.3).

To show the applicability of this simple expression for the layer thickness to ternary systems, the expression for the changing rate of the solute concentration, which corresponds to 1/m in binary systems, must be derived. In section IV.3, it has been expressed as a form using partial differential expressions which can be calculated from the phase diagram. In Ga-Al-As system, the meaning of eq.(IV.12) is as follows. In this equation, the numerator $(\partial X_{As}{}^{L}/\partial\theta)_{X_{Al}}{}^{L}$ in right side terms corresponds to $dX_{As}{}^{L}/d\theta$ in Ga-As system. In the denominator, the second term is equal to zero in Ga-As system because $(X/2 - X_{Al}{}^{L})$ is equal to zero. In Ga-Al-As system, as a result that $-(\partial X_{As}{}^{L}/\partial X_{Al}{}^{L})_{\theta}$ and $(X/2 - X_{Al}{}^{L})/(X_{As}{}^{S} - X_{As}{}^{L})$ always have positive values, the denominator has a greater value than 1 Therefore, the second term in the denominator can be regarded as the correction term which corresponds to the effect caused by introducing aluminum into Ga-As system.

$dX_{As}^{L}/d\theta$ calculated from eq.(IV.12) is based on the pseudoequilibrium assumption because this equation is derived from eq.(III.9). Then, the value of $dX_{As}^{L}/d\theta$ in Fig.IV-4 might show only a decreasing rate of X_{As}^{L} at the beginning of the growth. In the process of an actual growth, as the cooling interval increases, the value of $dX_{As}^{L}/d\theta$ could vary substantially because the diffusion would dictate a different deposition path. However, within a small amount of a cooling interval, or in a case that the diffusion length of arsenic in the liquid is sufficiently longer than the melt thickness. A clear increasing tendency of T in proportion to $\Delta^{3/2}$ in Fig.IV-7, and a fairly good linear relationship of T with $(dX_{As}^{L}/d\theta)/X_{As}^{S}$ in Fig.IV.8 show that the calculated value of $dX_{As}^{L}/d\theta$ gives a reasonable approximation of the decreasing rate of arsenic concentration at the solid-liquid interface under such experimental conditions.

Though numerous theoretical and experimental studies have been reported on the growth rate of GaAs LPE growth, there have been only a few papers which reported on the growth rate of $Ga_{1-x}Al_xAs$[6),11),12),16),17)]. In these papers, only Moon and Kinoshita's[6)] can be compared directly with ours. They examined LPE layer thickness of $Ga_{1-x}Al_xAs$ on GaP (111) and obtained a simple relationship:

$$T = 9.5\alpha t^{3/2} \times 10^{-7} \text{ (in cm, t in sec, } \alpha \text{ in °C/min)} \quad .. \quad (IV.16)$$

Their experimentally set values of X = 0.5 and θ = 910°C give

$(dX_{As}^{L}/d\theta)/X_{As}^{S} = 3.1\times10^{-4}\,°C^{-1}$ from our calculation. The calculated arsenic diffusivity using eq.(IV.15) is 1.4×10^{-5} cm^2/sec. Although this value is somewhat lower than the value obtained in the present work, it is reasonable because their experimentally obtained values in GaAs system are $0.6\text{-}1.9\times10^{-5}$ cm^2/sec[6),18)].

Arsenic diffusivities obtained in the present work are summarized in Fig.IV-9 with the data in literatures. These data except for Moon's are seen to follow an activation process expressed as follows:

$$D = D_0 \exp(-\theta''/\theta) , \qquad .. \text{(IV.17)}$$

where D_0 and θ'' are the proportionality constant and the diffusion activation temperature, respectively. Rode's data[9)] are expressed by $D_0=5000$ cm^2/sec and $\theta'' = 12600°K$. As is pointed out in his paper, this is indeed a strong temperature dependence even as compared to the arsenic solubility with the solubility activation temperature of $\theta' = 12600°K$. On the other hand, Moon's data[18)] show no temperature dependence. However, his data are thought to be unreasonable because the values are too low compared with other data. Our data for 850°C, 900°C, and 950°C give $D_0 = 6.1\times10^{-3}$ cm^2/sec and $\theta'' = 4600°K$. The extraporated line for lower temperature agrees with Dawson's data[19)] of $D = 8\times10^{-5}$ cm^2/sec at 800°C, and comes close to Doi's data[20)] of $D = 5\times10^{-5}$ cm^2/sec at 744°C. According to Rode's data, a temperature change by one percent of absolute

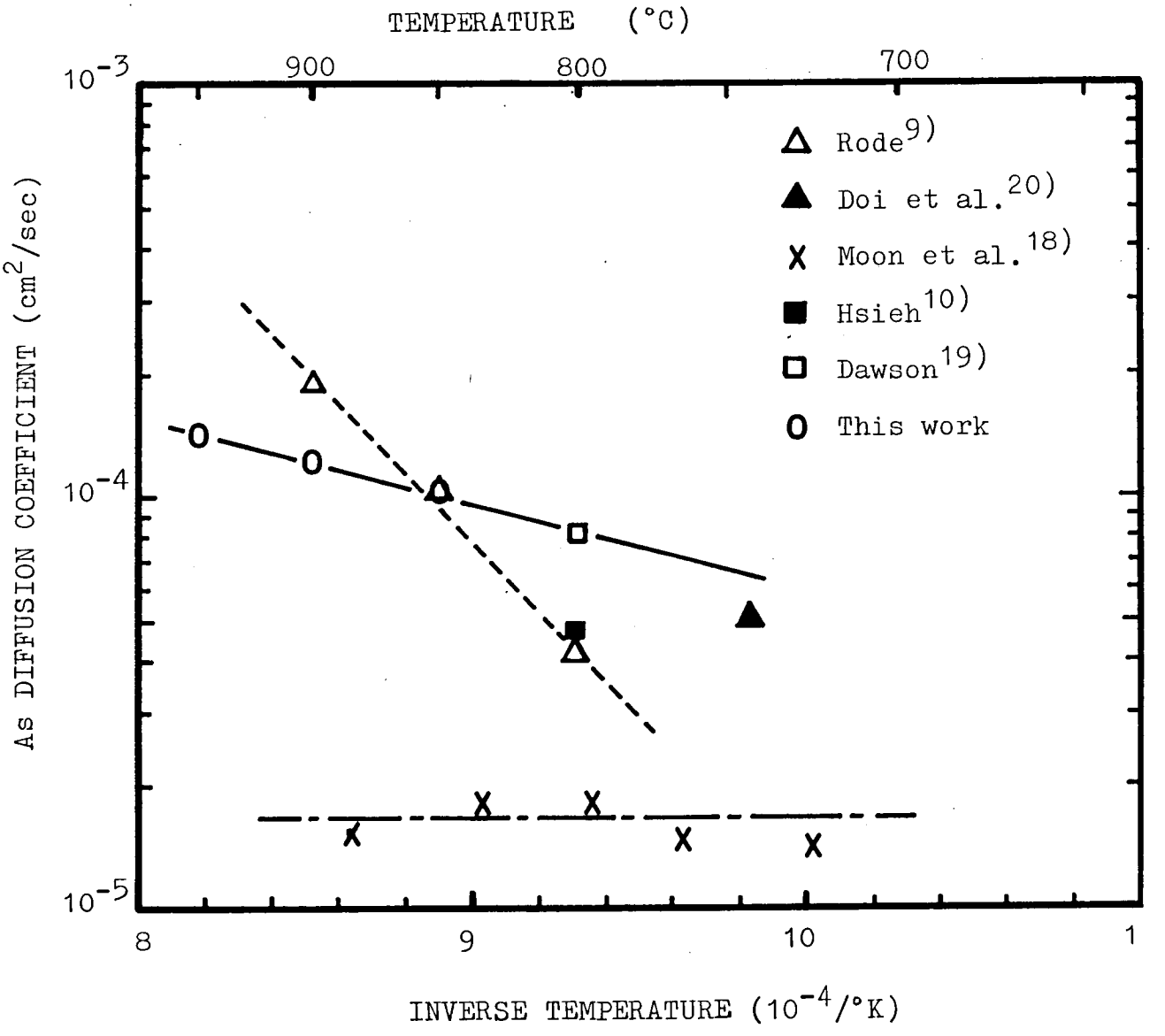

Fig.IV-9. Temperature dependence of the diffusion coefficient of As in Ga.

value at 800 °C yields a change in D near twenty percent, whereas arsenic solubility changes by thirteen percent. Such a larger temperature dependence of D than that of the arsenic solubility is unreasonable even assuming the association of arsenic with gallium or arsenic itself in the liquid. The data of the present work give a change in D about three percent for a temperature change by one percent of absolute value at 800 °C. Such a smaller dependence of D than that of arsenic solubility may be reasonable assuming the associations of arsenic in the liquid as reported by Osamura and Murakami[21].

IV.6. Conclusions.

The theories of LPE growth rate in binary and ternary systems were described. The equations for the LPE layer thickness in binary systems were derived from the diffusion equation based on a diffusion limitted growth model. The derived equations have simple analytical forms, especially in a case of the growth from a semi-infinite melt, the layer thickness is proportional to the cooling rate, to the reciprocal of the slope of the liquidus line, and to the growth time taken to the 3/2 power.

To examine the applicability of this equation in binary systems to ternary ones, basic equations for the slope of the deposition path over the liquidus surface in ternary systems were derived. From these equations, the changing rate of arsenic and aluminum concentrations in the Ga-Al-As liquid during the LPE growth cycle were calculated. From the comparison between the calculated values of the changing rate of arsenic concentration in the liquid, and the LPE layer thicknesses of $Ga_{1-x}Al_xAs$ obtained by the growth experiments, it has been shown that the linear relationship between these two quantities holds in Ga-Al-As system. The another series of the growth experiments have shown that the LPE layer thickness of $Ga_{1-x}Al_xAs$ is proportional to the growth time taken to the 3/2 power. These facts means that the growth process of $Ga_{1-x}Al_xAs$ is mainly arsenic diffusion controlled, and that the simple equation for the layer thickness in binary systems

is applicable in Ga-Al-As system.

From the results of the comparisons described above, arsenic diffusivities in the Ga-Al-As liquid were estimated to be 1.0×10^{-4}, 1.2×10^{-4}, and 1.4×10^{-4} cm^2/sec at 850°C, 900°C, and 950°C, respectively. These values show a relatively weak temperature dependence compared with the published data.

REFERENCES OF CHAPTER IV.

(1) W. A. Tiller, J. Crystal Growth 2 (1968) 69.

(2) W. A. Tiller and C. Kang, J. Crystal Growth 2 (1968) 345.

(3) R.Ghez, J. Crystal Growth 19 (1973) 153.

(4) H. T. Minden, J. Crystal Growth 6 (1970) 228.

(5) M. B. Small and J. F. Barnes, J. Crystal Growth 5 (1969) 9.

(6) R. L. Moon and J. Kinoshita, J. Crystal Growth 21 (1974) 149.

(7) D. L. Rode, J. Crystal Growth 20 (1973) 13.

(8) R. J. Moon, J. Crystal Growth 27 (1974)62.

(9) D. L. Rode, J. Crystal Growth 20 (1973) 13.

(10) J. J. Hsieh, J. Crystal Growth 27 (1974) 49.

(11) I. Crossley and M. B. Small, J. Crystal Growth 15 (1972) 268.

(12) H. Ijuin and S. Gonda, J. Crystal Growth 33 (1976) 215.

(13) I. Crossley and M. B. Small, J. Crystal Growth 11 (1971) 157

(14) J. Crank, Mathematics of Diffusion (Oxford Univ. Press, London 1957) ch.4.

(15) S. Isozumi, Y. Komatsu, N. Okazaki, S. Koyama and T. Kotani, J. Crystal Growth 41 (1977) 166.

(16) H. Ijuin and S. Gonda, J. Electrochem. Soc. 123 (1976) 1109.

(17) G. H. B. Thompson and P. A. Kirkby, J. Crystal Growth 27 (1974) 70.

(18) R. L. Moon, J. Crystal growth 32 (1976) 68.

(19) L. R. Dowson, J. Crystal Growth 27 (1974) 86.

(20) A. Doi, T. Asano and M. Migitaka, J. Appl. Phys. 47 (1976) 1589.

(21) K. Osamura and Y. Murakami, J. Phys. Chem. Solids 36 (1975) 931.

V. THICKENING OF EPITAXIAL FILMS

V.1. Introduction.

The external quantum efficiency of a light emitting diode (LED) is determined by a product of the internal quantum efficiency and the extraction efficiency of the light emitted from the crystal. The former depends mainly on the crystal quality, which is sufficiently high in LPE crystals because of few native defects in them. Whereas, the latter is directly dependent on the device stsucture.

There is a disadvantage in $Ga_{1-x}Al_xAs$ LPE crystals for designing a device structure suitable for effective extractions of the emitted light. In Fig.V-1(a), a schematic illustration of a $Ga_{1-x}Al_xAs$ LPE wafer for LEDs is shown. As is described in chapter III, AlAs mole fraction X within the LPE layer decreases from the interface with the GaAs substrate to the surface in the composition region of $X < 0.5$ which is usually used for the device. This leads to the gradient of the bandgap in the LPE layer from the interface to the surface. Then, the light emitted from the p-n junction toward the surface is absorbed in the p-region in which the bandgap energy is lower than that of the light. On the other hand, the light emitted toward the GaAs substrate is completely absorbed because of its sufficiently lower bandgap energy.

To overcome this difficulty, Burrus et al.[1] extracted the light from the interface side after removing a part of the

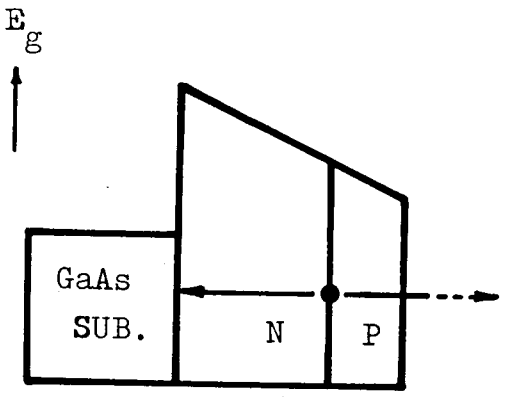

(a) A LED structure with GaAs substrate.

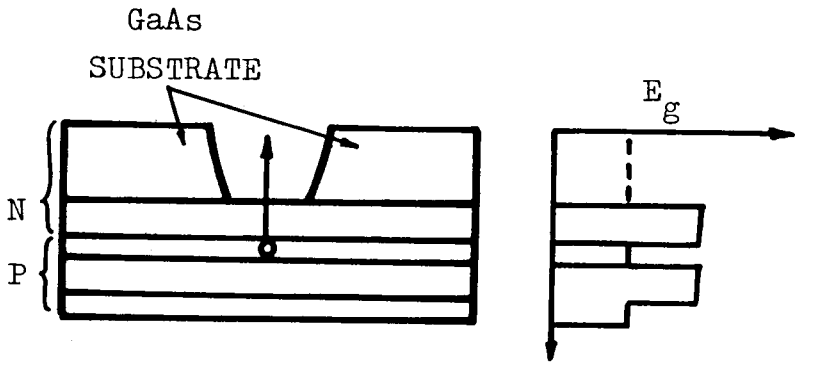

(b) A LED structure with partially dissolved GaAs substrate.

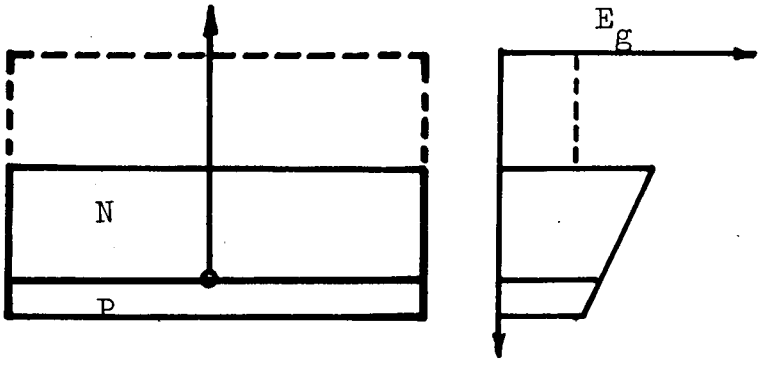

(c) A LED structure without GaAs substrate.

Fig.V-1. Schematic illustrations of $Ga_{1-x}Al_xAs$ LPE wafers for LEDs.

GaAs substrate as shown in Fig.V-1(b). In this LED, the emitted light passes through only the region with the higher bandgap energy, and the resultant absorption is remarkably reduced. However, this structure requires complicated fabrication processes such as a partial etching of the GaAs substrate. Moreover, LEDs with this structure have been believed to be disadvantageous in the reliability[2], because the partial removal of the GaAs substrate induces a concentrated stress on the light emitting region. For simple fabrication processes and high reliabilities, the GaAs substrate should be completely removed as shown in Fig.V-1(c). Whereas, such structure requires the LPE layer to be thick enough to ensure the mechanical strength by itself.

To realize such a thick $Ga_{1-x}Al_xAs$ LPE layer, knowledges of the solidus composition changing and the growth rate are essential. In this chapter, stuties on the analyses for obtaining a 50 μm thick LPE layer are described based on the theories described in the preceding chapters.

V.2. Control of Solidus Composition at The Surface.

In the growth of a thin $Ga_{1-x}Al_xAs$ LPE layer, the phase diagram gives almost complete data because the solidus composition changing in such a thin layer is usually negligible. Whereas, the growth of a thick $Ga_{1-x}Al_xAs$ requires a cooling interval of more than a few tens °C, and the solidus composition distributes within the layer. In this case, it is neccessary to define the region which sould be accurately controlled for device performances. In the LEDs shown in Fig.V-1(c), the composition at the surface (i.e. the composition at the end of the growth) is important in this meaning because the wavelength of the emiited light is determined by the composition near the p-n junction which is usually formed near the surface. In a case of LEDs for fiber-optical communication systems, the AlAs mole fraction at the surface should be coltrolled within 0.09 ± 0.02 in order to restrict the emitted light to the low loss wavelenght region of optical fibers from 8000 Å to 8500 Å [3]. Provided that the growth is started from 900°C with a solidus composition of $X > 0.09$, X decreases as the cooling interval increases, and subsequently reaches the value of 0.09. Then, just at this temperature, the growth must be terminated by the reason described above.

The analytical method of the deposition path described in chapter III provides a very powerful technique for the analyses on this theme. Using this technique, the solidus composition changing during the cooling cycle from 900°C to 800°C was cal-

culated. The result is shown in Fig.V-2. In this figure, AlAs mole fraction X corresponding to each temperature during the cooling cycle is shown as a function of the aluminum weight introduced into 1 g of gallium. (The unit of Al wight/ 1 g Ga is very useful for the actual growth.) From this figure, both the initial AlAs mole fraction (X_0) at 900°C, and the temperature at which X reaches 0.09 were predicted.
In Fig.V-3, the temperature at which X reaches 0.09 ($\theta_{X=0.09}$) and the solidus composition at 900°C are shown versus the aluminum composition in the liquid. This figure gives complete data for the actual growth of thick layers with controlling the solidus composition at the surface. Another calculation in the same manner will provide the growth conditions for another solidus composition at the surface.

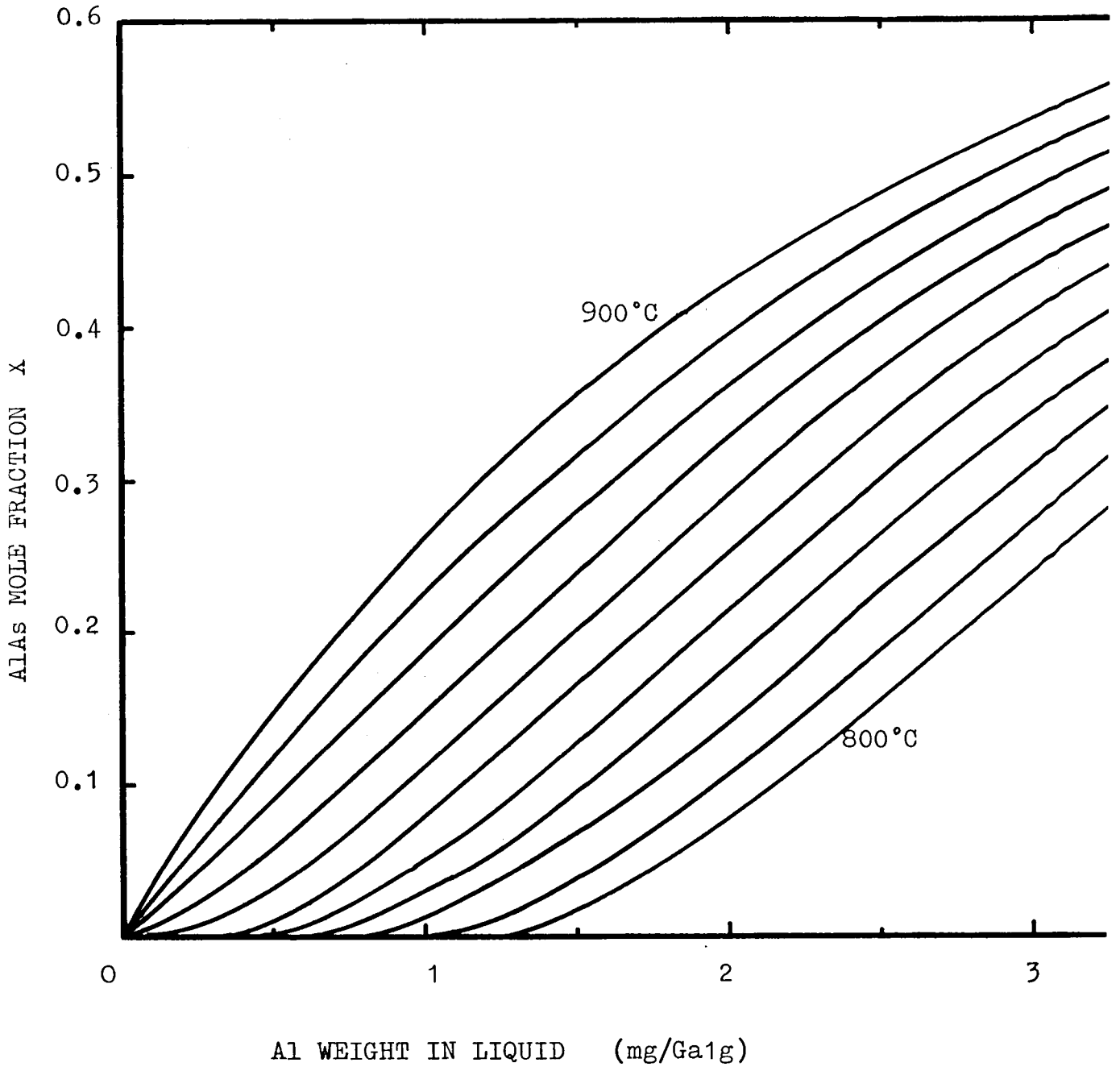

Fig.V-2. Change of AlAs mole fraction during the cooling cycle from 900°C as a function of Al weight in the liquid.

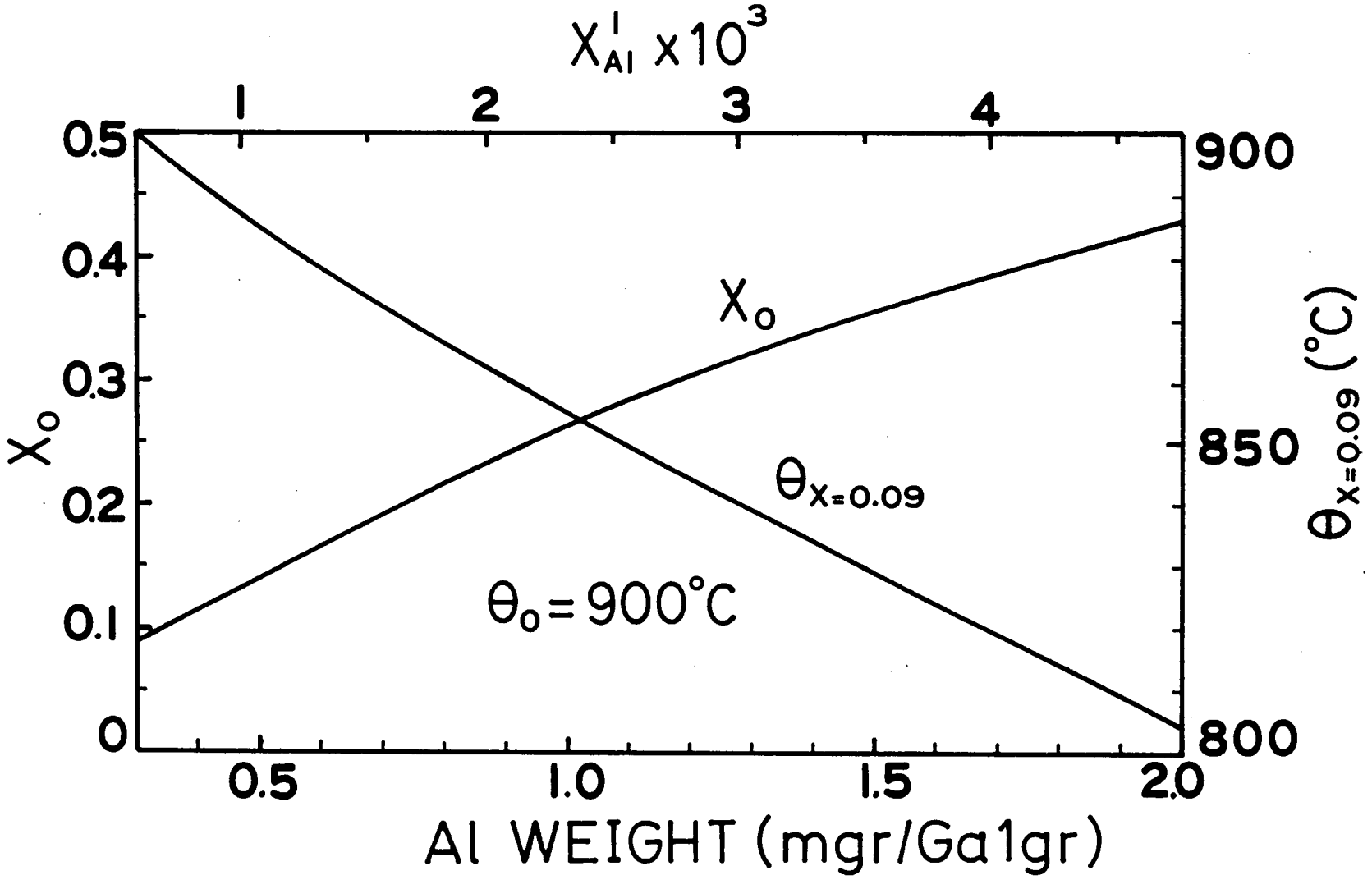

Fig.V-3. AlAs mole fraction at 900°C and the temperature at which X reaches 0.09 as a function of Al weight in the liquid.

V.3. Growth of Thick $Ga_{1-x}Al_xAs$ Layer without Spontaneous Nucleations in The Solution.

To make the growth time to obtain a LPE layer with a certain thickness as short as possible, the growth condition should be chosen as to give a high growth rate. Then, thick melt for the growth might seem to be advantageous for this purpose. However, constitutional supercooling in the melt distant from the substrate is substantially caused as the growth proceeds, and spontaneous nucleation occurs when the melt there is supercooled above the value of a critical supercooling temperature (Δ_c)[4]. In such a case, the volume of the melt which effectively contributes the growth becomes small. Spontaneous nucleations decrease the neighboring solute concentration. This leads to the decrease of the growth rate on the substrate below there, or to the surface irregularity of the LPE layer. Consequently, to optimize the growth condition for thick LPE layers, it is neccessary to analyze the maximum melt thickness in which the magnitude of supercooling never exceeds the value of a critical supercooling temperature.

The LPE growth experiments were carried out for this purpose using the same growth system described in chapter IV. The growth was started from 900°C, and was terminated at 840°C. X_O and X_{Al}^L were 0.3 and 2.7×10^{-3}, respectively. Under this condition, the thickness of the solution for the growth (1) was varied for each growth run from 0.6 mm to 3.6 mm. The adopted cooling rate (α) were 0.15, 0.22, and 0.33°C/min. The LPE

layer thickness was obtained by averaging 5 values measured at different positions of the LPE wafer. The results were shown in Fig.V-4. In this figure, the solid line represents the theoretical value predicted by the calculation described in chapter III. In the region of a thin solution, the LPE layer thickness is proportional to the solution thickness, and agrees with the theoretical line. Whereas, the experimental data deviate from the theoretical line as the solution thickness increases. In this region, the layer thickness is weakly dependent on the solution thickness owing to spontaneous nucleation in the solution. Then, the optimum solution thickness (l_o), which is defined as the maximum solution thickness without spontaneous nucleations in the solution, was determined for each cooling rate from the intersection of the theoretcal line and the experimental one. In Fig.V-5, the optimum solution thicknesses are plotted as a function of cooling rates in a logarithmic scale. The data show a clear dependence of l_o on $\alpha^{-1/2}$. Then, the relationship was approximated as follows:

$$l_o = 1.04 \times 10^{-2} \alpha^{-1/2} \quad (\text{in cm}, \alpha \text{ in } ^\circ\text{C/sec}) . \qquad \ldots (V.1)$$

As long as the growth condition conforms to this relationship, the deposition efficiency, which is defined as a ratio between the layer thickness actually deposited and the predicted by the calculation, becomes near 100 % because the spontaneous nucleation in the solution does not occur. The maximum growth rate

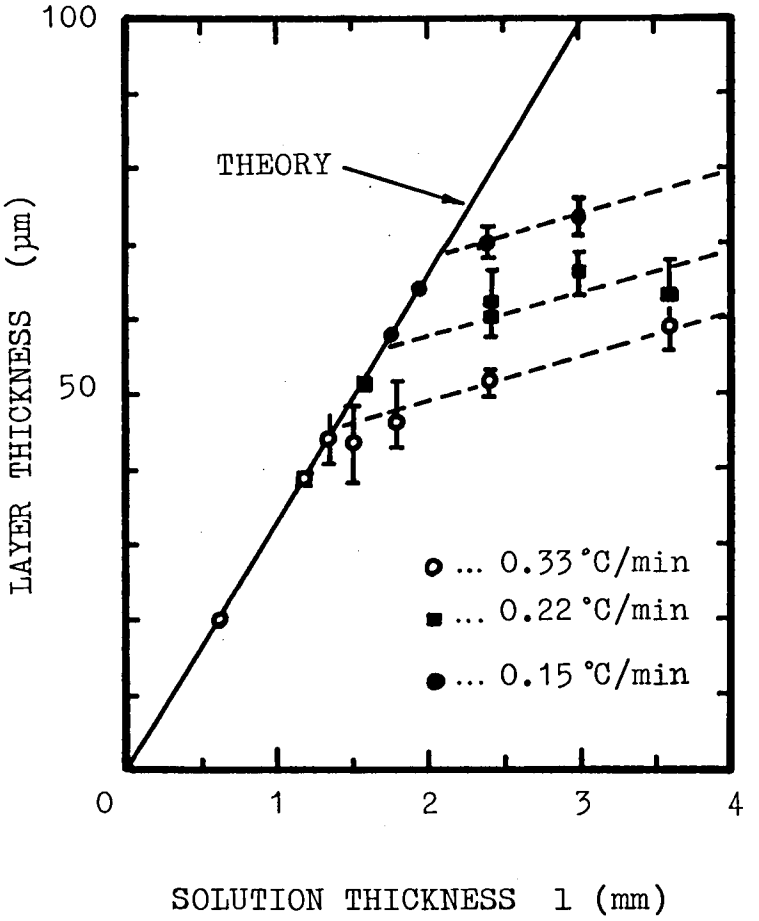

Fig.V-4. LPE layer thickness as a function of the solution thickness.

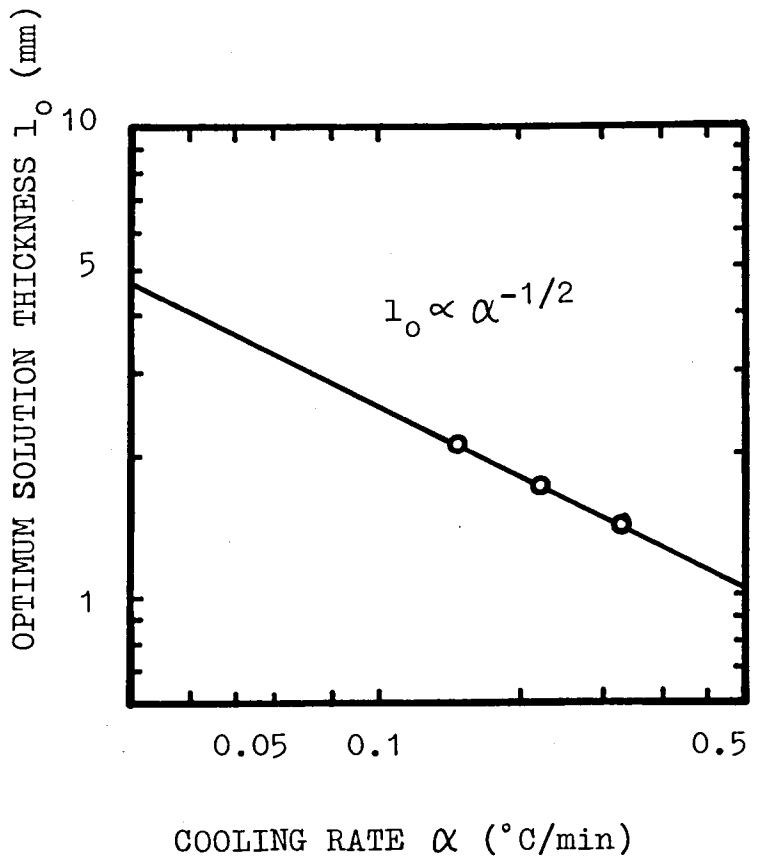

Fig.V-5. Optimum solution thickness as a function of cooling rate.

and the flat surface are also expected by the same reason.

In the previous section, the growth condition of $Ga_{1-x}Al_x$-As is determined when the composition at the surface is fixed at X = 0.09. From the calculation described in chapter III, the layer thickness corresponding to this deposition path can be calculated for a given solution thickness. Reversely, when the layer thickness is given, the optimum solution thickness can be determined. Then, the cooling rate is also determined from eq.(V.1). The results of these analyses are shown Fig.V-6 in a case of a 50 μm thick LPE layer. In this figure, the optimum solution thickness and the corresponding cooling rate are plotted versus the solidus composition at 900°C. This figure and Fig.V-3 give the complete data for the growth of 50 μm thick layers with the control of the surface composition at X = 0.09.

In Fig.V-7, the growth time corresponding to Fig.V-6 is shown. This figure shows that the growth time decreases in the region of $X_0 < 0.4$, whereas, it increases in the region of $X > 0.4$. Then, it can be concluded that the region of $X_0 \simeq 0.3 \sim 0.4$ is advantageous in the actual growth of a 50 μm thick layer.

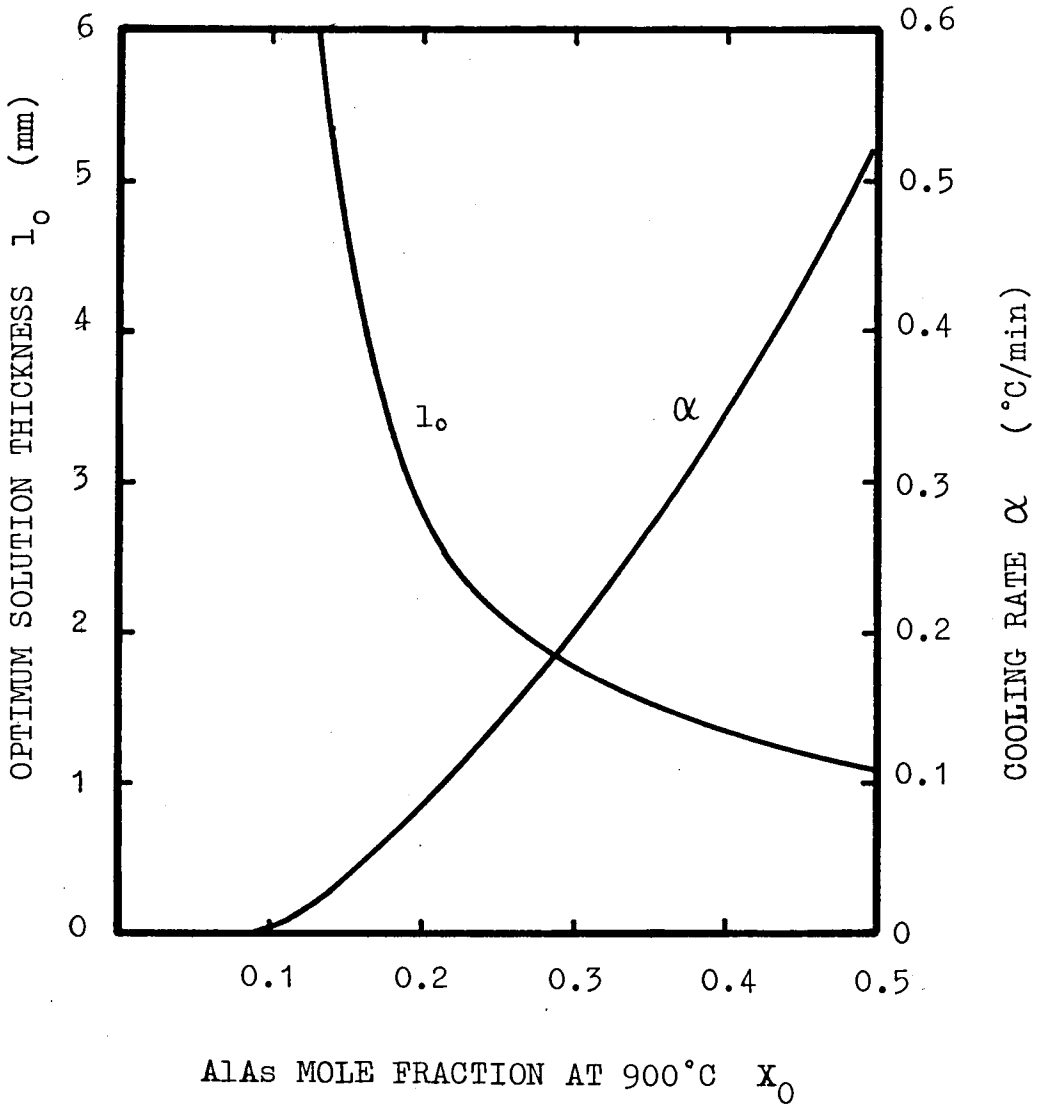

Fig.V-6. Growth condition for a 50 μm thick $Ga_{1-x}Al_xAs$ LPE layer. The optimum solution thickness and the corresponding cooling rate are plotted as a function of AlAs mole fraction at 900°C.

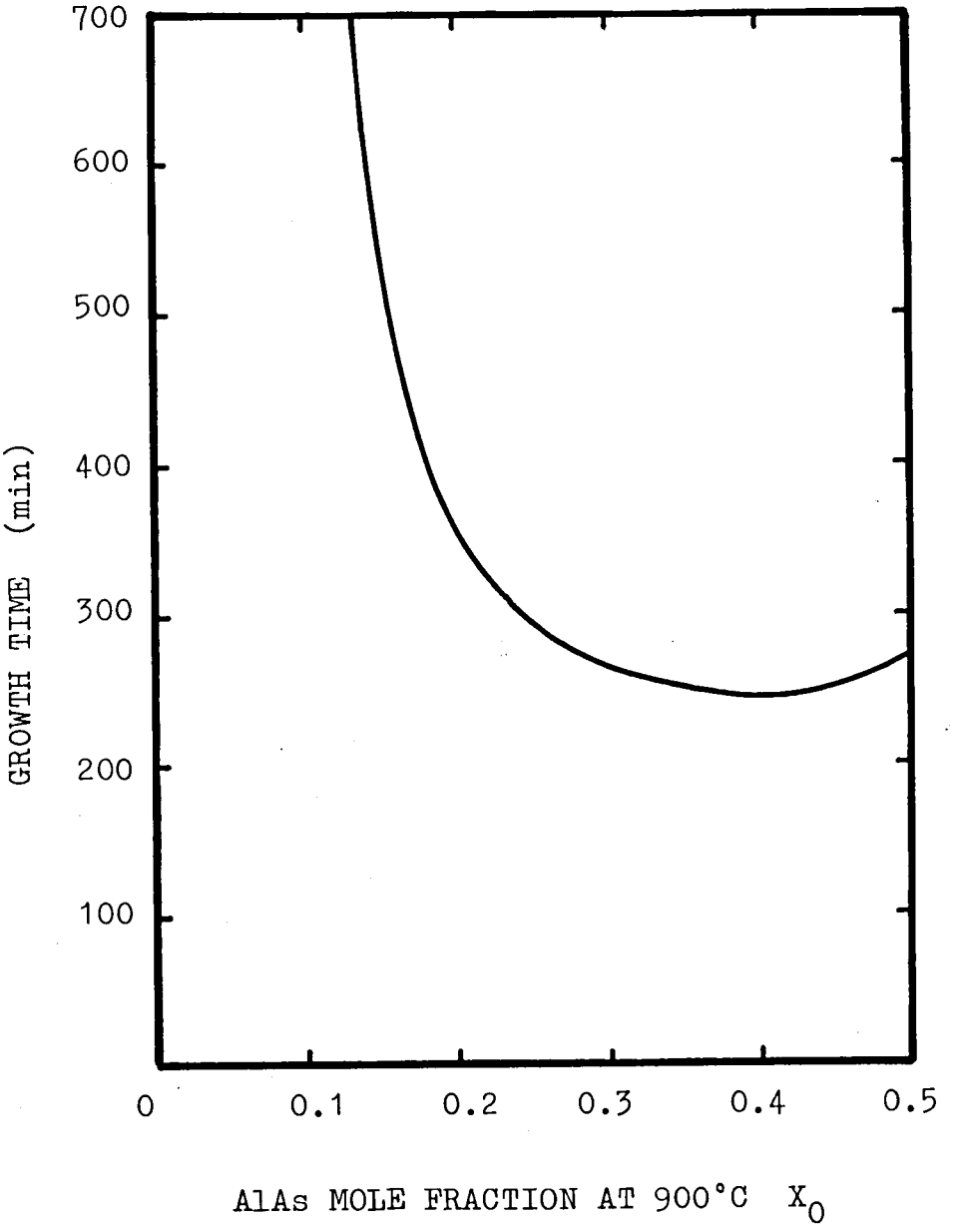

Fig.V-7. Growth time for obtaining a 50 μm thick $Ga_{1-x}Al_xAs$ LPE layer.

V.4. Discussion.

In section V.3, the equation for the optimum solution thickness has been determined, experimentally. The physical meaning of this equation is considered based on the theory. According to the theory described in chapter IV, the solution at the solid-liquid interface is always equilibrated with the solid, whereas the solution at the free surface is most supercooled after the growth is initiated. From eq.(IV.5), the difference of the equilibrium temperature (Δ_θ) between the solution at the interface and the one at the free surface is expressed as follows:

$$\Delta_\theta = m(C(0,t) - C(1,t))$$
$$= \frac{\alpha l^2}{D} \left(\frac{1}{2} - 2 \sum_{n=0}^{\infty} \frac{(-1)^n}{\lambda_n^3} \exp\left(- \frac{\lambda_n^2 Dt}{l^2}\right) \right) . \qquad \ldots (V.2)$$

The second series term in eq.(V.2) comes to zero when Dt becomes much larger than l^2. The growth conditions discussed in this chapter belong to this case. Then, eq.(V.2) is simplified as follows by neglecting the second term:

$$\Delta_\theta = \alpha l^2/2D . \qquad \ldots (V.3)$$

The optimum growth condition described in section V.3 is considered as the one in which Δ_θ does not exceed the value of a critical supercooling temperature. This is alternatively expressed as follows:

$$\Delta_c = \alpha l_o^2/2D \qquad \ldots (V.4)$$

Then, the optimum solution thickness l_o is

$$l_o = (2D\Delta_c)^{1/2}\alpha^{-1/2} . \qquad \ldots (V.5)$$

Comparing eq.(V.5) with eq.(V.1), it is found that the both have the same formula. Assuming that eq.(V.5) is applicable to Ga-Al-As system, Δ_c was calculated from eqs.(V.1) and (V.5) with $D = 1\times10^{-4}$ cm^2/sec. The calculated value is 0.54°C.

This value is too small compared with the reported values in Ga-As system[4)-6)]. However, the critical supercooling temperature is not a physical constant, but is dependent on the surrounding conditions such as the cooling rate and the surface condition of the solution. Bryskiwics[6)] reported that Δ_c decreased as the cooling rate decreased in Ga-As system. Ijuin and Gonda[7)] reported Δ_c in Ga-Al-As system was 2.5°C when the cooling rate was 1°C/min. This value is much lower than the value of 6°C in Ga-As system[4)] at the same cooling rate. These facts imply that the present small value in Ga-Al-As system is probable at such low cooling rates.

V.5. Conclusions.

Growth conditions for obtaining a 50 μm thick $Ga_{1-x}Al_xAs$ LPE layer were analyzed based on the theories described in the preceding chapters.

From the calculation of the solidus composition changing, the relationship between the liquidus composition at 900°C, and the temperature at which solidus composition X reaches 0.09 was obtained in a case of the growth from 900°C.

To optimize the growth condition for obtaining a 50 μm thick LPE layer, LPE growth experiments from 900°C were carried out using the same growth apparatus described in chapter IV. The results of the experiments revealed the relationship between the LPE layer thickness and the solution thickness. In the region of a thin solution, the LPE layer thickness was proportional to the solution thickness, and agreed with the theoretical value. Whereas, the experimental data deviated from the theoretical values as the solution thickness increases, because spontaneous nucleations in the solution caused in such a thick solution reduced the growth rate on the substrate. From these experimental results, the optimum solution thickness, which is the maximum solution thickness without causing spontaneous nucleations in the solution, was found to be proportional to the cooling rate taken to the -1/2 power. Finally, the cooling rate, the optimum solution thickness, the initial solidus composition at 900°C, and the growth time were reciprocally related with one another.

From the theory based on a diffusion limitted growth model, a equation which explained the experimentally obtained relation between the cooling rate and the optimum solution thickness was derived. The comparison between the theory and the experiment gave a value of a critical supercooling temperture Δ_c = 0.54°C when D = 1×10^{-4} cm^2/sec. Although this value is small compared with the one in Ga-As system, it is probable at such low cooling rates adopted in this study.

REFERENCES OF CHAPTER V.

(1) C. A. Burrus and B. I. Miller, Opt. Commun. 4 (1971) 307.

(2) M. Abe, O. Hasegawa, Y. Komatsu, Y. Toyama and Y. Yamaoka, IEEE Trans. Electron Dev. 25 (1978) 1344.

(3) Y. Suematsu and K. Iga, Introduction to Optical Fiber Transmissions. (Ohom-sha, Tokyo 1976) chap. 7.

(4) A. Doi, T. Asano and M. Migitaka, J. Appl. Phys. 47 (1976) 1589.

(5) M. B. Small and I. Crossley, J. Crystal Growth 27 (1974) 35.

(6) T. Bryśkiewicz, J. Crystal Growth 43 (1978) 101.

(7) H. Ijuin and S. Gonda, J. Electrochem. Soc. 123 (1976) 1109.

VI. EPITAXIAL GROWTH OF THICK FILMS WITH A MULTIPLE-LAYERS STRUCTURE.

VI.1. Introduction.

In the previous section, the growth condition to obtain a 50 μm thick $Ga_{1-x}Al_xAs$ layer were given from the theoretical and experimental analyses. Homojunction LEDs fabricated from such thick LPE wafers by zinc diffussion have shown a high output power because the emitted light is free from the bulk absorption[1]. However, heterostructures are required for higher perfomances of LEDs, because the high current density and low thermal resistance are essential for high coupling efficiency into optical fibers[2].

In Fig.VI-1, the structure of a LED suitable for this purpose is schematically shown[3]. The LPE wafer consits of a 50 μm thick window layer and the subsequent thin layer for the carrier confinement. Whereas, to achieve this structure, there exsists such a difficulty that the precise control of both the composition and the layer thickness in the subsequent thin layer is required after the growth of the first thick layer. Moreover, a smooth photoprocessable surface is also required for the formation of fine electrode patterns at the surface.

In chapter II, it was reported that a conventional sliding method as shown in Fig.II-5 was disadvantageous because of the formation of Al_2O_3 scums on the surface of the melt, and the resultant irregularity of the LPE layer. The growth apparatus

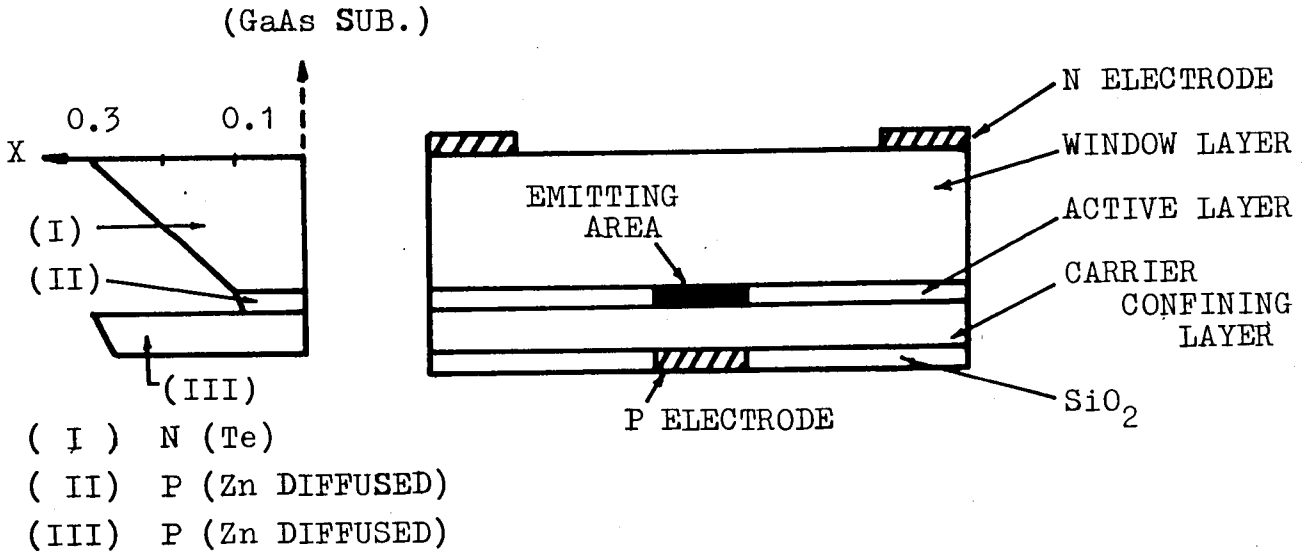

Fig.VI-1. Schematic illustrations of $Ga_{1-x}Al_xAs$ LED, and the LPE wafer.

shown in Fig.IV-6 improved these points by introducing the GaAs source wafer beneath the solution. In this system, the bottom of the solution, which is in contact with the substrate during the growth cycle, is protected from the oxidation during the heating cycle. Then, the LPE wafers by this system were free from the scums. However, a part of the solution was always left on the partially disolved source wafer. If the same structure as this is adopted in the growth apparatus for the multiple-layers, this will lead to the cross contamination between the solutions in adjacent bins.

It was also reported, in chapter II, that the solution removal after the growth could not be sometimes accomplished in the growth of thick LPE layers. This was caused by the the excess growth at the edges of the wafer, which interrupted a smooth slide of the bin in the result. This problem must be overcome in the growth of muptiple-layers, by all means.

In this chapter, a new LPE growth method developed for the growth of a thick $Ga_{1-x}Al_xAs$ wafer with a multiple-layer structure is described. It will be found that this method is very powerful in overcoming the difficulties described above.

VI.2. A New LPE Growth System.

As is analyzed in chapter V, the cooling interval of a few ten's is required to obtain a 50 μm thick $Ga_{1-x}Al_xAs$ LPE layer. In the growth of two LPE layers as shown in Fig.VI-1, during the growth of the first thick layer, the soution for the second layer is also cooled. Then, if the conventional sliding system as shown in Fig.I-7 is used for the growth, the second solution will be covered with precipitated $Ga_{1-x}Al_xAs$ because the magnitude of the supercooling is a few °C at most. To improve this point, it is neccessary to equilibrate the second solution with the solid during the growth of the first thick layer.

The growth system shown in Fig.VI-2 was designed as to improve this points and the ones described in the previous section. In this figure, a noticeable characteristic is that all the surfaces of the solutions except for the upper ones are in contact with the GaAs sources before the growth. They are used for both arsenic sources into the solutions, and the saturation seeds. Each GaAs source is dissolved and is equilibrated with each saturated solution before the growth of first layer (Fig.VI-2(a)). Then, the first solution and the second one are slid from each bottom source wafer onto the substrate and the first source wafer, respectively (Fig.VI-2(b)). During the growth of the first thick layer, the solidus deposition from the second solution onto the first source wafer results in keeping the solution in a equilibrium condition.

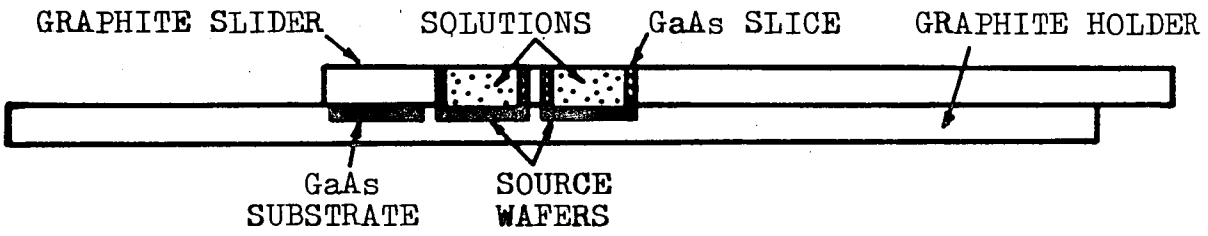

(a) Prior to the growth.

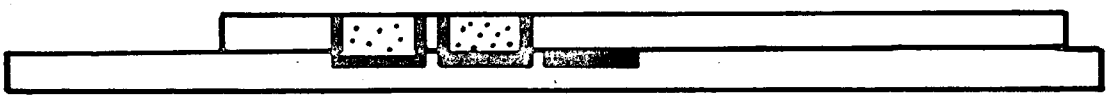

(b) 1st layer growth.

(c) 2nd layer growth.

(d) After the growth.

Fig.VI-2. A sliding boat for the growth of multiple layers.

After the growth of the thick layer, the second thin layer growth is initiated by sliding the second solution from the second source wafer onto the substrate. Since the solution has been equilibrated with the source wafer just before the growth of this layer is initiated, the precise control of both the thickness and the composition can be expected as shown later.

Another difficulty caused by the excess edge growth can be overcome by the effect produced by the GaAs source slices surrounding the solution. The excess edge growth is related to the relatively high convection transport of the solute caused by the direct heat transport between the edges of the solution attached to the bin walls of the graphite boat[4]. Since the solution shown in Fig.VI-2 is not attached directly to the bin walls, but is in contact with the GaAs source slices, the convection transport of the solute is thought to decrease. In addition to this effect, the deposition onto these slices decreases the gradient of the solute concentration at the edge of the solution, and leads to the suppression of the growth rate there. The experimental evidence of this effect will be shown in the following section.

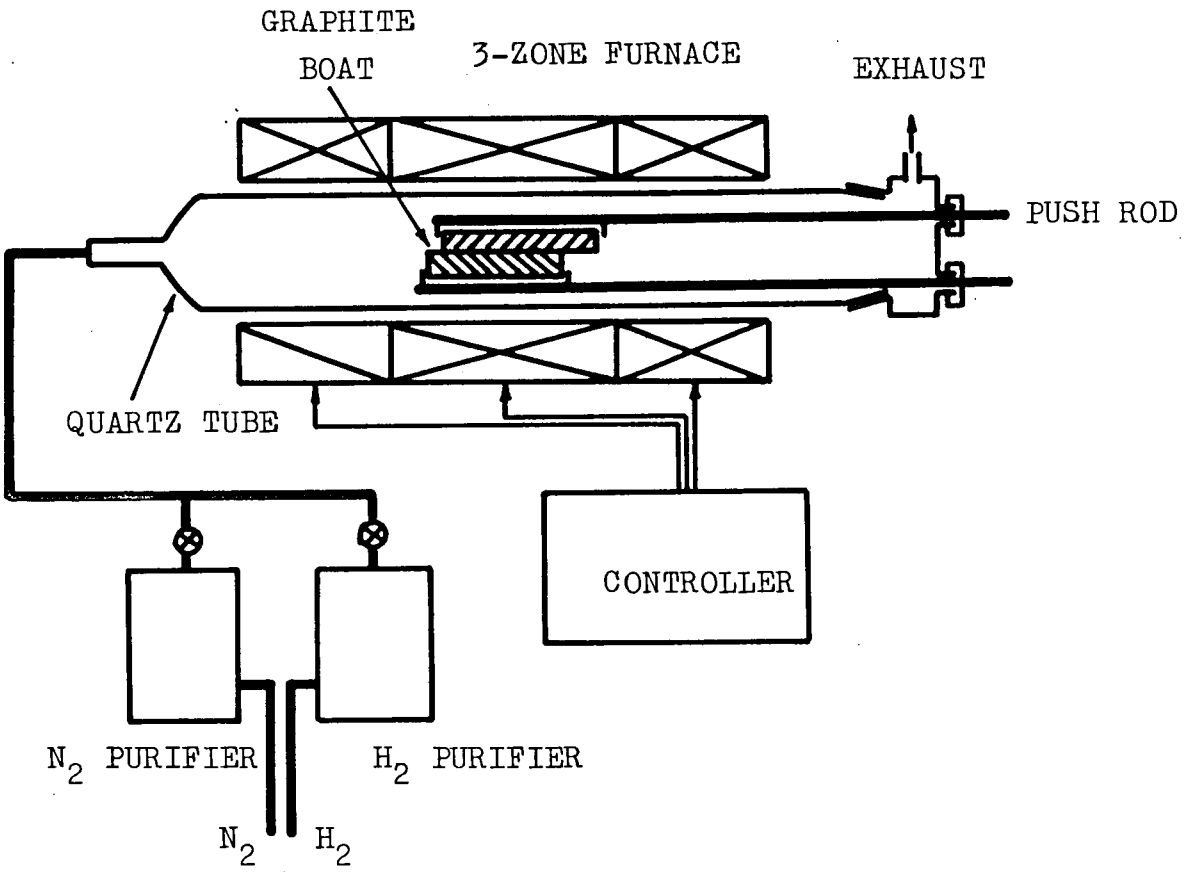

Fig.VI-3. Schematic illustration of the growth system.

VI.3. LPE Growth of Multiple Layers.

Growth experiments of the $Ga_{1-x}Al_xAs$ LPE wafer for LEDs shown in Fig.VI-1 were carried out using the sliding boat described in the previous section. A schematic illustration of the whole growth system is shown in Fig.VI-3.

Figs.V-3 and V-6 in chapter V give a sufficient knowledge of the growth condition for the first thick layer. In a multi-layers growth, a subsequent thin layer is grown from the temperature at which the growth of the first layer is terminated. From the requirement of the carrier confinement, the composition of the second layer should be chosen as X = 0.3. Since, in the present growth system, the second solution is also saturated at 900°C, and is cooled down to the temperature at which the the composition of the first layer comes to 0.09, the composition of the solid deposited from the second solution has been also changing until the growth of the second layer is initiated. Consequently, the similar alaysis on the composition changing is neccessary to control the composition of this layer at X = 0.3. In Fig.VI-4, the result of this analysis is shown with the condition for the first layer. In this figure, aluminum weight for the second solution which gives the composition of X = 0.3 at the end temperature of the first layer. In Fig.VI-5, the cooling rate and the optimum solution thickness are shown using the same horizontal scale as Fig.VI-4.

Any growth condition shown in Figs. VI-4 and VI-5 will give the LPE wafer with the 50 μm thickness and the

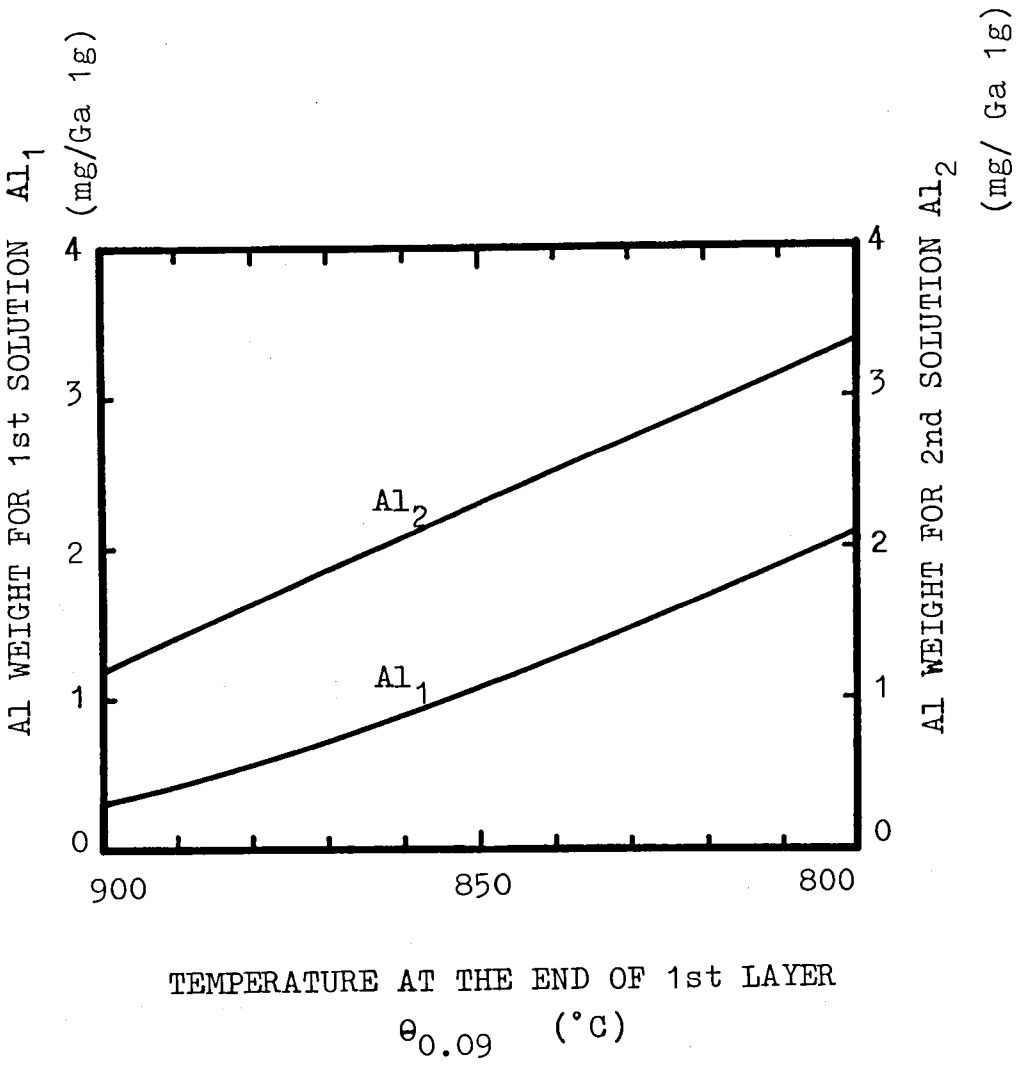

Fig.VI-4. Al wights for the first solution (Al_1) and the second solution (Al_2) as a function of the temperature at which the growth of the first layer is terminated.

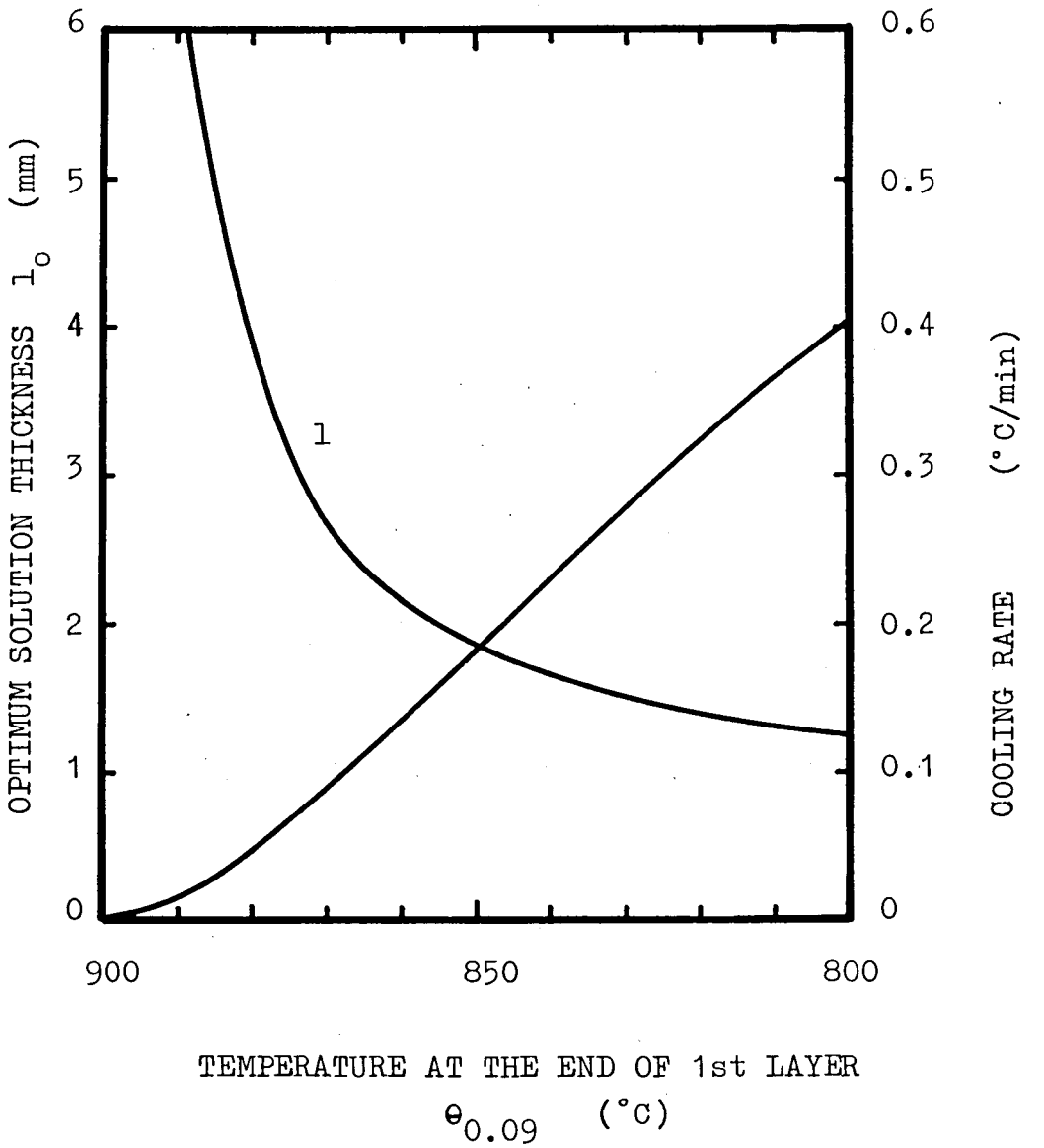

Fig.VI-5. Optimum solution thickness and the corresponding cooling rate as a function of the temperature at which the growth of the first layer is terminated.

desired compositions. From the points of the growth time and the magnitude of the composition distribution in the thick layer, the cooling rate, the solution thickness, and the cooling interval for the growth of the first layer were determined as 0.22 °C/min, 1.6 mm, and 60°C, respectively. Since the growth area was 5.8 cm^2, the total weight of gallium for the solutions was 5.2 g. From Fig.VI-4, the weights of aluminum for the first and the second solutions were determined as 1.3 mg/Ga 1g and 2.5 mg/Ga 1g, respectively. Tellurium was used for n-dopant in the first layer, and the second layer was undoped.

The cooling interval for the second thin layer (Δ_2) was determined from the result of the growth experiments in which only Δ_2 was varied with fixing the cooling interval for the first layer at 60°C. From the result shown in Fig.VI-6, the growth rate of the second layer is known 0.6 μm/°C. Then, Δ_2 = 3.5°C for 2 μm thickness was finally determined.

In Figs.VI-7, VI-8, and VI-9, the photographs of the as-grown wafer, and the cross sectional views at the center and the edge of the LPE layers are shown, respectively. The surface of the LPE wafer was enough smooth for photoprocessings, and any kind of surface defect was not observed. As is shown in Fig.VI-9, the layer thickness at the edge region continuously decreased toward the outside of the wafer. This means the GaAs source slices surrounding the solution were effective for suppressing the excess edge growth.

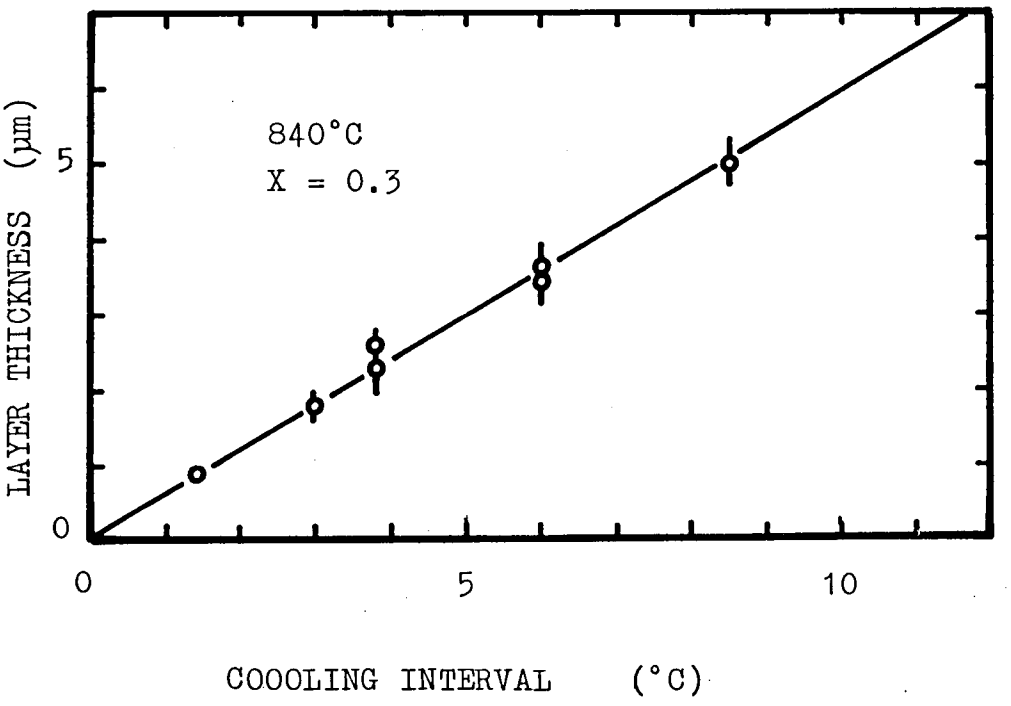

Fig.VI-6. LPE layer thickness of the second layer as a function of the cooling interval.

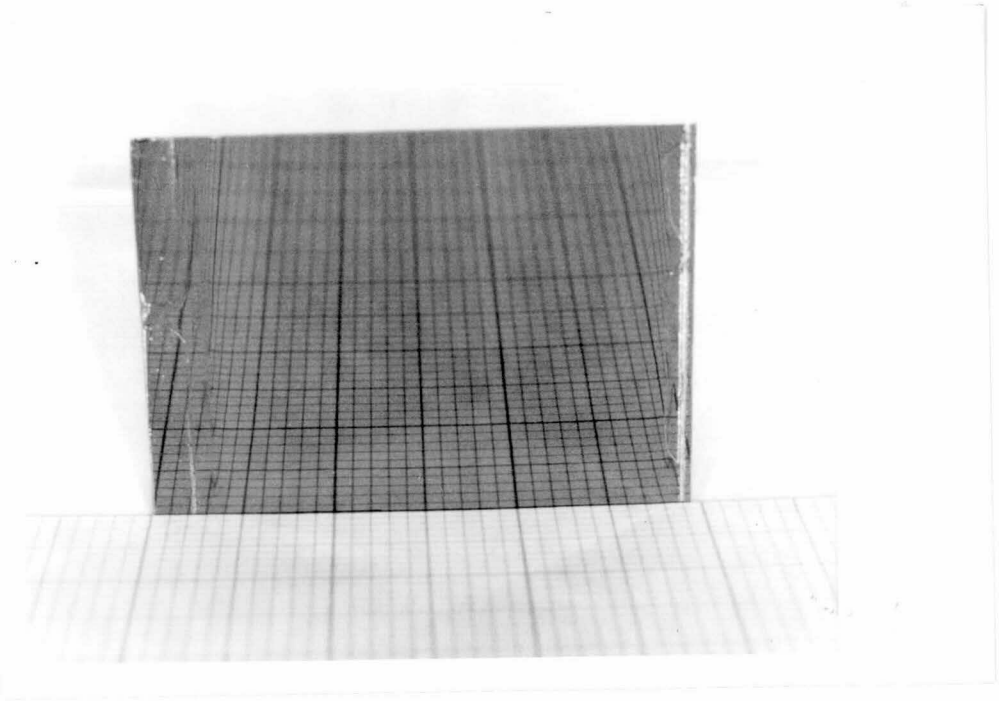

Fig.VI-7. A photograph of the surface of the as-grown LPE wafer.

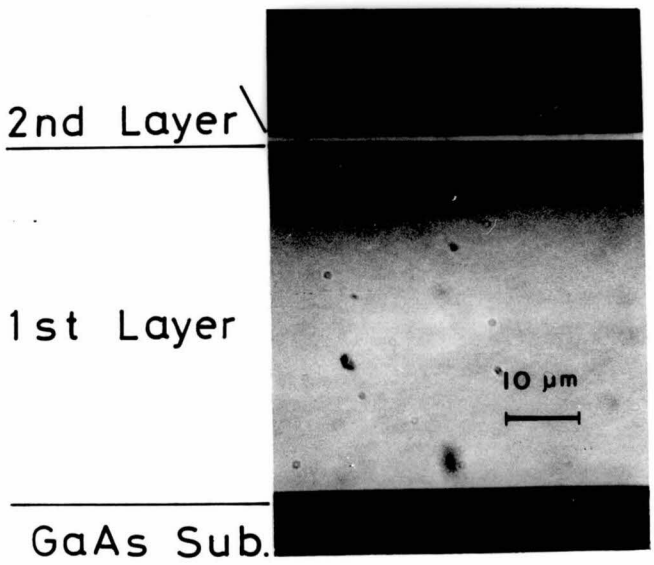

Fig.VI-8. A cross sectional view of the LPE wafer at the center of the grown area.

Fig.VI-9. A cross sectional view near the edge of the LPE layer.

VI.4. Discussion.

A thick and multistructured $Ga_{1-x}Al_xAs$ has been desired as a LPE wafer for LEDs used in optical-fiber communications. However, it has been thought difficult to realize such a structure by a temperature-cooling method. Then, Ueyanagi et al[5] grew single-heterostructured p-n layers on a polished thick $Ga_{1-x}Al_xAs$ LPE layer which was obtained by a temperature gradient method[6], and fabricated spherically-shaped LEDs. Whereas, such a two-stage growth technique is thought useless in the actual productions. On the other hand, the sliding method, which is one of temperature-cooling methods, enables us to grow multilayers at one cooling cycle. Although this point is very attractive, there exsisted some difficulties in the preparation of such thick LPE wafers by a conventional sliding method.

A new LPE growth system was developed for this purpose. It was found that the developed growth system was effective for the suppression of the excess edge growth and the equilibration of each solution at any time during the growth cycle. As is well known, the excess edge growth often causes poor wiping of the solution after the growth of the final layer, or cross-contamination between solutions in adjacent bins. This leads to a fatal problem in the growth of thick layers because the amount of the excess edge growth becomes larger as the LPE layer is grown thicker. In the present system, GaAs slices surrounding the solution completely solved this problem. Besides, they contributed to completely wiping the solution from the substrate,

or the source wafer by the force of the adhesion to themselves

Another important point in the present system exists in the thin solutions. The solution thickness adopted in the present work is 1.6 mm for the cooling rate of 0.22°C/min. A thicker solution or a higher cooling rate would result in a irregular thick layer because of the effect of the spontaneous nucleations in the solution. In Fig.VI-10, a photograph of the surface of the LPE wafer grown at a cooling rate of 1°C/min. The irregularity of the surface is obvious from this figure.

The analytical approach described in chapter V, and the growth technique described in this section are applicable to the growth of a more complicated multilayers. From a point of the device performance, a double heterostructure is promissing because a less absorption of the emitted light in the window layer, and a higher density of carriers confined in the active layer are expected. However, a higher AlAs concentration in the window layer is required in such a structure. This leads to a lower growth rate and the larger cooling interval for the window layer. Although these difficulties will cause a longer growth period, it is believed that the same approach will realize such a structure[7].

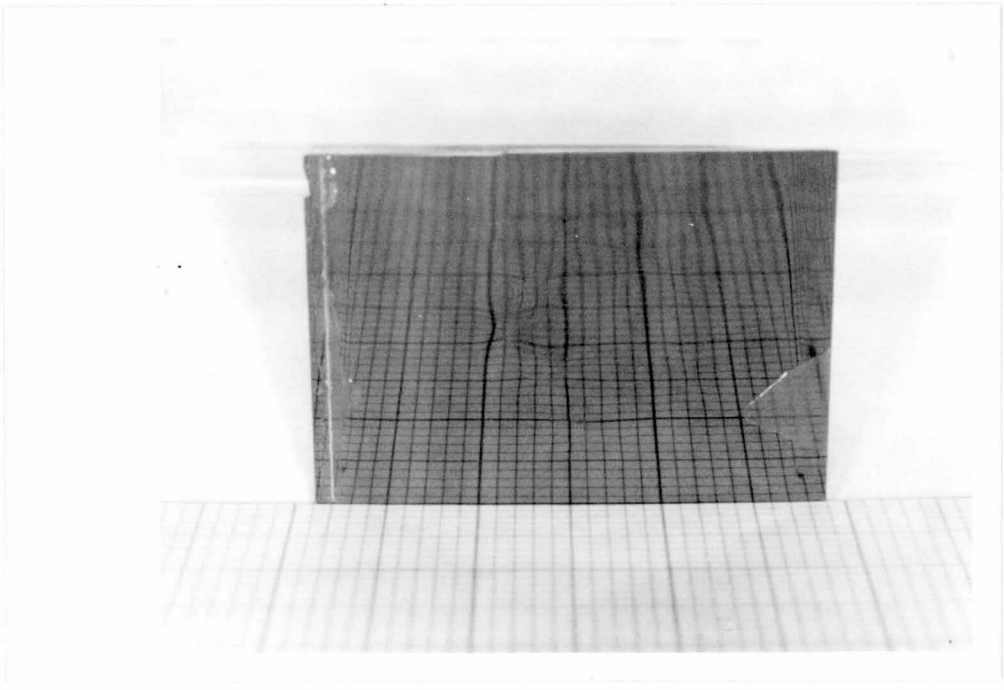

Fig.VI-10. A photograph of the surface of the as grown LPE wafer which was grown at a high cooling rate.

VI.5. Conclusions.

A new sliding system was developed for the LPE growth of thick $Ga_{1-x}Al_xAs$ wafers with a multiple-layers structure. The growth apparatus was designed as to suppress the excess edge growth, and to equilibrate the solution with the solid during the whole cooling cycle.

The growth conditions for a 50 μm thick window layer and the 2 μm thick subsequent thin layer were determined by the analyses based on the theory described in chapter V. The solution thickness and the cooling rate were 1.6 mm and 0.22 °C/min, and the aluminum weight for the first and second layers were 1.3 mg/Ga1g and 2.5 mg/Ga1g, respectively.

The LPE wafers obtained by the experiment were found to contain photoprocessable surfaces and the expected values of both the compositions and the thicknesses. The suppression of the excess edge growth and the wiping of the solution after the growth were completely accomplished. Then, it is concluded that the developed growth system is very powerful for the preparation of thick $Ga_{1-x}Al_xAs$ wafers with a multiple-layers structure. The application of this system to LPE growth for other devices will be also possible.

REFERENCES OF CHAPTER VI.

(1) Y. Komatsu, S. Isozumi and T. Kotani, FUJITSU Scientific and Technical J. 12 (1976) 125.

(2) O. Hasegawa, M. Abe and T. Yamaoka, J. Appl. Phys. 49 (1978) 4353.

(3) M. Abe, I. Umebu, O. Hasegawa, S. Yamakoshi, T. Yamaoka, T. Kotani, H. Okada and H. Takanashi, IEEE Trans. Electron Device ED-24 (1977) 990.

(4) R. L. Rode and R. G. Sobers, J. Crystal Growth 29 (1975) 61.

(5) K. Ueyanagi, K. Ito, Y. Ono and K. Kurata, OYOBUTSURI 44 (1975) 971.

(6) L. E. Stone, K. Kadden and R. W. Haisty, J. Electronic Mater. 1 (1972) 111.

(7) M. Abe, O. Hasegawa, Y. Komatsu, Y. Toyama and T. Yamaoka, IEEE Trans. Electron Dev. 25 (1978) 1344.

VII. CHARACTERISTICS OF $Ga_{1-x}Al_xAs$ LIQUID PHASE EPITAXIAL FILMS.

VII.1. Introduction.

$Ga_{1-x}Al_xAs$ LPE wafers described in the previous section were used for LEDs for fiber-optical communications. As is well known, semiconductor devices for communication systems are required for very high reliabilities. In order that a communication system has been operating without any trouble for over than one year, each component in the system must be alive for over than ten years. This value of the device life time is, at present, assured in silicon devices owing to intensive efforts by many workers.

On the other hand, studies on reliabilities of opto-electroni devices using III-V compounds are still in the early stage. Degradations in these devices sometimes look very complicated, and differnt from that of silicon devices. One of the reasons of this problem is that III-V compound crystals contain many complex defects in themselves. Another reason is that these devices utilize the recombination process of minority carriers. This process is strongly influenced by the crystal defects, and multiplies themselves. Mutual interactions between the recombination process and the crystal defects make it very difficult to understand the degradation phenomena in these devices.

In this chapter, characteristics of $Ga_{1-x}Al_xAs$ LPE films are described from the points of the degradation phenomena in LEDs. Fabrication processes and some properties of the LEDs

are also described for better understandings.

VII.2. Structure and Properties of $Ga_{1-x}Al_xAs$ Light Emitting Diodes[1].

$Ga_{1-x}Al_xAs$ LEDs shown in Fig.VII-1 were fabricated from the LPE wafer as follows. First, zinc was diffused to convert both the X = 0.09 region of the first layer and the second layer into p-type at 710°C in a quartz ampoule for 6 hours. $ZnAs_2$ was used as a source at 650°C. The thickness of the active layer was about 0.7 μm. By this fabrication method, a peak emission wavelength of about 8000 Å was obtained to match the low-loss spectral range of the fiber. The emitting area was defined by the Au-Zn p-electrode, whose diameter was chosen to be 35 μm. The plated gold heat sink with the thickness of about 20 μm was used to facilitate heat removal. Finally, the GaAs substrate was removed to extract the light, and then, the Au-Ge-Ni n-electrode was formed as shown in Fig.VII-1. The size of the LED chip is 500 μm. A cross-sectional view of the LED-fiber mounting package is shown in Fig.VII-2. The spherical-ended fiber had a length of 3 cm and is fixed to the cap by the epoxy. The cap with the fiber is adjusted to the LED by monitoring the optical output power from the fiber, and then fixed to the stem.

Electrical and optical characteristics of the fiber-mounted LEDs were measured at an ambient temperature of 20°C. Fig.VII-3 shows the output powers from the fiber end (P_f) and from the LED chip (P_c) as a function of forward current (I_f). At a forward current of 100 mA, the LED had a P_f of 305 μW and a P_c of 4.7 mW. The output power increased almost linearly up to about

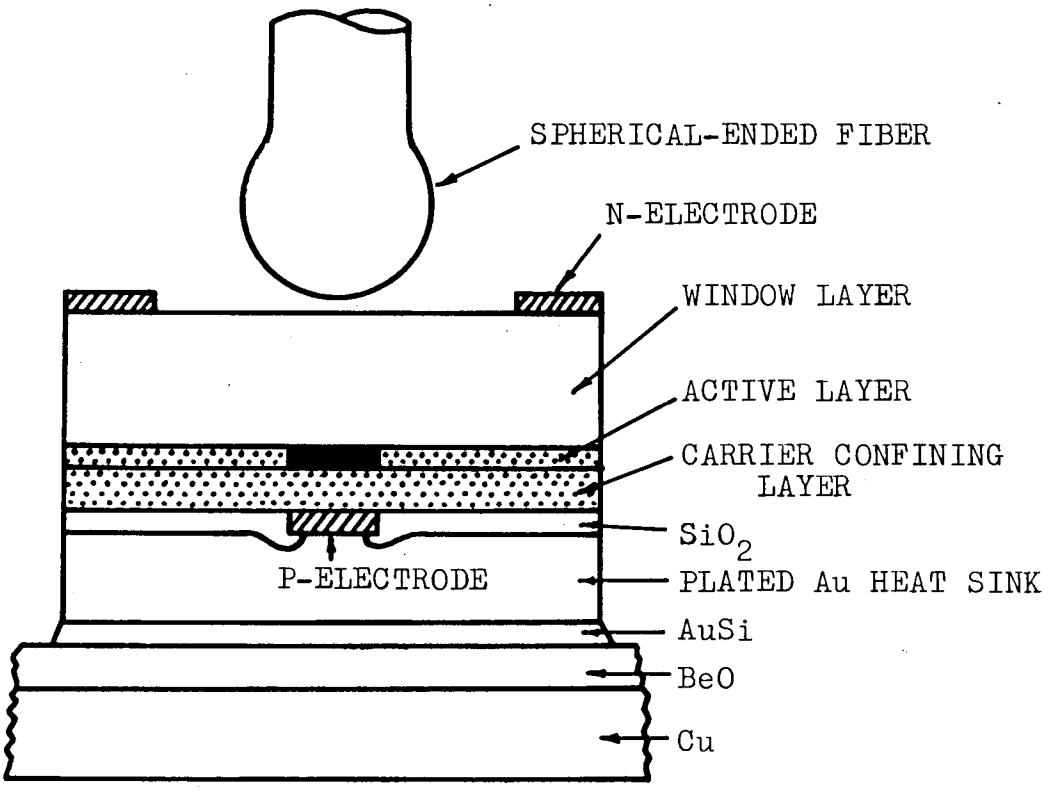

Fig.VII-1. Structure of the fiber-mounted $Ga_{1-x}Al_xAs$ LED.

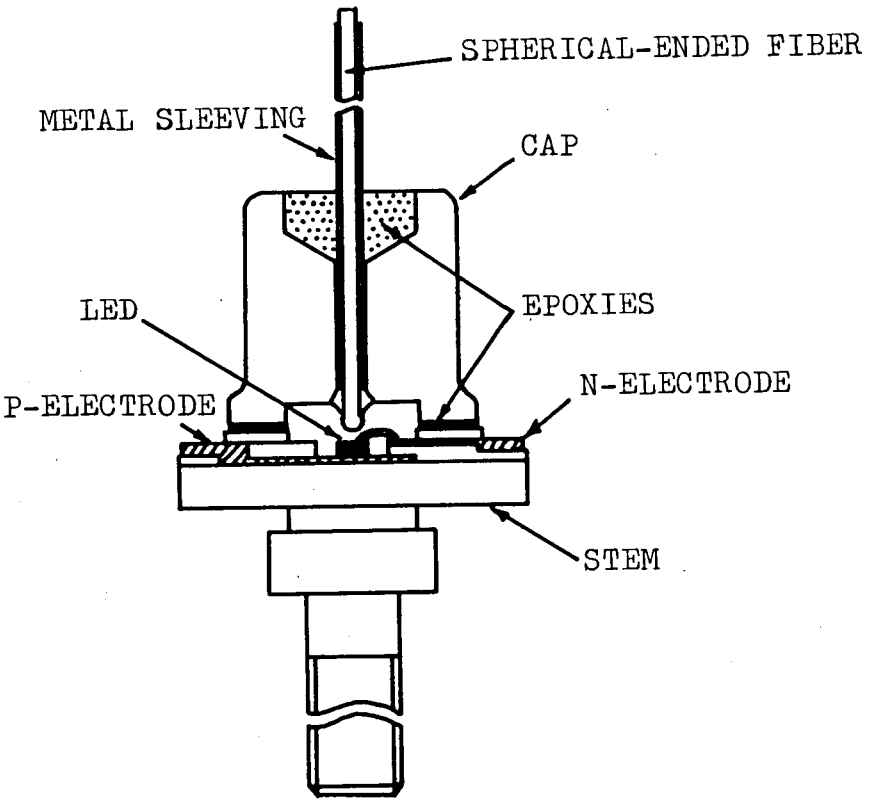

Fig.VII-2. Cross sectional view of the LED-fiber mounting package.

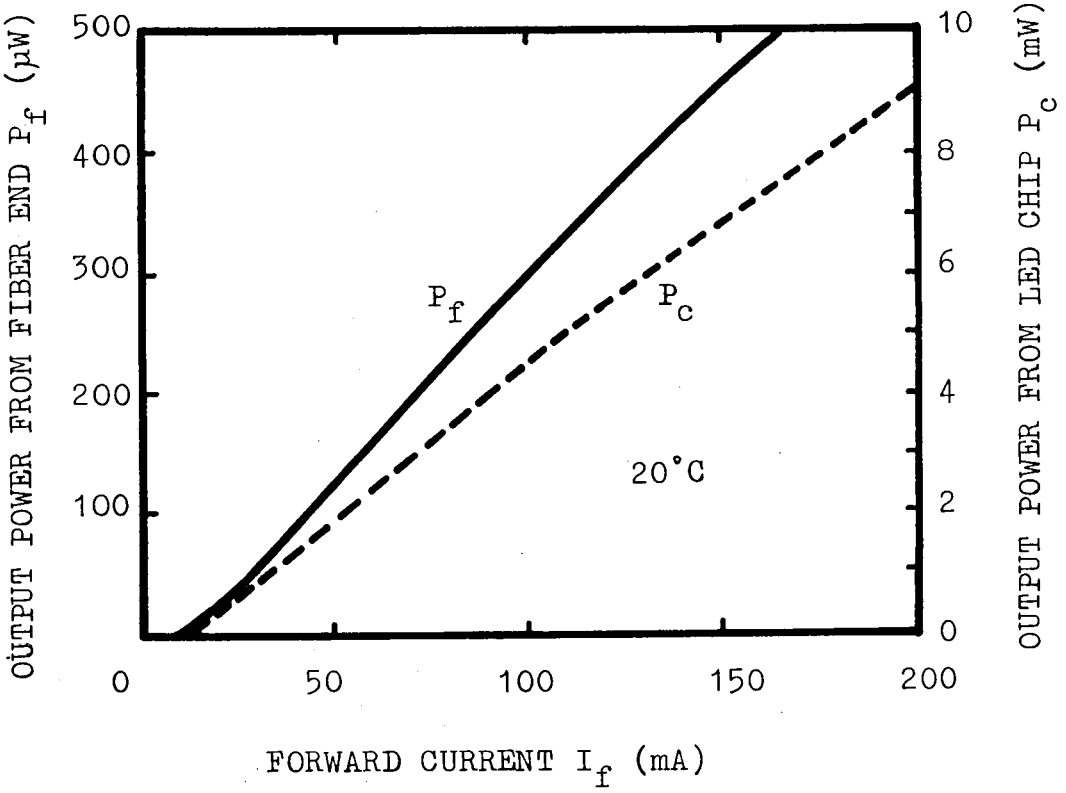

Fig.VII-3. Optput powers from the fiber end P_f and from the LED chip P_c as a function of the forward current I_f.

200 mA as seen in this figure. Typical emission spectra of this LED are shown in Fig.VII-4, in the conditions of forward currents of 50, 100, and 150 mA, respectively. The peak emission wavelength was 8010 Å and the half spectral width was very narrow (200 Å) at a current of 100 mA. This narrow emission spectrum is mainly caused by the interband transition. By increasing the current, the peak position of the emission shifted to shorter wavelength due to band filling at a sufficiently low current level. As seen from this figure, multi-peak emission spectra were observed as a result of an optical interference effect in the LED chip.

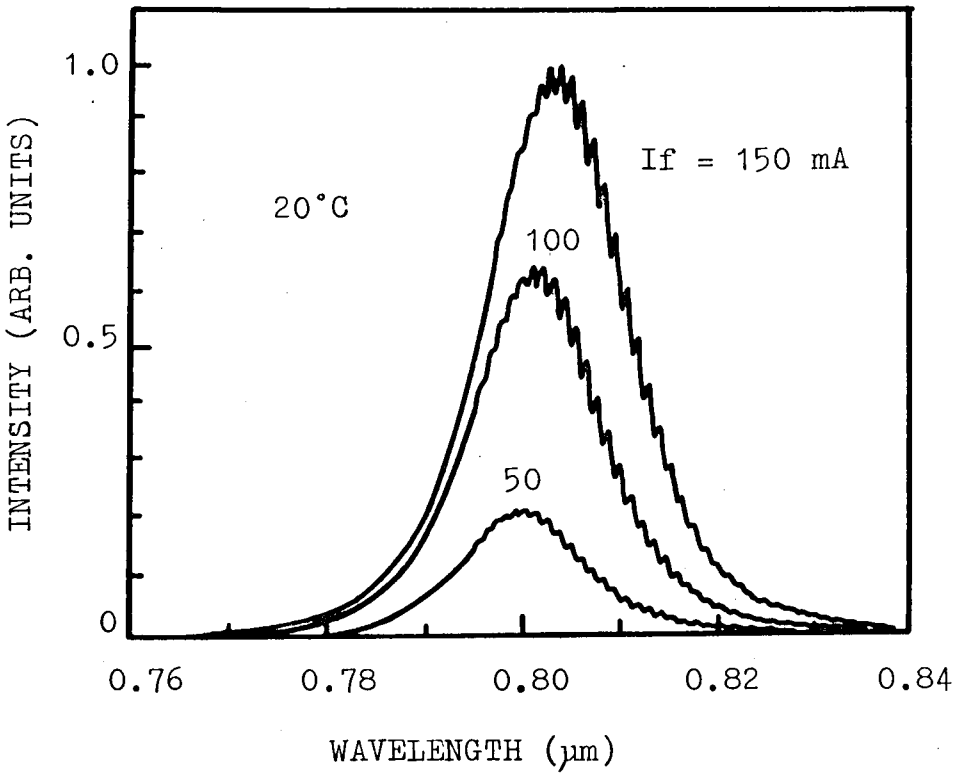

Fig.VII-4. Typical forward-current dependence of emission spectra.

VIII.3. Degradation Phenomena of $Ga_{1-x}Al_xAs$ Light Emitting Diodes[2),3)].

The light output power of the LED usually decreases with respect to the operating time. This phenomenon is called "degradation", and occurs in almost all light emitting devices. In Fig.VII-5, the normalized output power from the LEDs described in the previous section is shown as a function of operatimg time. It is obvious that there are three tipes of samples. Sample (A) shows a constant output power within the operating time of 100 hours. Whereas, samples (B) and (C) show rapid decreases of the output power in the eary stage of the operation. The output power of sample (D) increases with respect to time, but such a case was very rare. The increasing trend of the output power in this sample may be responsible to a poor contact of electrodes. In Fig.VII-6, electroluminescence micrographs of the emitting areas in the samples (A) and (B) are shown. Fig.VII-6(a) shows the sample (A) emits the light uniformly. Whereas, there are dark regions in the emitting area of the sample (B) as shown in Fig.VII-(b). In these regions, it looks like that linear non-radiative defects oriented to <110> and <100>direction are gathering. They are called "dark line defects (DLDs)" in relation with their linear shapes. Hasegawa et al.[2)] and Yamakoshi et al.[3)] reported that DLDs were always observed in the degraded LEDs like the samples (B) and (C), and they were generated in an early stage of the operation. They also reported the LEDs free from DLDs could be selected after 100 hours operation with

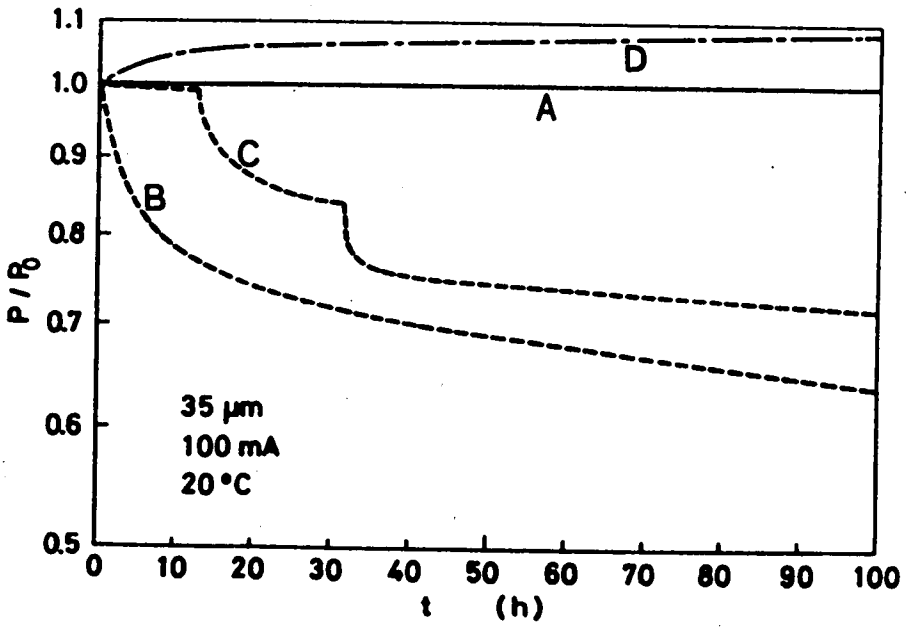

Fig.VII-5. Normalized output power as a function of operating time.

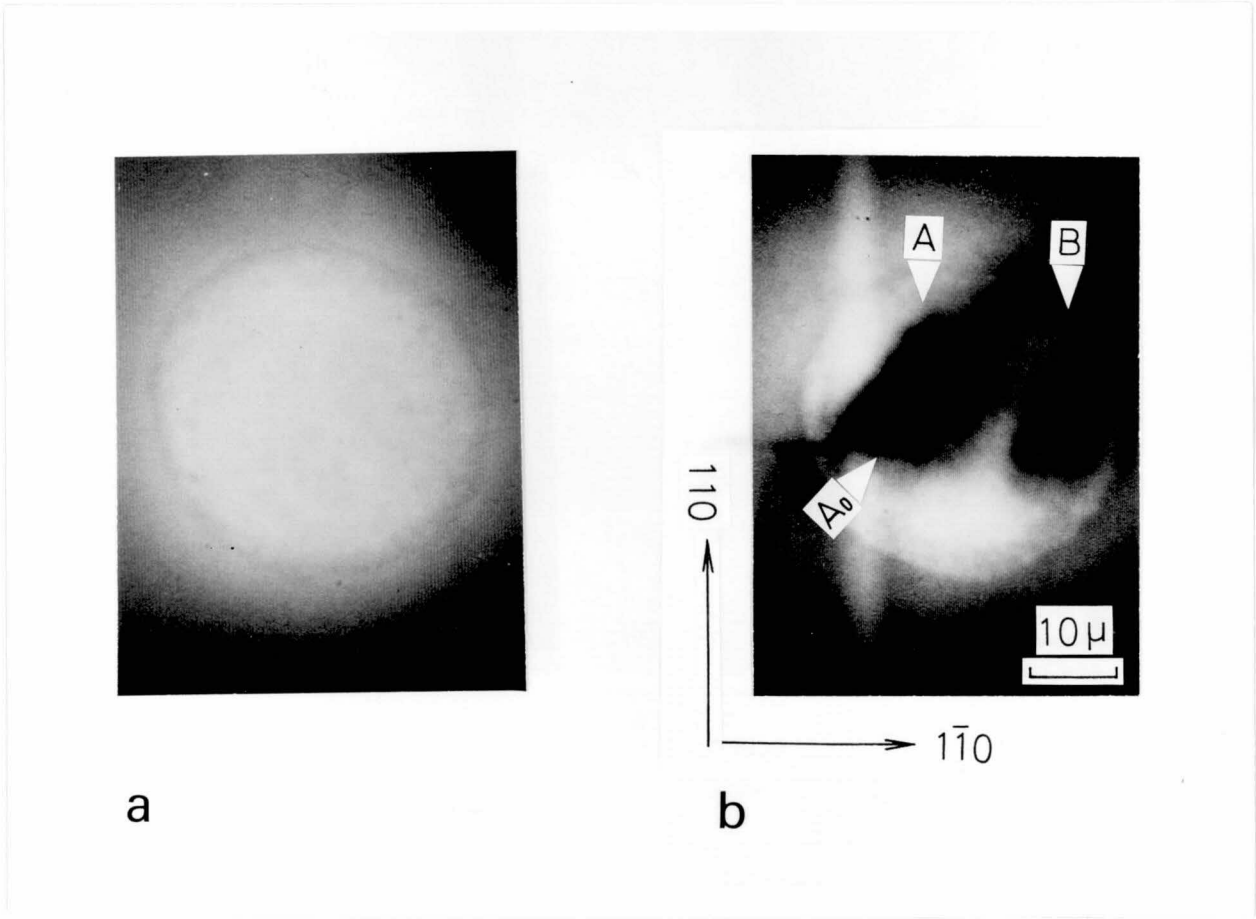

Fig.VII-6. Electroluminescence patterns of (a) the DLD-free LED and (b) the rapidly degraded LED.

good reproducibilities.

Within a range of the operating time shown in Fig.VII-5, the output power of the sample (A) is seen to show no decrease. DLD-free LEDs such as the sample (A) exhibit a characteristic of very slow degradation at room temperature. Since the magnitude of the slow degradation at room temperature is too small to measure, accelerated aging tests are required to estimate the life of the DLD-free LEDs. Yamakoshi et al.[3] showed that the speed of the slow degradation was strongly dependent on the operating temperature. They examined the slow degradation at 20, 60, 120, 180, and 250°C in dry-nitrogen ambient. The results are shown in Fig.VII-7. The data in this figure were periodically measured at 20°C. Duing these accelerated aging tests, DLDs were not observed in the samples.

As is shown in Fig.VII-7, the output power (P) can be expressed as an exponential function with time (t),

$$P = P_0 \exp(-\beta t), \qquad \ldots \text{(VII.1)}$$

where P_0 and β are the initial power and the degradation coefficient, respectively. An output power for LEDs running at 20°C remained constant over an operational period of 15000 hours. At the ambient temperature of 60°C, the degradation did not exceed the range of error of the optical power measurements ($\sim 2\%$). β depended on the temperature (θ) at the active region, and was found to obey the following equation:

$$\beta = \beta_0 \exp(-E_0/k\theta) \qquad \ldots \text{(VII.2)}$$

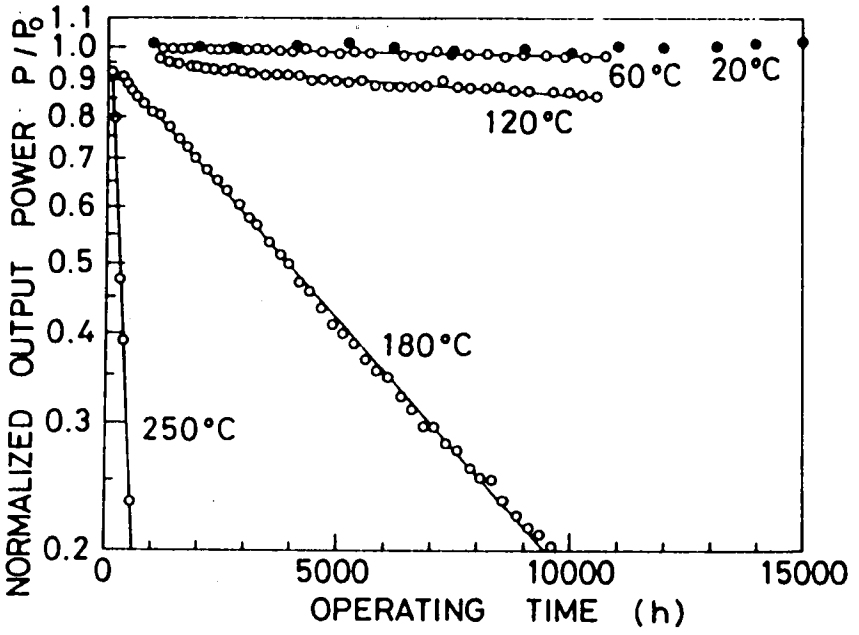

Fig.VII-7. Normalized output power as a function of operating time. The data points of a typical diode for respective ambient temperature are shown.

where β_0, E_0, and k are the proportionality constant, the activation energy, and the Boltzmann constant, respectively. Fig.VII-8 shows the temperature dependence of the degradation coefficient. From this figure, the activation energy and the value of β_0 are found to be 0.57 eV and 93 h^{-1}, respectively. By extrapolating the degradation coefficient to the temperature of 40°C, it is estimated that the room-temperature half-life of these LEDs is over 5×10^6 hours. Besides, the results obtained from the mesa-etched LEDs with an emitting diamter of 85 μm[4), whose operating current density was 3.5 KA/cm^2, are also plotted in Fig.VII-8. They show that the value of β does not significantly depend on the current density and the structure of the LED. Then, it is believed that the slow degradation is caused by some effects induced in the bulk during the operation.

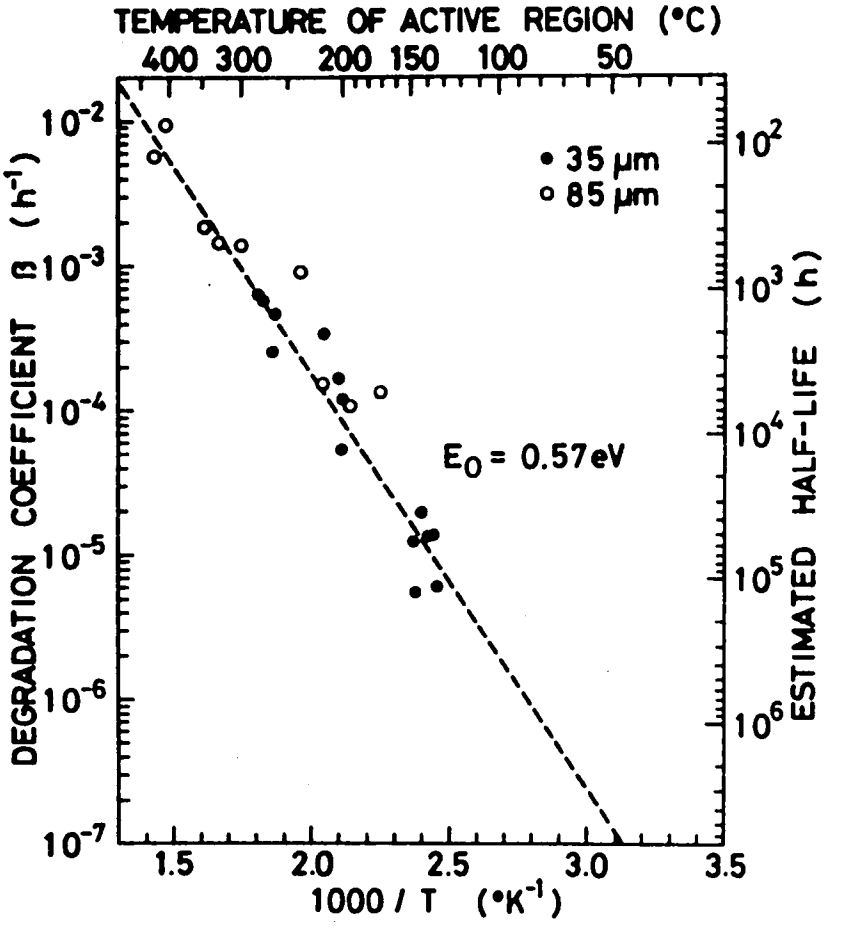

Fig.VII-8. Temperature dependence of the degradation coefficient.

VII.4. Defect Structure of Dark Lines in The Active Region of Rapidly Degraded $Ga_{1-x}Al_xAs$ Light Emitting Diodes.

In this section, the defect structure of the dark lines which are responsible to the rapid degradation of $Ga_{1-x}Al_xAs$ LEDs is analyzed by transmission electron micrograph (TEM) measurements.

In GaAs-$Ga_{1-x}Al_xAs$ double heterostructure lasers, the rapid degradation in an early stage of the operation have been observed by many workers[5)-7)]. According to their results, the generation and the multiplication of DLDs oriented to <100> and <110> directions are responsible for the rapid degradation of double heterosturcture lasers. Petroff and Hartman[5)] showed that dislocation networks, which included many dislocation dipoles, helical dislocations, and small dislocation loops, were associated with <100> DLDs in the degraded regions. They concluded that the Burgers vector of the dislocation networks as a/2[011] inclined at 45° to the junction plane, and that the networks were intrinsic. Contrarily, more detailed analyses by Hutchinson et al.[6)] indicated that three types of dislocation networks, with Burgers vectors of (a) a/2 [011] inclined at 45° to the (001) junction plane, (b) a/2 [110] laying in the junction plane, and (c) a[011] normal to the junction plane were observed in the active region of the degraded lasers, and that they were extrinsic in character. However, up to present, there have been no report about the observation of <100> or <110> DLDs in $Ga_{1-x}Al_xAs$ LEDs by TEM.

The rapidly degraded LED shown in Fig.VII-6(b) was used for the TEM sample. One <110> DLD (A_0) and some <100> DLDs (A and B) were observed in the light emitting area. For the preparation of the specimen for TEM, thick gold heat sink and SiO_2 mask were removed by chemical etching. The second layer was then removed by ion thinning, in order to observe the active region. The first layer was chemically etched from the side of the n-electrode by an echant of $40H_3PO_4$: $40H_2O$: $1H_2O_2$ until the etched surface reached near the junction. Finally, the specimen was mounted on a TEM mesh, and thinned down to about 0.1-0.5 μm by ion thinning. The specimen was observed by a JEM-120 electron microscope operated at 120 kV with a specimen-tilting-and-rotating mechnism. The processes of the sample preparation is schematically shown in Fig.VII-9.

Figs.VII-10(a) and VII-10(b) are transmission electron micrographs which correspond to A and B, respectively. They were obtained from the $2\bar{2}0$ and $\bar{2}20$ reflections. Many dislocation dipoles and helical dislocations were observed in both regions. The dipoles extended in the <100> or <210> direction as shown in Fig.VII-10(a). Small circular loops (100-500 Å in diameter) and larger irregular circular loops existed in the vicinity of them. Figs.VII-11(a) and VII-11(b) are stereo electron pairs of the dipole X in Fig.VII-10(a), where g=220 and $s > 0$, and the beam direction is close to $[\bar{1}\bar{1}6]$ and $[1\bar{1}6]$, respectively. Figs. VII-12(a)-(d) were obtained from the $\bar{2}\bar{2}0$, 400, $0\bar{4}0$, and 040 reflections, respectively, and $s > 0$ in all cases. The dipole

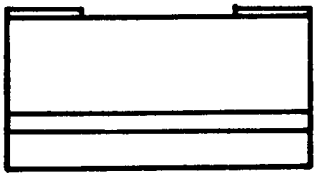

a) The degraded sample is removed from the stem.

b) Thick Au heat sink and SiO_2 mask are removed by chemical etching.

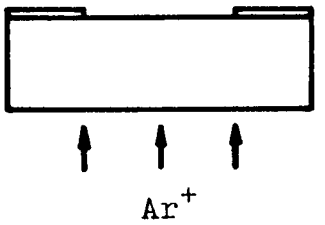

c) The second layer is removed by Ar^+ ion sputtering.

d) The first thick layer is chemically etched from the side of N-electrode.

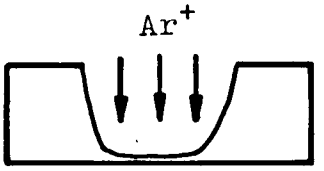

e) The first layer is thinned down to 0.1-0.5 μm by ion sputtering.

Fig.VII-9 Schematic illustration of the TEM sample preparation.

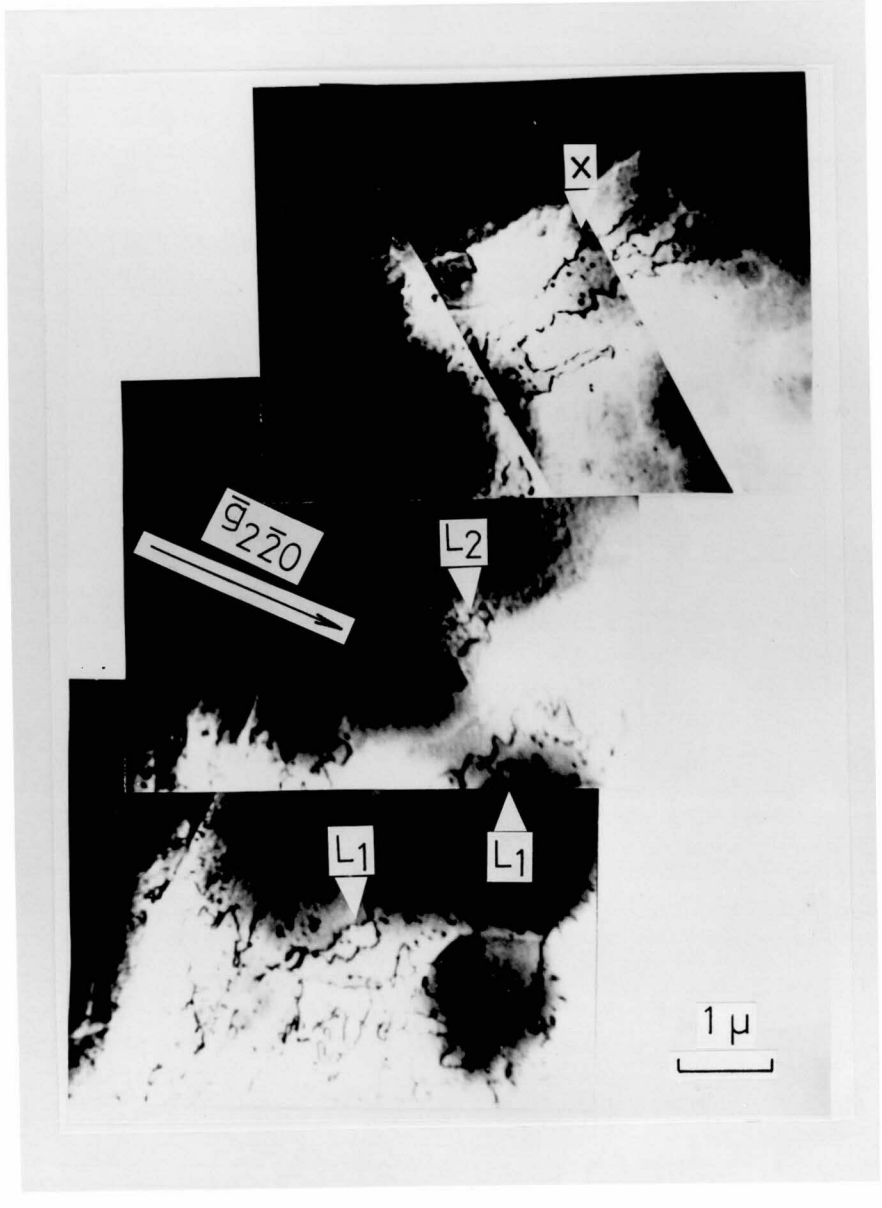

Fig.VII-10(a). Transmission electron micrograph of the degraded region A in Fig,VII-6(b). $\bar{g} = 2\bar{2}0$, $s > 0$.

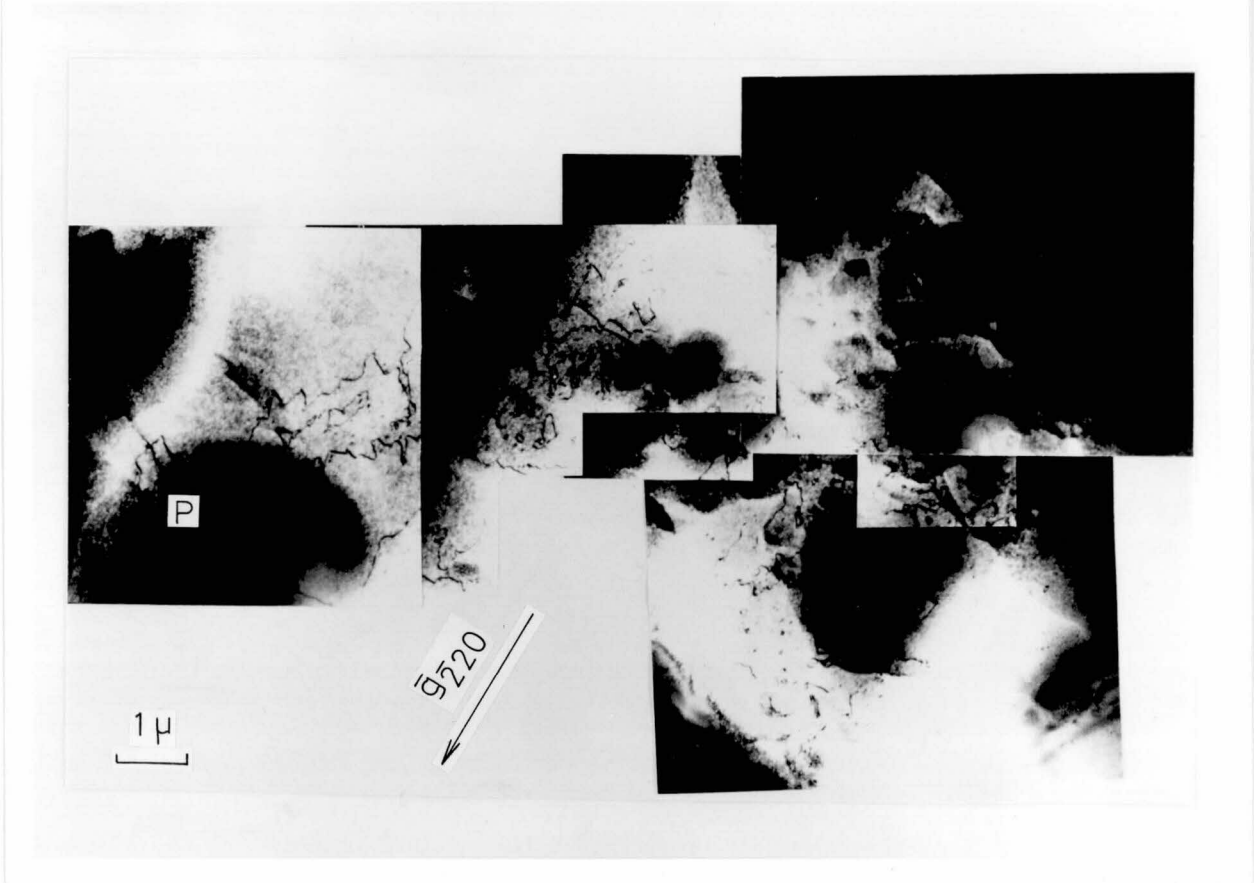

Fig.VII-10(b). Transmission electron micrograph of the degraded region B in Fig.VII-6(b). $\bar{g} = \bar{2}20$, $s > 0$.

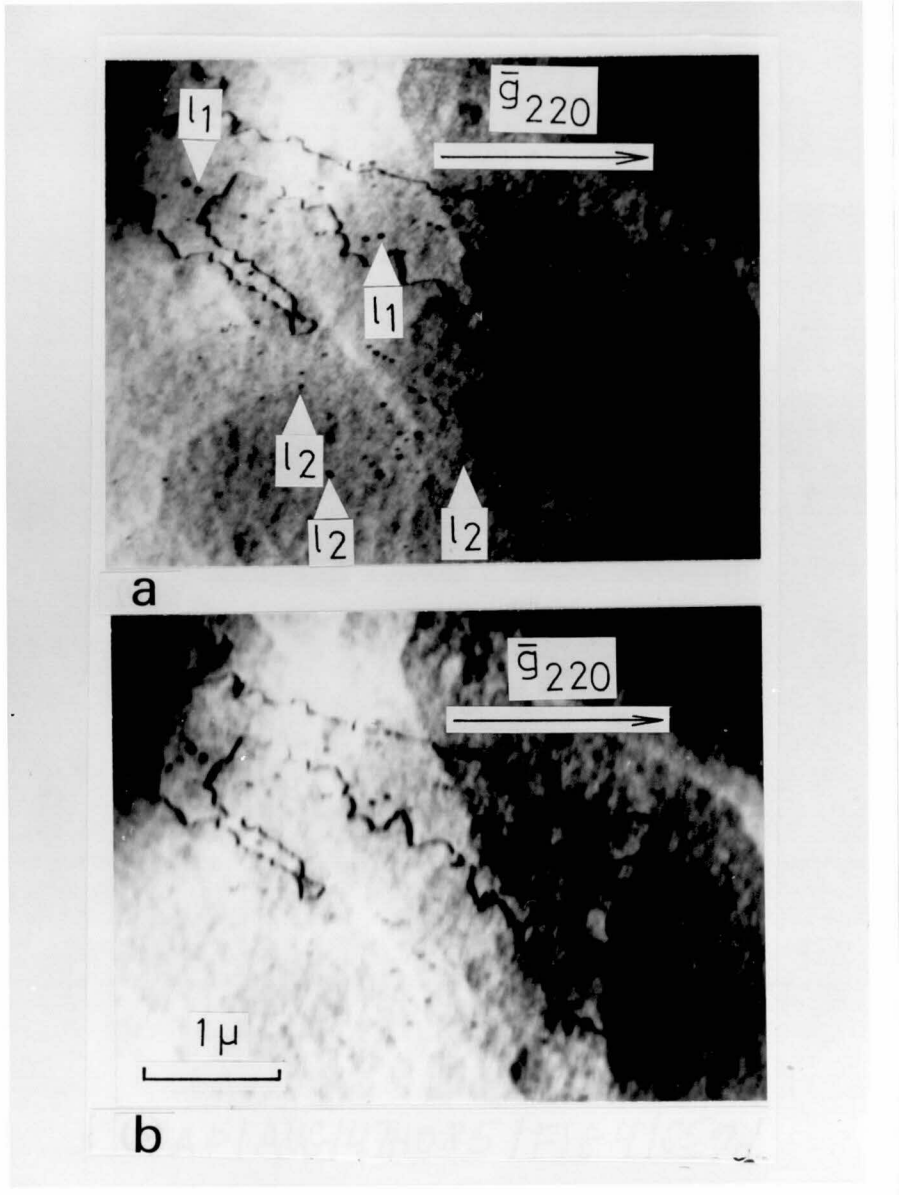

Fig.VII-11. Stereo electron pair of the part of the network shown in Fig.VII-10(a). $\bar{g}$ = 220, s > 0, the beam direction: (a) $[\bar{1}16]$; (b) $[1\bar{1}6]$.

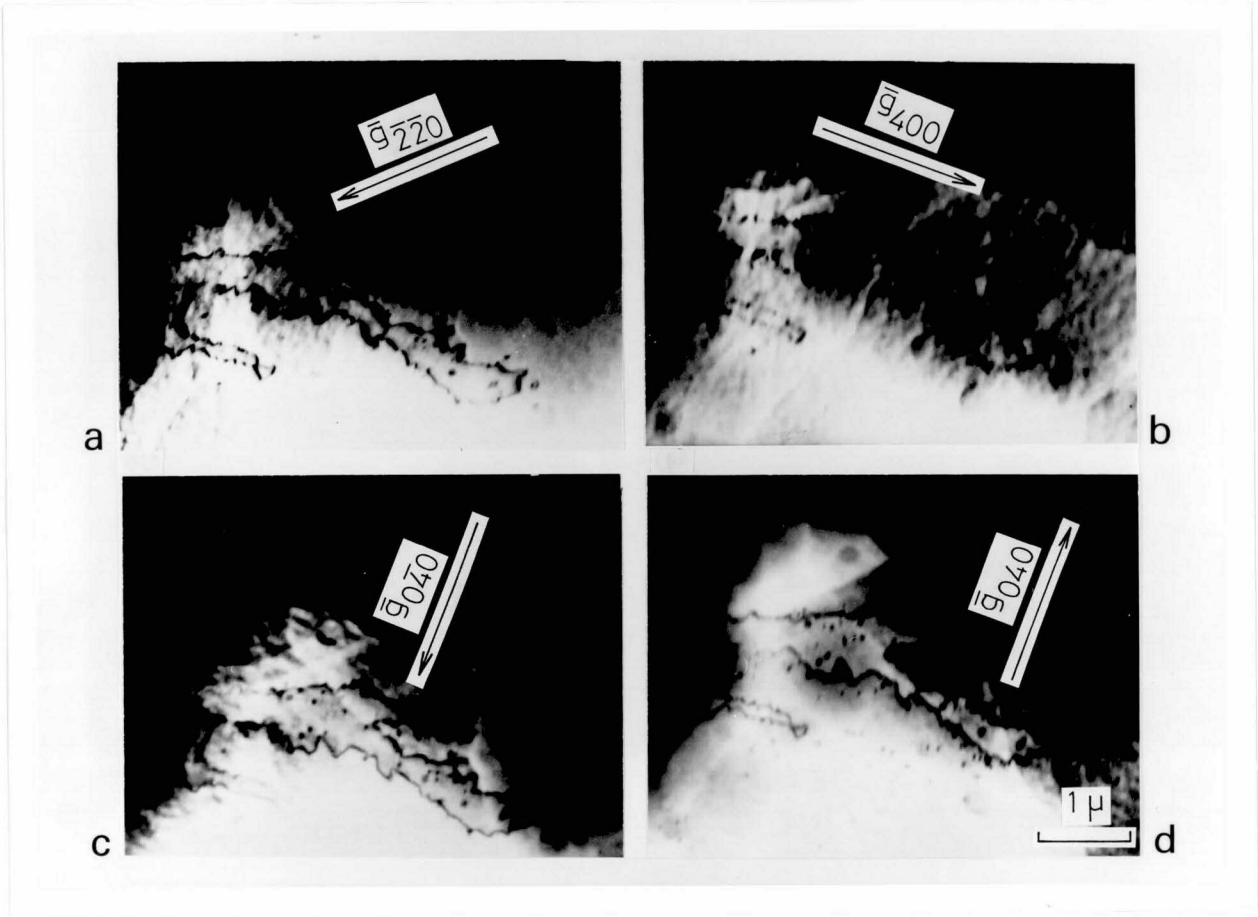

Fig.VII-12. Variation of the diffraction contrast of dipole X shown in Fig.VII-10(a). (a) $\bar{g} = \bar{2}\bar{2}0$, $s > 0$; (b) $\bar{g} = 400$, $s > 0$; (c) $\bar{g} = 0\bar{4}0$, $s > 0$; (d) $\bar{g} = 040$, $s > 0$.

X was out of contrast when g=400, and in contrast when g=220, $2\bar{2}0$, 040, and $0\bar{4}0$. From these results, the Burgers vector of the dipole X was determined to be $\pm a/2[0\bar{1}1]$ inclined at 45° to the junction plane. On the other hand, a dislocation dipole exhibits inside contrast for $(g\cdot b)\cdot s < 0$, and outside contrast for $(g\cdot b)\cdot s > 0$. The dipole X exhibited inside contrast when g=040 and $s > 0$, and outside contrast when $g=0\bar{4}0$ and $s > 0$. Therefore, its Burgers vector was $a/2[0\bar{1}1]$ and it was extrinsic in character. The same analyses were performed on the dislocation loops which existed in the vicinity of the dipoles. They indicated that small circular loops and larger irregular circular ones inside the dipoles were intrinsic in character, and that those outside the dipoles were extrinsic in character. The results described above indicate that dislocation networks which contain extrinsic dislocation dipoles, helical dislocations , and dislocation loops are associated with <100> DLDs in a rapidly degraded $Ga_{1-x}Al_xAs$ LED.

Although the origin of these defects in the degraded region A could not be observed, a threading dislocation is expected to be one of the origins of them. A <110> DLD was observed along the edge of <100> DLDs in degraded region A in the micrograph, while the dislocation P in FigVII-10(b) contained a helical dislocation and was lying in the [1$\bar{1}$0] direction, though the <110> DLD corresponding to this could not be observed in Fig. VII-6(b). Therefore, it could be also expected that dislocations parallel to the <110> direction were generated by local stress

(i.e., the stress between the diode and the electrode) during LED operation, and then, helical dislocations and dislocation dipoles grew from them. The larger irregular circular loops inside the dipole L_1 in Fig.VII-10(a) and those outside the dipole L_2 in Fig.VII-10(a), which were intrinsic and extrinsic, respectively, were considered to be generated by unusual climb motion of the dipole. On the other hand, the small dislocation loops inside the dipole (l_1 in Fig.VII-11(a)) which were also intrinsic, were perhaps generated by pinning several segments of the dislocation line with dragging points. However, it is also possible that these intrinsic loops in Fig.VII-11(a) were generated by the condensation of vacancies inside the dipole. This would be reasonable provided that the dislocation climb is subjected to the absorption of interstitial atoms. Because, if interstitial atoms were generated in the crystal, the same number of vacancies would also be generated in it. Recently, Petroff et al.[8] showed that dislocation networks were associated with the degraded region of the GaP LED, and that the number of small dislocation loops inside the dipole increased during TEM observation. They concluded that still-existing vacancies inside the dipole condensed during the operation. However, this phenomenon did not occur in the present experiment. This may be due to the absence of excess vacancies inside the dipole. Apart from this, one of the typical features peculiar to the dislocation networks in the degraded region of $Ga_{1-x}Al_xAs$ LED was the existence of extrinsic small dislocation

loops outside the dipole (l_2 in Fig.VII-11(a)). These loops were localized in the vicinity of the dipole. At present, the origin of these loops is not clear.

VII.5. Discussion.

$Ga_{1-x}Al_xAs$ LEDs fabricated from thick wafers have exhibited high performances as described in section VII.2. The output power of 4.7 mW at an operating current of 100 mA corresponds to the internal quantum efficiency of about 80 % under considering a perfect reflection at the back side (i.e., p-electrode) and no internal optical absorption. Then, assuming that a reflection at the back side is not perfect, and that the emitted light is somewhat absorbed in the crystal, the internal quantum efficiency would come up to the value of about 100 %. This means the concentration of nonradiative recombination centers in the crystal is negligibly small compared with the concentration of the injected minority carrier.

In the present $Ga_{1-x}Al_xAs$ LEDs, the light emitting region is confined in a very small area of about 35 μm in diameter. Then, the current density at 100 mA operation is about 10 kA/cm^2. This value is much higher even than semiconductor lasers (2-3 kA/cm^2, typically). In the early stage of the development of this LED, we were afraid that such a high current density would accelerate the degradation. However, as is described in section VII.3, the slow degradation was found to be independent of the current density. Under the low current density of 10-100 A/cm^2 which is an usual operation condition of LEDs for photo-lamps, the generation and the multiplication of DLDs occur with a very slow rate. In this case, it is difficult to distinguish the slow degradation from that caused by DLDs. Whereas, in the pre-

sent LEDs, the generation and the multiplication of DLDs occured at a high speed owing to the very high current density. This phenomenon was effectively applied to the selection of the DLD-free LEDs.

TEM analyses described in section VII.4 have revealed that dislocation networks, which contained dislocation dipoles and a number of dislocation loops, were associated with DLDs oriented to <100> direction. In these analyses, the origin of <100> DLDs could not be identified, completely. However, a number of works on the degradation of semiconductor lasers[5)-7)] have shown that most of threading dislocations grow to be <100> DLDs. Hasegawa et al.[2)] reported that the density of DLDs corresponded with the dislocation density in the crystal. Petroff and Hartman[5)] reported that the network was seen to originate from the threading dislocation in the active region of the semiconductor laser by TEM observations. These results strongly indicate one of the origins of <100> DLDs in $Ga_{1-x}Al_xAs$ LEDs is a threading dislocation.

In the present work, <110> DLD dnoted by A_0 in Fig.VII-6(b) colud not be identified. Recent works by Ueda and Isozumi[9)] have identified that the multiple stacking faults which laid in <110> directions, or the half dislocation loops which also laid in <110> directions and had Burgers vectors of the type a/2<011> inclined at 45° to the junction plane or a/2 <110> parallel to the junction plane were associated with <110> DLDs. They suggested the half dislocation loops which corresponded to <110>

DLDs were introduced from the surface by local stress (i.e., the stress between the diode and the electrode or the SiO_2 mask) during the operation. They also observed that herical dislocations and dislocation dipoles grew from the half dislocation loop. This fact indicates that the another origin of <100> DLDs is <110> DLD.

Some models for the growth mechanisms of dislocations [10)-12)] have been proposed to explain the multiplications of helical dislocations and dislocation dipoles, which are responsible for <100> DLDs. However, the growth mechanism of <100> DLDs cannot be fully explained by these models. One of the important points for considering this problem is that these dislocations cannot be easily moved or multiplied at the usual operating temperature. The activation energy of a glide motion of dislocations in GaAs is about 1 eV[13)]. Whereas, in the actual experiments, it is observed that the dislocation easily grows in the operation at room temperature, but cannot grow out of operation. This fact indicates that the recombination process of the injected carriers enhances the growth of dislocations.

Lang and Logan[14),15)] proposed a model to explain this puzzle. According to their model, the deep levels in crystals are often strongly coupled to the lattice. This coupling can cause rapid nonradiative recombinations in which the released electronic energy causes violent vibrations of the lattice near the defect. The vibrations can promote the defect motion at low temperature. This phenomenon, in result, enhances the

growth of dislocations and the multiplication of nonradiative recombination centers. This idea well explains the degradations in light emitting devices. It is also supported by the fact that the semiconductor devices in which the majority carrier transportation is used, such as Gunn diodes and IMPATT diodes, live much longer. There are still too many difficulties, however , in complete understanding of the degradation phenomena because of few reliable data on this problem.

VII.6. Conclusions.

$Ga_{1-x}Al_xAs$ LPE wafers described in the previous chapter were used for the fabrication of LEDs for fiber-optical communication systems. The 50 μm thick window layer enabled the complete removal of the GaAs substrate in the fabrication processes. The LEDs exhibited a very high output power of 4.7 mW at 100 mA. Such a high performance of this LED proved that the crystal was almost perfect and contained few nonradiative recombination centers.

Some of the fabricated LEDs, however, rapidly degraded during the operation. In these LEDs, dark line defects oriented in the <100> or <110> direction were observed. From the analyses by a transmission electron microscopy, dislocation networks, which contained dislocation dipoles and a number of dislocation loops, were associated with <100> DLDs. The dipole extended in the <100> or <210> direction, and was extrinsic in character; its Burgers vector was a/2 <011> inclined at 45° to the junction plane. Since these results were very similar to those of GaAs-$Ga_{1-x}Al_xAs$ double heterostructure lasers, the major origins of <100> DLDs in the present LED were believed to be threading dislocations propagated from the GaAs substrate. On the other hand, half dislocation loops which also lay in {110} directions and had Burgers vectors of the type a/2 <011> inclined at 45° to the junction plane or a/2 <110> parallel to the junction plane were associated with <110> DLDs. They were believed to be introduced by the local stress under the operating condition.

Some indications of the growth of <100> DLDs from the half dislocation loops were observed. This strongly suggest that the another origin of <100> DLDs are <110> DLDs.

From the accelerated aging tests, the room-temperature half-life of the DLD-free LEDs was estimated in excess of 5×10^6 hours. This is the longest value in the previously reported papers. It is believed that such a high reliability has been achieved by the perfection of the LPE grown $Ga_{1-x}Al_xAs$, and by completely removing the GaAs substrate in the LEDs fabrication.

REFERENCES OF CHAPTER VII.

(1) M. Abe, I. Umebu, O. Hasegawa, S. Yamakoshi, T. Yamaoka, T. Kotani, H. Okada and H. Takanashi, IEEE Trans. Electron Device ED-24 (1977) 990.

(2) O. Hasegawa, S. Yamakoshi, I. Umebu, H. Hamaguchi, M. Abe T. Yamaoka, Optical and Quantum Electronics group meeting of IECE, OQE 76-96 (1976).

(3) S. Yamakoshi, O. Hasegawa, H. Hamaguchi, M. Abe and T. Yamaoka, J. Appl. Phys. 31 (1977) 627.

(4) Y. Komatsu, S. Isozumi and T. Kotani, FUJITSU Scientific and Technical J. 12 (1976) 125.

(5) P. Petroff and R. L. Hartmann, Appl. Phys. Lett. 23 (1973) 469.

(6) P. W. Hutchinson, P. S. Dobson, S. O'Hara and D. H. Newman, Appl. Phys. Lett. 26 (1975) 250.

(7) P. W. Hutchinson and P. S. Dobson, Philos. Mag. 32 (1975) 745.

(8) P. M. Petroff, O. G. Lorimor and J. M. Ralston, J. Appl. Phys. 47, (1976) 1583.

(9) O. Ueda, S. Isozumi, S. Yamakoshi and T. Kotani, J. Appl. Phys. to be published.

(10) J. Matsui, K. Ishida and Y. Nannichi, Japan J. Appl. Phys. 14 (1975) 1555.

(11) P. M. Petroff and R. C. Kimerling, Appl. Appl. Phys. Lett. 29 (1976) 461.

(12) T. Kamejima, K. Ishida and J. Matsui, Japan J. Appl. Phys. 16 (1977) 233.

(13) Y. Nannichi, OYOBUTSURI 46 (1977) 558.

(14) D. V. Lang and R. A. Logan, Phys. Rev. Lett. 39 (1977) 635.

(15) D. V. Lang and L. C. Kimerling, Phys. Rev. Lett. 33 (1974) 489.

(16) O. Ueda, S. Isozumi, T. Kotani and T. Yamaoka, J. Appl. Phys. 48 (1977) 3950.

VII. SUMMARY.

In chapter II, the theory of the phase diagrams of ternary III-V systems was described based on the quasi-regular solution model, and was applied to the calculation of the phase diagram of the Ga-Al-As system. From the comparison between the calculated values and the experimental ones, the best thermodynamic data for the Ga-Al-As system were chosen from the literatures. A conventional sliding method used in the growth experiment was found disadvantageous for the growth of $Ga_{1-x}Al_xAs$ because of the formation of the Al_2O_3 scums on the surface of the solution. It was also found that the AlAs mole fraction considerably distributed in the thick LPE layer.

In chapter III, the theory of the composition change in ternary III-V compounds was described. A theoretical expression about the decreasing rate of each nutrient in the solution was derived, and the calculation of the deposition path in Ga-Al-As system was carried out based on it. The calculated results have shown that the solidus composition change during the growth cycle is determined by a competing process between the depletion of aluminum in the liquid, and the increase of the distribution coefficient of aluminum. The calculated result was compared with the experiment of the growth from 950°C. Then, it was found that the solidus compositions obtained by the experiment slightly deviate from the calculated values as the growth proceeds , whereas, the deviation between the actual layer thicknesses and the theoretical ones is seriously large.

In chapter IV, the theories of LPE growth rate in binary and ternary systems were described. The equations for the LPE layer thickness in binary systems were derived from the diffusion equation based on a diffusion limitted growth model. The derived equation has a simple analytical form in a case of the growth from a semi-infinite solution. In this case, the layer thickness is proportional to the cooling rate, to the reciprocal of the slope of the liquidus line, and to the growth time taken to the 3/2 power. To examine the applicability of this equation in binary systems to ternary ones, the basic equations for the slope of the deposition path over the liquidus surface in ternary systems were derived. From these equations, the changing rate of arsenic and aluminum concentrations in Ga-Al-As liquid during the LPE growth cycle were calculated. From the comparison between the calculated values of the changing rate of arsenic concentration in the liquid, and the LPE layer thickness obtained by the experiments, it was shown the linear relationship between these two quantities held in the Ga-Al-As system. The another series of the growth experiments showed that the LPE layer thickness of $Ga_{1-x}Al_xAs$ was proportional to the growth time taken to the 3/2 power. These facts indicate that the growth process of $Ga_{1-x}Al_xAs$ is controlled mainly by the diffusion of arsenic, and that the simple equation for the layer thickness in binary systems is applicable in Ga-Al-As system. From the results of the comparisons described above, arsenic diffusivities in the Ga-Al-As liquid were estimated

to be 1.0×10^{-4}, 1.2×10^{-4}, and 1.4×10^{-4} cm^2/sec at 850°C, 900°C, and 950°C, respectively. These values show a relatively weak temperature dependence compared with the published data in the Ga-As system.

In chapter V, growth conditions for obtaining a 50 μm thick $Ga_{1-x}Al_xAs$ LPE layer with fixing the solidus composition at the surface at X = 0.09 were analyzed based on the theories described in the preceding chapters. From the results of LPE growth experiments in which the solution thickness was varied for each growth run, it was found that the spontaneous nucleations in the solution remarkably reduced the layer thickness, and seriously disturbed the flatness of the layer. Then, the maximum solution thickness without causing the spontaneous nucleations in the solution was obtained as a function of the cooling rate. Within the range of the cooling rate from 0.15 °C/min to 0.33°C/min, it was proportinal to the cooling rate taken to the -1/2 power. This relation was well explained by the theory based on the diffusion limitted growth model, and the value of a critical supercooling temperature was obtained as 0.54°C when the arsenic diffusivity was 1×10^{-4} cm^2/sec. Although this value is small compared with the one in Ga-As system, it is probable at such low cooling rates. Finally, the cooling rate, the optimum solution thickness, the initial solidus composition, and the growth time were reciprocally related with one another.

In chapter VI, a new sliding system was developed for the

LPE growth of thick $Ga_{1-x}Al_xAs$ wafers with a multiple-layers structure. The growth apparatus was designed as to suppress the excess edge growth, and to equilibrate the solution with the solid during the whole cooling cycle. From the results of the previous analyses, the growth condition for a 50 μm thick window layer and the 2 μm subsequent thin layer were determined as the solution thickness of 1.6 mm, the cooling rate of 0.22°C/min, and the aluminum weights of 1.3 mg/Ga1g for the first layer and 2.5 mg/Ga1g for the second layer. The obtained LPE wafers were found to contain photoprocessable surfaces and the expected values of both the compositions and the thicknesses. The suppression of the excess edge growth and the wiping of the solution after the growth were completely accomplished.

In chapter VII, the light emitting diodes were fabricated using the LPE wafer described in the previous chapter for the purpose of the characterization of the epitaxial layers. The fabricated LEDs exhibited a very high output power of 4.7 mW at 100 mA. Such a high performance of this LED proved that the crystal was almost perfect and contained few nonradiative recombination centers. However, some of the LEDs rapidly degraded during the operation. In such LEDs, dark line defects oriented in the <100> or <110> direction were observed. From the analyses by a transmission electron microscopy, dislocation networks, which contained dislocation dipoles and a number of dislocation loops, were associated with <100> DLDs. The dipole

extended in the <100> or <210> direction, and was extrinsic in character; its Burgers vector was a/2<011> inclined at 45° to the junction plane. The major origins of <100> DLDs were thought to be threading dislocations propagated from the GaAs substrate. On the other hand, half dislocation loops which lay {110} directions and had Burgers vectors of the type a/2<011> inclined at 45° to the junction plane or a/2<110> parallel to the junction plane were associated with <110> DLDs. They were believed to be introduced by the local stress during the operation.

ACKNOWLEDGEMENTS

The present thesis has been submitted to Kyoto University for the partial requirements of the degree of Doctor of Engineering. The research work presented in this thesis was performed in Semiconductor Materials Laboratory, FUJITSU Laboratories Ltd., from 1971 to 1978.

The author wishes to express his sincere thanks to Dr. Osamu Ryuzan and Mr. Tsuyoshi Kotani for their appropriate advices and continuous encouragement. He also indebted to Professor Yotaro Murakami and Dr. Kozo Osamura for introducing him to the study of the phase diagrams and their encouragement throughout this work. Further, he is deeply indebted to Messrs. Toyoshi Yamaoka, Yasuaki Komatsu, Osamu Ueda and Osamu Hasegawa, and Drs. Masayuki Abe and Shigenobu Yamakoshi for their helpful discussions and earnest contributions throughout this work.

THE LIST OF PUBLISHED PAPERS

(1) "Liquid Phase Epitaxial Growth of $Ga_{1-x}Al_xAs$ LEDs Used in Optical Communication Systems." Yasuaki Komatsu, Shoji Isozumi and Tsuyoshi Kotani, FUJITSU Scientific and Technical J. 12 (1976) 125.

(2) "Dependence of $Ga_{1-x}Al_xAs$ LPE Layer Thickness on Solution Composition" Shoji Isozumi, Yasuaki Komatsu, Niro Okazaki, Shuichi Koyama and Tsuyoshi Kotani, J. Crystal Growth 41 (1977) 166.

(3) "Defect Structure of <100> Dark Lines in The Active Region of A Rapidly Degraded $Ga_{1-x}Al_xAs$ LED" Osamu Ueda, Shoji Isozumi, Tsuyoshi Kotani and Toyoshi Yamaoka, J. Appl. Phys. 48 (1977) 3950.

(4) "TEM Observation of $Ga_{1-x}Al_xAs$ LPE Crystals for An Optical Source for Optical Communications." Osamu Ueda, Shoji Isozumi and Tsuyoshi Kotani, FUJITSU Scientific and Technical J. 14 (1978) 87.

(5) "Defect Structure of Degraded $Ga_{1-x}Al_xAs$ Double-Hetero-Structure Light Emitting Diodes." Osamu Ueda, Shoji Isozumi, Shigenobu Yamakoshi and Tsuyoshi Kotani, J. Appl. Phys. 50(2) (1979) 765.

(6) "Analyses on The Composition Control and The Growth Rate of $Ga_{1-x}Al_xAs$ LPE Layer." Shoji Isozumi, Yasuaki Komatsu and Tsuyoshi Kotani, FUJITSU Scientific and Technical J. 15 (1979) to be published.